EFFECTS OF DYNAMIC ENTRAPPED AIR ON HYDRAULIC CONDUCTIVITY

THE EFFECTS OF DISCONNECTED ENTRAPPED AIR ON HYDRAULIC CONDUCTIVITY IN THE PRESENCE OF WATER TABLE FLUCTUATIONS

By

MARICRIS MARINAS, B.Sc.

A Thesis

Submitted to the School of Graduate Studies

in Partial Fulfillment of the Requirements

for the Degree

Master of Science

McMaster University

MASTER OF SCIENCE (2009) **McMaster University**

(Earth Science) **Hamilton, Ontario**

TITLE: The Effects of Disconnected Entrapped Air on Hydraulic Conductivity in the Presence of Water Table Fluctuations

AUTHOR: Maricris Marinas, B.Sc. (McMaster University)

SUPERVISOR: Professor James E. Smith

NUMBER OF PAGES: xi, 97

ABSTRACT

The hydraulic conductivity of a groundwater system can possess high spatial and temporal variability in the presence of an entrapped air phase (quasi-saturated soils) which is a key factor in controlling hydraulic behaviour. Previous studies have provided evidence of reduced hydraulic conductivity caused by entrapped air; however, these did not address the dynamic behaviour of the entrapped gaseous phase. In this study, the hypothesis that the decreases in hydraulic conductivity caused by entrapped air are sensitive to fluctuations in the water table was tested using laboratory experiments. The effects of applying increasing confining pressures (water table elevation) on the nature of entrapped air and its effects on quasi-saturated hydraulic conductivity was investigated for a range of sands and for air entrapment by both upward water flow and ponded infiltration (downward flow). Laboratory experiments were conducted using the constant flux method on saturated/ quasi-saturated horizontally positioned sand columns using 1% bleach as the solution. Induced pressures ranged from 0 to 250 cm with changes in hydraulic conductivity calculated using collected timed-interval outflow discharge and the pressure gradient measured by a differential pressure transducer. The sand core was also instrumented to measure volumetric moisture (or air) content with time domain reflectometry (TDR) probes. Results show that a 250-cm increase in water pressure above atmospheric pressure induced changes in the volume of entrapped gas according to the ideal gas law indicating the primary and tertiary roles played by air phase compression and capillary pressure, respectively. The reduction in air content at the 250-cm pressure increased the quasi-saturated hydraulic conductivity by a factor of 1.20 to 1.64. The results were fitted to the van Genuchten (1980) and Faybishenko (1995) functions for unsaturated and quasi-saturated hydraulic conductivity, respectively. The changes in quasi-saturated hydraulic conductivity due to changes in air content are expected to ubiquitously occur in the presence of a fluctuating water table. Thus the understanding of this fundamental mechanism and its incorporation into current general models of flow and transport will aid in better understanding the unique role of entrapped air in groundwater systems.

ACKNOWLEGMENTS

First and foremost I would like to express my gratitude and appreciation to my supervisor Dr. James E. Smith for providing the opportunity to investigate, learn, and develop skills that also apply beyond the world of academia. I would like to thank Dr. Jim W. Roy of the Canada Centre for Inland Waters of Environment Canada (Burlington, Ontario) who acted as co-supervisor providing research assistance, thoughtful discussion, and guidance throughout this entire experience. To Jennie Kirby of McMaster University, I extend my sincere gratitude for her technical and moral support. I am thankful to my family and friends who provided their constant and endless encouragement during each victory and obstacle faced during this research experience.

TABLE OF CONTENTS

LIST OF TABLES

LIST OF FIGURES

1.0 INTRODUCTION

One approach in assessing the importance of groundwater is to recognize that two-thirds of the world's freshwater resource is groundwater (Freeze and Cherry, 1979). Traditionally, the study of groundwater has been motivated by its importance as a resource. In addition to understanding the occurrence and quantity of groundwater, growing interest in a number of processes that occur within groundwater including biochemical reactions, the dissolution and exsolution of gases, and the transport and cycling of nutrients and contaminants has emphasized the unique role of groundwater. Analysis of the physical parameters that define the groundwater system aids in illustrating the flow system dynamics within this portion of the subsurface.

The groundwater table is the level at which groundwater pressure is equal to atmospheric, with pressures decreasing above and increasing below this level. The vadose zone extends from the water table to the ground surface and is generally unsaturated (air and water fill the pores) except for the tension-saturated capillary fringe directly above the water table. The saturated (phreatic) zone reaches below the water table and is commonly treated as completely filled with water (Figure 1.1). However, groundwater table fluctuations constantly introduce air below the water table through trapping of gas bubbles and ganglia occluded by water in the pore spaces of soils (i.e. entrapped air; Christiansen, 1944). This leads to a hydraulically complex multi-phase (air and water) region below the capillary fringe that can affect a number of processes including groundwater flow and the transport of dissolved gases and contaminants (e.g. Cirpka and Kitanidis, 2001; Amos and Mayer, 2006).

The trapped gaseous phase can occupy both dead-end and open pores thereby impacting the conduits traveled by water (Faybishenko, 1995) and effectively reducing the hydraulic conductivity (Christiansen, 1944; Fayer and Hillel, 1986; Faybishenko, 1995; Fry et al., 1997; Ryan et al., 2000). As a result, there can be an appreciable reduction in the effective rate of recharge as compared to a saturated aquifer (Christiansen, 1944, Faybishenko, 1995). A fundamental property of entrapped air that has been overlooked to date is the dynamic nature of entrapped air beyond dissolution and exsolution (Figure 1.2). The only other work is that of Emmerton (2001) who's undergraduate thesis work under the supervision of Dr. J.E. Smith in the School of Geography and Earth Sciences at McMaster University constituted preliminary investigations into this system. There is a lack of research and a gap in our knowledge concerning 1) how entrapped air reacts to water table changes and 2) what effects this has on hydraulic conductivity. The relationship between hydraulic conductivity and water content in the presence of continuous air within unsaturated soils is well studied and understood; however, the behaviours generated by entrapped air in the presence of water table fluctuations, i.e. under quasi-saturated conditions, are less well known and require further study to fill this gap in knowledge (Figure 1.1).

Although studies have shown that hydraulic conductivity is reduced below saturated values in soils as a result of trapped gas (Christiansen, 1944; Faybishenko, 1995; Fry et al., 1997; Sakaguchi et al., 2005), multi-phase and unsaturated flow simulators generally do not incorporate any consideration of the entrapped gaseous phase into models. Failing to integrate the concept and effects of entrapped air within a multifluid simulation could result in significant errors in flow rates and travel times across and near the groundwater table. In addition, this lack of sufficient knowledge has also meant that remediation technologies have not fully considered/ exploited the role of entrapped air.

A number of studies have addressed the issue of emplacement methods and the effects of the corresponding static volume of entrapped air, but they fail to directly address the dynamics of entrapment during changing water pressures, such as that from groundwater table fluctuations. Recognizing hydraulic conductivity as a function of entrapped air content and water table position is a fundamental and dynamic relationship that will provide a greater understanding of flow and transport near the groundwater table which is continuously subjected to natural fluctuations and to manipulation during resource exploitation and remediation interventions

1.1 Hypotheses and Research Goal

The hypotheses of this experimental investigation stipulate that:

1. An increase in water table elevation will effectively result in a significant and substantial decrease in entrapped air content.
2. The ideal gas law is a sufficient first order approximation of the change in volume of entrapped air in response to water table fluctuations.
3. Decreases in air content in a porous medium as a result of increasing water pressure will result in significant increases in the quasi-saturated hydraulic conductivity.

4. The texture of a porous medium is a primary factor in air entrapment and hydraulic behaviour under quasi-saturated conditions.

The goal of this research was to design and conduct a series of systematic laboratory-based experiments to address these hypotheses and quantify the observed processes, thereby enhancing our fundamental understanding of shallow groundwater systems and our ability to simulate their dynamic behaviour.

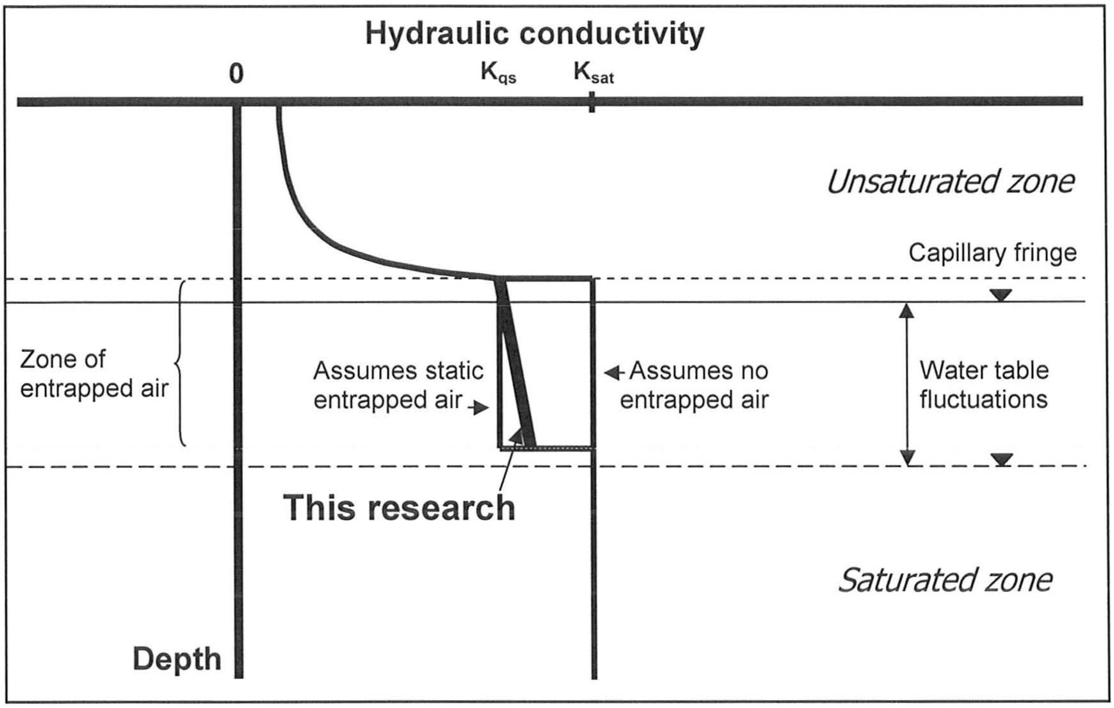

Figure 1.1: Conceptual illustration of the interrelationship between entrapped air content, quasi-saturated hydraulic conductivity and water table position

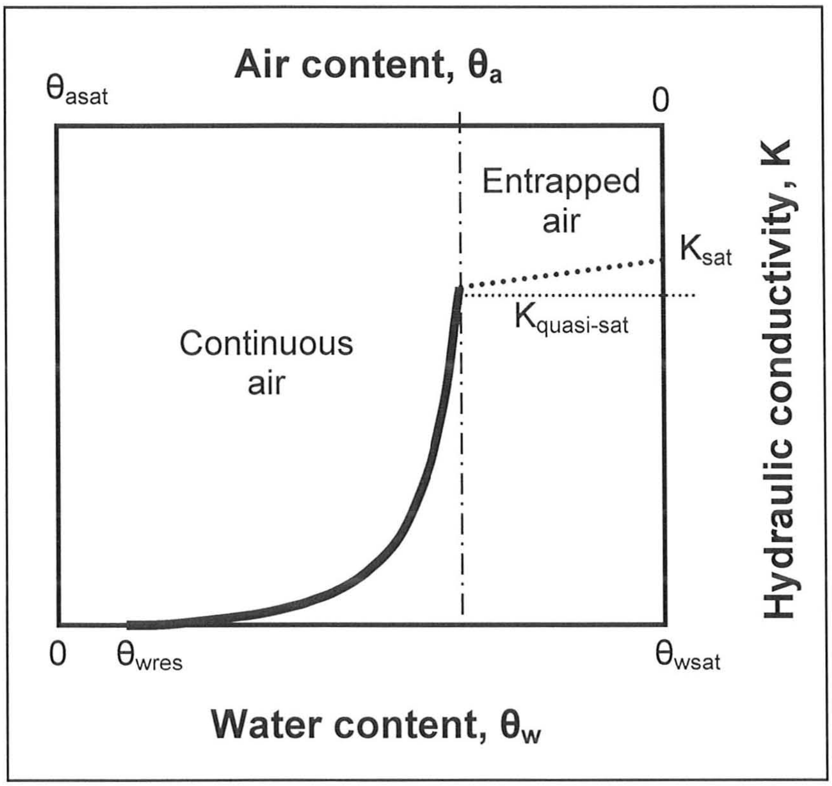

Figure 1.2: Schematic hydraulic conductivity versus water content curve

2.0 BACKGROUND

2.1 Air and Water in the Subsurface

Flow in multi-phase systems composed of water and entrapped air beneath the water table differs from that under saturated conditions. The analysis of the volumetric water content (ratio of volume of water and total volume- the sum of soil volume, water volume, and air volume) and porosity (fraction of void space in the material) aids in understanding the degree of saturation within a porous medium. Saturation is defined as the ratio of the volume of water and volume of the void spaces. Moisture is contained within pore spaces through surface tension- a function of the radius of curvature of each meniscus (Freeze and Cheery, 1979). Flow within the unsaturated regions of an aquifer is driven by gravity and capillary potential in which surface tension forces cause negative (compared to atmospheric) pore water pressures (Fetter, 1999). The capillarity of a porous medium is a function of the volumetric water content- the lower the water content the lower (more negative) the capillary pressure (Fetter, 1999).

Considering water drainage, the porous medium will be in a water saturated state at atmospheric pressure; then, as pressure declines, the air entry pressure of the soil will be reached and water will start to drain from pore spaces (largest pores generally drain first) (Fetter, 1999). As pressure head continues to decrease, the soil moisture content will decline as smaller pores drain, until an irreducible minimum water content is reached upon which the moisture content will not drain further regardless of any additional increase in negative pressures (Fetter, 1999). This process gives the main drying curve for a soil (Figure 2.1). For the reverse process of wetting, air present within pore spaces is displaced by water. Soils that did not completely drain and were then re-wetted, or vice versa, follow an intermediate scanning curve that expresses volumetric moisture content and pressure head (Freeze and Cherry, 1979). A multitude of scanning curves dependent upon the conditions at wetting/drainage reversal exist between the main drainage and imbibition curves (Fetter, 1999). The lack of a purely functional relation between the drying and wetting curves classify this physical system as hysteretic, i.e. dependent upon wetting history. The process of hysteresis includes the presence of entrapped air influencing the water retention curves of saturated versus quasi-saturated porous media and consequently the curves possess different shapes during drainage and imbibition (Freeze and Cherry, 1979).

2.2 Basic Characteristics of Entrapped Air

2.2.1 *Entrapped Air Terminology*

The term “entrapped air” describes a discontinuous gaseous phase within otherwise water saturated soils beneath the water table. Areas within an aquifer that possess both air and water do not reflect the conditions described by the commonly used terms “saturated soils” and “unsaturated soils,” the latter being a conventional term that describes continuous connected air within the vadose zone above the capillary fringe (Faybishenko, 1995). Faybishenko (1995) coined the phrase “quasi-saturated soils” to describe multi-phase systems of water and entrapped air beneath the water table. Furthermore, Faybishenko (1995) proposed the term “quasi-saturated hydraulic conductivity” to more accurately express the Darcy coefficient (to be discussed in detail in a later section) of water conductivity in the presence of entrapped air content.

Introduction of this designation distinguishes the parameter from "saturated hydraulic conductivity" (applicable to flow in saturated soils) and "unsaturated hydraulic conductivity" (used to describe fluid flow of unsaturated soils possessing continuous air phase within the vadose zone) (Faybishenko, 1995).

The terminology adopted by Roy and Smith (2007) in describing the different forms of entrapped air is applied within this thesis. Gaseous phase present as small disconnected entrapped air on the scale of the size of pores is described using the general term "bubble" whereas gas occupying several pores in size is a "gas cluster." Disconnected gas phase that possesses branches is referred to as entrapped air "ganglia." Multi-phase system experiments have demonstrated that the non-wetting phase commonly becomes trapped in the form of ganglia (Roy and Smith, 2007; Mumford et al., 2009). The complex shapes formed by disconnected ganglia differ in size due to the grain size and distribution of porous material (Figure 2.2).

Use of the term "bubbles" in association with entrapped air is made in order to better justify simple empirical relationships. For example, the radius of curvature of an air bubble is more easily defined than the geometry of ganglia. Empirically, the concept that entrapped air is analogous to gas bubbles may be a sufficient first order approximation; however, it is necessary to understand that these structures exist and behave as trapped ganglia which possess more complex geometry.

2.2.2 *Types of Entrapped Air*

There are two primary types of entrapped air: (I) mobile air and (II) immobile air that is trapped within pores and can only be removed through dissolution under most natural groundwater conditions (Christiansen, 1944; Faybishenko, 1995). Faybishenko (1995) observed the development of an entrapped air region behind the wetting front upon initial saturation of the porous media. As the unsaturated soils become satiated, free air partitions into either immobile or mobile air (Faybishenko, 1995). Christiansen (1944) and Faybishenko (1995) determined and confirmed that mobile air can be present within soil and discharged in the free state through upward saturation leaving only immobile entrapped air within the quasi-saturated soils. Christiansen (1944) determined that materials of low permeability would require long periods of time to dissolve air entrapped within pore spaces through the process of dissolution.

Residual saturation of the gaseous phase in water-wet systems is controlled by the capillary, buoyancy, and viscous forces (Fry et al., 1997). Capillary forces are a result of adhesion and interfacial tension between fluid phases; cause immobility by trapping air thereby disabling movement through pore throats (Fry et al., 1997). Buoyancy forces are an effect of the differences in fluid densities with viscous forces being proportional to fluid velocities caused by media permeability and pressure gradient (Fry et al., 1997). The rate of gaseous phase mobility is governed by such buoyancy and viscous forces (Fry et al., 1997).

Through experimental investigation, Mumford et al. (2009) produced pore-scale images that captured transient behaviours of gas clusters located near the surface of a dense non-aqueous phase liquid (DNAPL) pool (Figure 2.3). Four gas clusters (A, B, C, and D) were identified and outlined. The images demonstrate expansion and dissolution of gas clusters A and B, respectively. Cluster C initially expands then undergoes fragmentation as cluster D partially dissolves then coalesces with neighbouring clusters (Mumford et al., 2009). A gas cluster must undergo mobilization and fragmentation to demonstrate such behaviours. Critical cluster length is useful in describing the geometry of the discontinuous gas phase based on the pressures acting on the top and bottom of the cluster and the decrease in pressure across the height of the cluster (Glass et al., 2000; Geistlinger et al., 2006),

$$h_{crit} = \frac{P_c^{top} - P_c^{bottom}}{\Delta \rho g} \qquad \text{Eq. [1]}$$

where, h_{crit} is the critical cluster length, P_c^{top} and P_c^{bottom} are the capillary pressures (pressure across any curved surface separating immiscible fluids) at the top and bottom of the cluster, respectively when fragmentation and mobilization occur, $\Delta \rho$ is the density difference between the wetting and non wetting fluid, and g is the acceleration due to gravity.

2.3 Parameters Affecting Entrapped Air Volume

2.3.1 *Temperature*

Christiansen (1944) conducted tests on saturated and unsaturated cores equipped with manometers, under variable temperature conditions, observed a relationship between temperature and head loss across a core during steady state flow. Higher temperatures caused an increase in the observed head loss in systems containing entrapped air unlike the decrease that resulted in saturated soils due to the lower viscosity of warmer water (Christiansen, 1944). Water viscosity decreases at a rate of 2.5% per degree Centigrade rise in temperature (Fireman, 1944). In quasi-saturated cores this change in water viscosity due to temperature effects is more than offset by the temperature effect on the volume of trapped air (Christiansen, 1944; Fireman, 1944). From this, Christiansen (1944) and Fireman (1944) identified an overcorrection error in rectifying permeability to a standard temperature based on the viscosity ratio in systems containing entrapped air.

2.3.2 *Pressure*

As depth below the water table increases, pressure and gas solubility will also increase. There are two hydrostatic pressure mechanisms that control the volume of entrapped air within the upper layer of a phreatic aquifer: (I) compression and (II) dissolution (Figure 2.4). Entrapped air content in wet porous media can be compressed through the application of static gauge pressure (Gupta and Swartzendruber, 1964). An approximation of gas behaviour in response to compression may be determined by the ideal gas law:

$$PV = nRT \qquad \text{Eq. [2]}$$

where, P is the absolute pressure of the gas, V is volume of the gas, n is the number of moles of gas present, R (8.314472 N·m mol^{-1}·K^{-1}) is the universal gas constant, and T is the absolute temperature. As we utilize later, for a given mass of gas at a constant temperature the volume of the gas is inversely proportional to the pressure.

The compression mechanism also affects capillary pressure which is the pressure discontinuity across any curved surface separating two immiscible fluids. Contact between a liquid and another substance (solid, immiscible liquid or gas) generates interfacial energy as a result of the difference of degrees of attraction of molecules in the interior of each phase (Domenico and Schwartz, 1998). Interfacial energy is defined as the work necessary to separate a unit area of one substance from another (Domenico and Schwartz, 1998). Interfacial tension and the ability of certain liquids to wet surfaces upon contact result in capillarity. Contact angles between the liquid and solid differ from 90° due to wetting which causes a curvature of the liquid surface (Domenico and Schwartz, 1998). The relationship between interfacial tension and capillary rise when contact angle between the liquid and wall is small can be written as

$$\Psi = \frac{2\sigma \cos\theta}{\rho g r} \qquad \text{Eq. [3]}$$

where, Ψ is the wetting phase pressure head, σ is the interfacial tension, θ is contact angle, and r is the effective radius of the pore.

Capillary pressure at the interface of the two immiscible liquids is defined by the LaPlace equation,

$$P_c = P_{nw} - P_w = \sigma\left(\frac{1}{r_1} + \frac{1}{r_2}\right) = \frac{2\sigma}{r} \qquad \text{Eq. [4]}$$

where, P_c is capillary pressure, P_{nw} is the pressure of the non wetting fluid which in this thesis is air, P_w is the pressure of the wetting fluid, and r_2 are the principal radii of curvature of the gas-liquid interface and r is the effective radius of curvature of the gas-liquid interface. This effect would be the direct result of forcing the air-water interface into a pore location of significantly differing size.

Dissolution is a response to the compressed internal pressures within the entrapped air; it occurs when the partial pressure of the gas exceeds the equilibrium partial pressure in the surrounding water (Ronen et al., 1989; Fetter, 1999). When groundwater is in equilibrium with the atmosphere, the air phase will continue to dissolve moving towards equilibrium with the aqueous phase thereby decreasing the volumetric water content.

2.4 Impact of Heterogeneity on Air Phase

The magnitude of the impact of entrapped air on hydraulic behaviours is dependant on the volume of the trapped gaseous phase. Although the primary focus of this study is that of air trapped within pores as discrete discontinuous entities occupying pore bodies and throats, air can become trapped on a larger scale as a result of capillary barriers associated with heterogeneity (Silliman et al., 2002; Dunn and Silliman, 2003). Although the impact of heterogeneity on the air phase is beyond the scope of this work, it is necessary to address the presence of the gaseous phase that is connected macroscopically throughout the porous media due to the heterogeneity of natural groundwater systems.

The presence of heterogeneity within the capillary fringe influences the flow path of recharge water (Silliman et al., 2002). Both horizontal and non-horizontal heterogeneity has been shown to act as a transport mechanism for the fluid movement between water below the capillary fringe and water table (Silliman et al., 2002). This behaviour is due to the presence of an "air entry barrier" (AEB), a phenomenon in which a coarse sand layer will remain at high saturation despite low (negative) water pressures (Silliman et al., 2002). This is caused by the overlying fine sands that possess high air entry values to air thereby preventing air from entering and desaturating the coarse sand (Silliman et al., 2002). The results presented in Dunn and Silliman (2003) support the observations concluded within Silliman et al. (2002) thereby confirming the existence of high moisture containing coarse sands at elevations high above the water table which would normally be expected to have undergone drainage.

Figure 2.5 shows that time domain reflectometry (TDR) Probes 1 and 3 are embedded within the medium's fine sand matrix whereas Probes 2 and 4 are situated within coarse sand lenses. Under imbibition conditions, Probes 1 and 3 undergo rewetting. Regardless of increased water table height above the coarse sand lenses, Probes 2 and 4 remain close to residual saturation demonstrating the behaviour of the AEB.

Understanding the complexity of the region surrounding the water table is further complicated by the heterogeneity of natural groundwater systems. Nonetheless, the acknowledgement of such a phenomenon aids in further understanding the presence of entrapped air within heterogeneous soils.

2.5 Emplacement Methods and Corresponding Entrapped Air Contents

2.5.1 *Immiscible Displacement*

Immiscible displacement occurs when the non-wetting phase (air) is displaced by the wetting phase (water) and vice versa. In essence, immiscible displacement is the primary process of the flow of water into and through the vadose zone (Wang et al., 1998). Residual saturation of gas is the entrapped air content within pore spaces. The study of immiscible displacement and its effects on hydraulic properties and the residual entrapment of air aids in understanding the movement of water within the vadose zone and the volume of gas trapped through changes in water table position. Reviewing the soil science literature unveils numerous studies showing considerable amounts of entrapped air (both continuous and discontinuous) near the water table (Table 2.1).

Faybishenko (1995) also analyzed the dependence of air entrapment within porous media on the direction of the wetting front during initial saturation. Faybishenko (1995) found that each method of saturation, ponded infiltration and upward saturation yielded different entrapped air contents. Ponded infiltration resulted in 5 to 10% entrapped air some of which was mobile as compared to the <5% of only immobile air trapped by upward saturation (Faybishenko, 1995).

The directional dependence of the non-wetting phase by the wetting phase in a water-wet system was also analyzed by Fry et al. (1997). The results of this comparison were evaluated through the analysis of capillary number (ratio of viscous to capillary forces) versus the normalized volume of trapped gas which determined that similar volumes of gas were emplaced for both directional immiscible displacement methods at the same capillary number (Fry et al., 1997). Fry et al. (1997) explained that such results demonstrate the negligible effects of buoyancy forces relative to capillary forces. That is, a bond number (ratio of buoyancy to capillary forces) which is relatively small compared to the critical bond number of the porous medium indicates that the buoyancy forces are insufficient in overpowering the capillary forces retaining the air phase within pore spaces (Fry et al., 1997).

2.5.2 *Exsolution*

Exsolution or degassing is the process by which bubble nucleation or growth occurs within water that becomes supersaturated by a gas due to a decrease in pressure or increase in temperature (Fry et al., 1997) or by increasing dissolved gas concentrations. Although exsolution can initiate the *in situ* formation of entrapped air (Fry et al., 1997; Jones et al., 1999), this emplacement mechanism is beyond the scope of this work. The process of supersaturation of water by air can be accomplished through the dissolution of the gas into the liquid at higher pressures. However, entrapped air near the water table is a direct result of entrapment due to water table fluctuations. This research focuses on the changes in gas volume as a function of changing water pressure thus the details of the exsolution process are irrelevant within this study but must be acknowledged as a method of air emplacement within the subsurface.

2.6 Effects of Entrapped Air on Hydraulic Conductivity

A fully saturated porous medium possesses pore spaces that are solely filled with and can transport water, with the exception of dead-end pores (Fetter, 1999). In quasi-saturated soils, a proportion of pore spaces are occupied by air. Water flow can only occur through the wetted cross section of pore space thus the presence of entrapped air reduces the flow of fluid within a phreatic aquifer (Fetter, 1999; Christiansen, 1944, Faybishenko, 1995, Fry et al., 1997).

Hydraulic conductivity expresses the ability to conduct water under a hydraulic gradient within a porous medium and can be measured using Darcy's law (Darcy, 1856)

$$Q = -KA\frac{\partial h}{\partial l} \qquad \text{Eq. [5]}$$

where, Q is the volumetric discharge, K is the hydraulic conductivity (also referred to as the Darcy coefficient), A is the cross-sectional area, and $\frac{\partial h}{\partial l}$ is the gradient of the hydraulic head. This equation is more commonly expressed in terms of specific discharge, or Darcy flux (q), which is the volumetric flow rate (Q) divided by the cross-sectional area (A). Hydraulic conductivity can be expressed as a function of volumetric water content (θ) within the Darcy-Buckingham Flux Law (Buckingham, 1907), i.e.

$$q = -K(\theta)\frac{\partial h}{\partial l} \qquad \text{Eq. [6]}$$

A number of studies that have investigated the effects of static entrapped air on the hydraulic conductivity are listed in Table 2.1. Christiansen (1944) conducted soil permeability tests that confirmed air trapped within the porous medium upon wetting significantly decreases the soils ability to transmit water. Following the removal of mobile trapped air and dissolution of immobile entrapped air, soil permeability increased and reached its maximum when gas was no longer present (Christiansen, 1944). Christiansen (1944) reported the relative increase from the minimum to maximum permeability (P_{max}/ P_{min}) ranged from 2.0 to 4.5 for Hisperia sandy loam and from 2 to 40 for other soils tested. This translates to a reduced relative hydraulic conductivity (K/ K_{sat}) of 0.04 to 0.5 (Christiansen, 1944).

A similar pattern of results was produced by Faybishenko (1995) where the effects of both mobile and immobile entrapped air on the temporal behaviour of conductivity of a loam were studied. Following the emplacement of 5 to 10% entrapped air, the presence of mobile and immobile trapped gas within pore spaces decreased the quasi-saturated hydraulic conductivity (Faybishenko, 1995). Discharge of mobile air and the dissolution of immobile trapped gas resulted in an increase in conductivity by approximately 1 to 2 orders of magnitude essentially achieving a value equaling the saturated hydraulic conductivity of the system (Faybishenko, 1995).

Fry et al. (1997) also observed a reduction in permeability rate caused by gas entrapment. By implementing three different emplacement methods (direct gas injection, injection of supersaturated water, and injection of hydrogen peroxide solution) Fry et al. (1997) entrapped air within 14 to 55% of pore spaces resulting in a relative hydraulic conductivity range of 0.62 to 0.05. Figure 2.6 compares the laboratory results (symbols) produced by the presence of continuous entrapped air with the van Genuchten- Mualem model (lines) of unsaturated conductivity for three grades of sand (Fry et al., 1997). The agreement between the experimental and simulated results indicates the dependency of hydraulic conductivity on the degree of saturation (% volume of pore space) of the porous medium with the gas phase and independence with regards to the method of emplacement (Fry et al., 1997).

It has been established through experimental analysis on a variety of scales that entrapped air reduces the quasi-saturated hydraulic conductivity of phreatic aquifers. In order to quantify this relationship, studies isolated these variables from the transient conditions present within the natural groundwater systems.

Table 2.1: Literature on continuous and discontinuous static entrapped gas

Type of Trapped Gas	Soil Type	Trapped Gas (% of Pore Space)	Porosity (% of Bulk Volume)	Relative Hydraulic Conductivity (K/ Ksat)	Type of Experiment	Emplacement Method	Reference
A. Air trapped in pore bodies and throats	Sintered glass beads	16.4	...	...	Laboratory	Unsaturated soil wetted from below	Poulovassilis (1970)
	Find sandy loam to loamy sand	4.3-12.6	50	...	Field	Unsaturated soil wetted from above	Fayer and Hillel (1986)
	Los gatos gravelly loam	12	43	0.1	Field	Unsaturated soil wetted from above	Constantz et al. (1988)
	Diablo sandy loam	4	45	0.21	Field	Unsaturated soil wetted from above	Constantz et al. (1988)
	Olympic sand	19	36	0.2	Field	Unsaturated soil wetted from above	Constantz et al. (1988)
	Aiken loam	12	51	0.2	Field	Unsaturated soil wetted from above	Constantz et al. (1988)
	Aiken aggregates	6.9	69	...	Laboratory	Unsaturated soil wetted from below	Stonestrum and Rubin (1989)
	Oakley sand	12.6	37	...	Laboratory	Unsaturated soil wetted from below	Stonestrum and Rubin (1989)
	Loam	~ 8-10	~ 43	0.04-0.06	Laboratory	Unsaturated soil wetted from above	Faybishenko (1995)
B. Lenses of trapped air	Hesperia sandy loam	15-40	...	0.22-0.5	Laboratory	Unsaturated soil wetted from below	Christiansen (1944)
	Silica sand	14-55	35	0.062-0.05	Laboratory	Direct gas injection, water supersaturated with gas and hydrogen peroxide solution	Fry et al. (1997)
	Loamy sand	15.4-30.5	40	...	Laboratory	Unsaturated and saturated soil wetted from above	Wang et al. (1998)
C. Pockets of trapped air	Silica sands	14.8-33.6	34.8	...	Laboratory	Saturated soil wetted from below	Dunn and Silliman (2003)

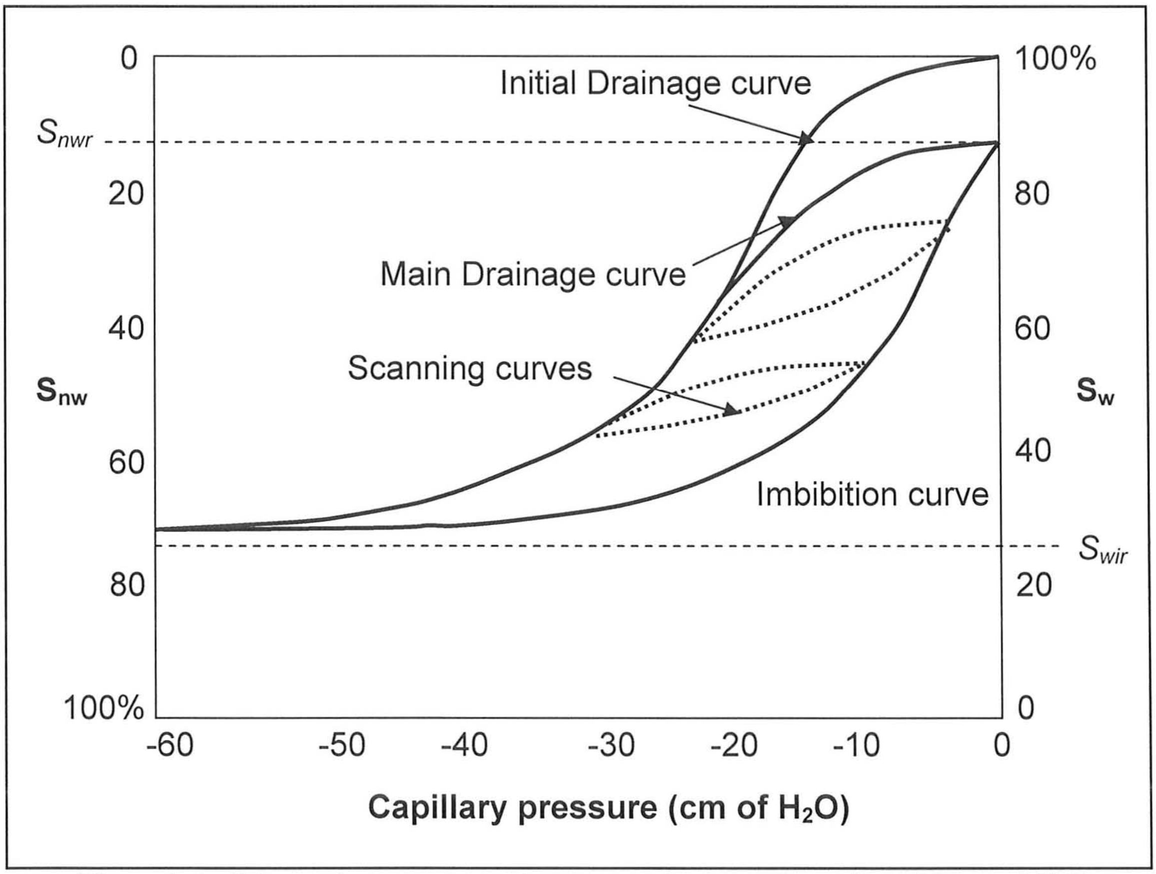

Figure 2.1: Schematic water retention curves for two-phase flow (Fetter, 1999)

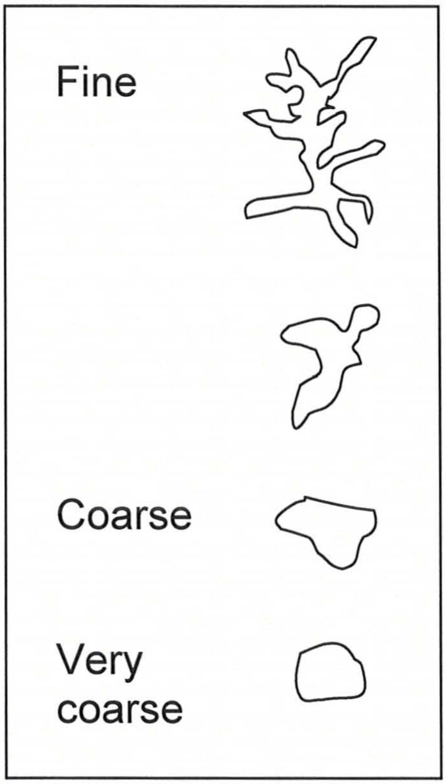

Figure 2.2: Schematic diagram of entrapped air ganglia size and shape which depend on porous material

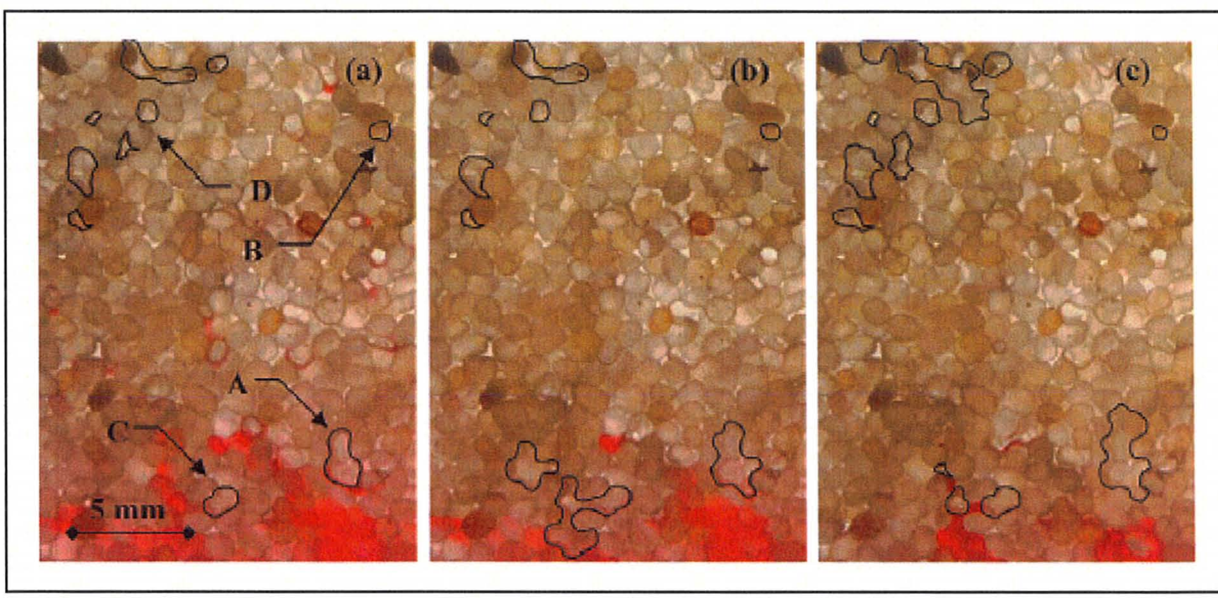

Figure 2.3: Pore-scale images of gas clusters after (a) 0 day (b) 5 days and (c) 10 days near the surface of a DNAPL pool (Mumford et al., 2009)

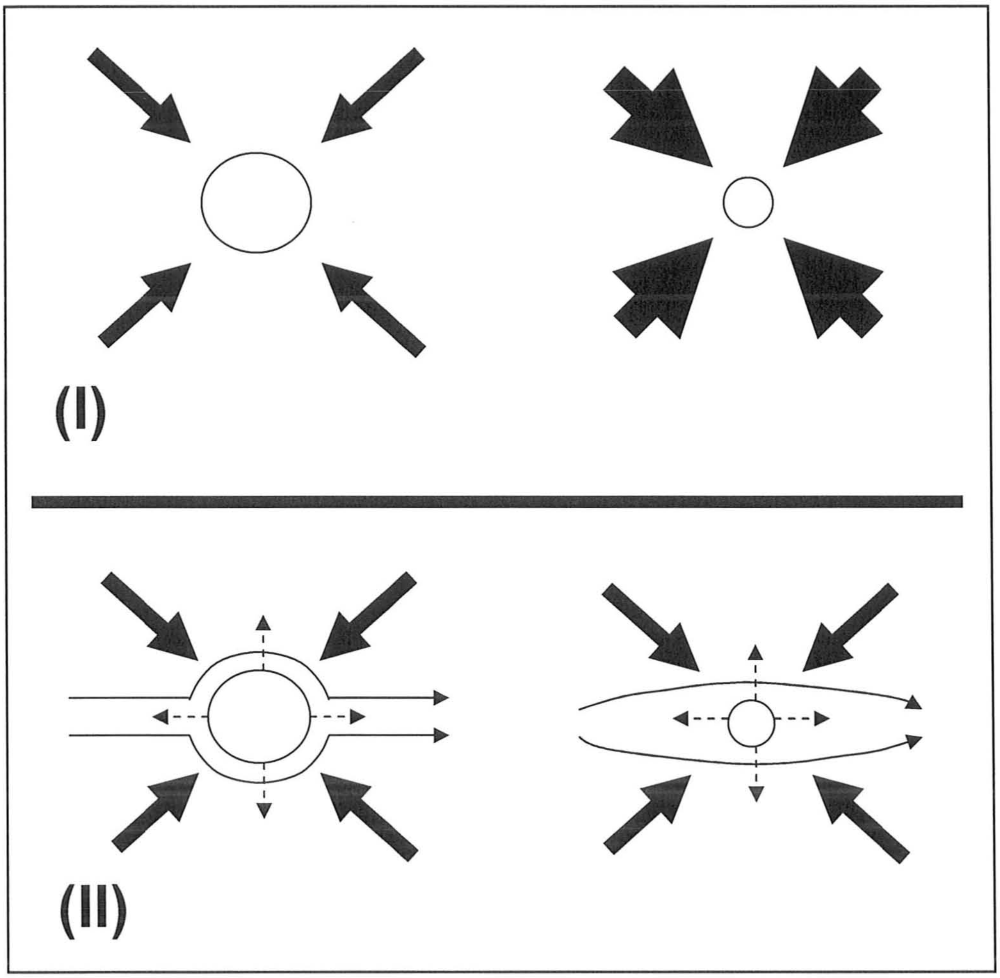

Figure 2.4: Schematic diagrams of squeezing (I) and dissolution (II) mechanisms for a spherical gas bubble (Emmerton, 2001)

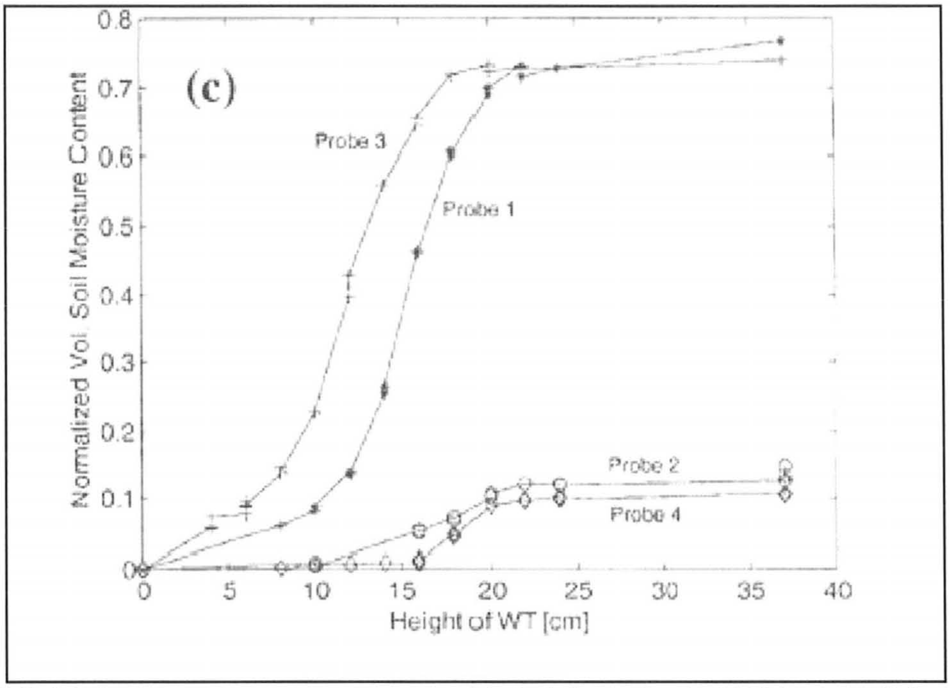

Figure 2.5: Moisture content versus water table height under imbibition conditions. TDR Probes 2 and 4 embedded within coarse sand lenses only partially resaturate (Dunn and Silliman, 2003)

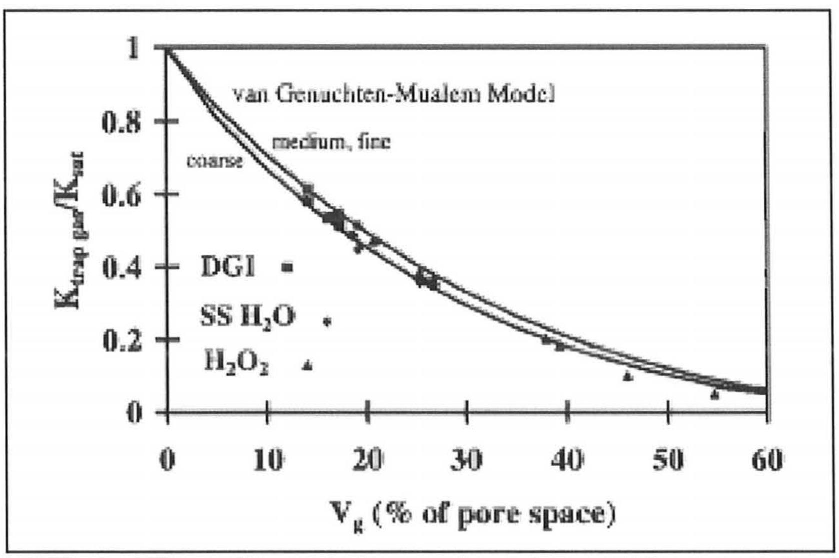

Figure 2.6: Comparison of the relative conductivity and % volume of pore space (continuous air saturation) attained through three emplacement methods and three grades of sand using the van Genuchten- Mualem model (Fry et al., 1997)

3.0 METHODS

3.1 Experimental Set-Up

3.1.1. *Porous Media and Packing of Flow Column*

Table 3.1 identifies the grades of fine to coarse sands used and the corresponding core designation for each of the five sand cores. The grain size distributions for all seven sand types are depicted within Figure 3.1.

A stainless steel splitter was used to divide the sand into practical portions of about 300 to 400 g which were weighed and wetted with water to a 3% (by volume) moisture content. Following a 24-hour equilibrium period, the sand was re-weighed and then used to pack the sand core.

Each sand column was composed of polyvinyl chloride (PVC) with a cross sectional area of 77.0 cm^2, an inner diameter of 9.9 cm, and a wall thickness of 0.4 cm with varying lengths (Table 3.2) and lucite end caps enclosing the sand core. Steel and nylon mesh affixed with glass wool was placed in each end cap to prevent the migration of particles from the sand pack.

Sand was added to the flow column in 1.0-cm layers which were packed manually using two custom instruments and a rubber mallet to attain a maximum bulk density. Each sand layer was subsequently disturbed using a raking instrument prior to the addition of the next layer to attain a homogeneous packing and bulk density throughout the entire core. A straight edged tool was used to ensure a level final layer and allow for even contact between the screens in the end cap and sand core. Silicon sealant was also applied to secure and seal the end caps of the flow columns.

3.1.2 *Installation of the Time Domain Reflectometry Probes and Differential Pressure Transducer*

A time domain reflectometry (TDR) system running TACQ software was used to measure volumetric water content within the sand core (Table 3.3). The stainless steel 3-rod TDR probes, possessing a rod diameter and length of 0.03 cm and 9.9 cm, respectively, were carefully positioned into pre-cut slots along the central axis of the column and installed into the sand core using gentle tapping with a rubber mallet. The probes were secured using silicon sealant between the probe handles and the core wall.

The TDR probes were connected to a metallic TDR cable tester through a shielded cable and a multiplexer which was used to switch to a select individual TDR probe to determine moisture content within the core. TDR measures the change in apparent dialectic constant of the soil which occurs with changes to soil water content (Topp, 1980). This technique is accomplished by measuring the speed of a high frequency electronic pulse that travels in the waveguide formed by rods inserted in the soil (Constantz et al., 1988). An empirical function (Topp et al. 1980) was used to convert the apparent permittivity to volumetric moisture content. The accuracy of the calibration to porosity was assessed and will be discussed in section 4.2.

The pressure gradient across the sand core was measured using a differential pressure transducer (PT) connected to the tubing system. The differential PT was composed of a stainless steel diaphragm clamped between two blocks of stainless steel. Embedded within each of the stainless steel blocks is an inductance coil that is sensitive to diaphragm deflection which is directly proportional to the pressure difference across the diaphragm (Validyne Engineering general operating instructions). The PT selected for the performed experiments can be calibrated for a range of pressures up the full scale pressure of 88.0 cm of H_2O while maintaining design specification precision of 0.25% of full-scale. This range met the design criteria for the experiments for the pressure gradients measured across the sand cores.

The PT was flushed and recalibrated between experiments. The calibration offset was determined by removing the tubing from the core for both sides of the PT and establishing a static positive water head of 0, 10, 20, 30, 40, and 50 cm across the transducer. The calibration slope was determined through comparison of the pressure deviation between the measured pressure head and transducer readings. A linear least squares best fit was used to determine the slope.

The tubing, with an inner diameter of 0.635 cm, was approximately 300 cm in length on each side of the sand core to allow for the application of up to 250 cm of additional water pressure above atmospheric.

3.2 Experimental Procedures

3.2.1 *Air Emplacement Methods: Upward Water Flow and Ponded Infiltration*

Two emplacement methods, upward water flow and ponded infiltration were implemented to attain entrapped air within the sand core. Each utilized a 1% bleach solution (included as a biocide) to saturate a vertically oriented column at a specific flow rate. It is the direction of displacement that distinguishes upward water flow from ponded infiltration- the former saturates the porous medium from below whereas the latter uses downward infiltration to saturate from above.

For the upward water flow method water was pumped into a vertically oriented core from the bottom at a rate of 20 cm^3 min^{-1} with quasi-saturation of the medium being complete when water emerged from the top of the column.

For the ponded infiltration method a tilted, vertically oriented sand core was saturated by pumping water into the top of the column at a rate of 10 or 20 cm^3 min^{-1}. Two flow rates were required to decrease the probability of continuous air entrapment; generally, the slower flow rate was used for the sand cores of mixed composition. Two air ports, located at the top and bottom of the column, were open during the infiltration process. The appearance of flow of water at the bottom of the column prompted closure of the lower air port allowing for continued filling of the core. When water began flowing from the air port located at the top of the column water flow was stopped and the port was closed.

3.2.2 *Removal of Entrapped Air at End Cap Ports*

During saturation, air could become lodged in the end cap ports of the flow column. The lodged air was removed using a syringe connected to the tubing. The tubing on the inlet side of the column was clamped off while the open end of the outlet tubing was placed into a water reservoir. The syringe plunger was gently pushed then pulled in order to purge the air lodged within the end cap on the inlet side of the column. This process was repeated for the outlet side of the flow column.

3.2.3 *Experimental Method: Quasi-Saturated Hydraulic Conductivity*

The hydraulic conductivity at water table positions ranging from 0 to 250 cm was determined using the constant flux method across a fixed horizontal sand core. An experimental trial begins at a water table height of 0 cm; a peristaltic pump was used to apply a constant flux of water to the core. The flux rate varied between sand cores and was dependant on the porous material as determined by establishing an acceptable pressure difference (5 to 50 cm) across the core well within the operational range of the PT. The PT was used to monitor the pressure head to determine when steady state conditions were established. After steady state was achieved, timed outflow was captured at this specific water table height multiple times to ensure a constant rate of flow. Simultaneously, pressure gradient and water content were measured using the PT and TDR systems, respectively.

Following the measurement of discharge rate, pressure gradient, and moisture content in triplicate, the peristaltic pump, inlet reservoir, and drip point were moved to an additional 250 cm simulating an increase in water table elevation by 250 cm. This change in water table elevation resulted in an essentially instantaneous (step) change in the moisture content and pressure gradient measured across the sand core with no measureable change in application rate. Once steady state was confirmed at a 250 cm water table elevation, the measurement procedure was repeated (Figure 3.2). Subsequently, timed outflow, pressure gradient, and moisture content were acquired at 50 cm intervals simulating a decrease (250, 200, 150, 100, 50, and 0 cm; first directional reversal) and increase (0, 50, 100, 150, 200, and 250 cm; second directional reversal) in water table elevation. The experimental trial is concluded with an instantaneous third directional reversal from 250 cm to a water table height of 0 cm.

The number of quasi-saturated experimental trials performed on each sand core is identified within Table 3.3. The following format was used to identify each sand core and experimental investigation within all tables and graph legends:

Core designation (Emplacement method- Trial number)

i.e. Ottawa (I-1)

where, the air emplacement methods of upward water flow and ponded infiltration are represented by I and II, respectively.

3.2.4 *Experimental Method: Saturated Hydraulic Conductivity*

Each sand core was pre-treated with carbon dioxide (CO_2) and de-aired water, a widely used effective and accepted practice, in order to attain a state of complete water saturation (Faybishenko, 1995; Zlotnik et al., 2007). A total of 50 pore volumes (50L) of CO_2 were passed through the sand core followed by a minimum of 25 pore volumes (25L) of de-aired 1% bleach solution.

The saturated flow column experiments were achieved using a similar procedure performed for the quasi-saturated sand core experiments; however, de-aired 1% bleach solution was used and timed outflow, pressure gradient, and moisture content measurements were taken at water table elevations of 0, 150, 200, and 250 cm only. Measurements at multiple heights were taken to ensure there was no entrapped gas and thus changes in hydraulic conductivity with confining pressure. Two experimental trials were completed under saturated conditions for each sand core.

3.3 Model Details

A number of numerical models use either the saturated hydraulic conductivity parameter or relative hydraulic conductivity as a function of pressure head, volumetric water content or saturation to determine unsaturated hydraulic conductivity (van Genuchten, 1980; Mualem, 1976). In this section, functions developed by Aver'yanov (1950), Faybishenko (1995), and van Genuchten (1980) are discussed.

Aver'yanov (1950) developed a power law functional relationship to describe water flow within unsaturated systems,

$$K(\omega) = K_s[(\theta - \theta_r)/(\theta_s - \theta_r)]^n \qquad \text{Eq. [7]}$$

where, $K(\omega)$ is the unsaturated hydraulic conductivity, θ is the volumetric water content, θ_s and θ_r are the saturated and residual volumetric water content, respectively, and n is a power factor fitting parameter that reflects the shape of the curvature of the conductivity function.

Faybishenko (1995) modified this function by acknowledging the effect of entrapped air so as to more accurately quasi-saturated hydraulic conductivity by the following line of reason:

(1) θ_{qs}, which is the quasi-saturated volumetric water content that corresponds to the minimum quasi-saturated hydraulic conductivity (K_0) and can replace θ_r

(2) assume relative hydraulic conductivity equates to $(K - K_0)/(K_s - K_0)$

(3) volumetric fraction of entrapped air (ω) is defined as $\omega = \theta - \theta_{qs}$

(4) maximum entrapped air content ($\omega_{\max}$) is defined as $\omega_{\max} = \theta_s - \theta_{qs}$

As a result, Faybishenko (1995) derived an empirical power function for quasi-saturated hydraulic conductivity

$$K(\omega) = K_0 + (K_s - K_0)\left(\frac{\theta - \theta_{qs}}{\theta_s - \theta_{qs}}\right)^n \qquad \text{Eq. [8]}$$

which can be written as

$$K(\omega) = K_0 + (K_s - K_0)\left(1 - \frac{\omega}{\omega_{\max}}\right)^n \qquad \text{Eq. [9]}$$

where, Faybishenko (1995) differentiates $K(\omega)$ to be a function of quasi-saturated systems.

Van Genuchten (1980) developed an empirical equation describing the relationship of soil-water content as a function of pressure head given as

$$\theta = \frac{\theta_s - \theta_r}{(1 + |\alpha\psi|^n)^m} + \theta_r \qquad \text{Eq. (10)}$$

where, Ψ is the pressure head and α, n, and m are soil-specific curve fitting parameters with m is commonly set to $1 - \frac{1}{n}$. The van Genuchten (1980) equation can be further developed to determine unsaturated hydraulic conductivity from water content resulting in

$$K(\Theta) = K_s \Theta^l (1 - (1 - \Theta^{\frac{1}{m}})^m)^2 \qquad \text{Eq. [11]}$$

where, $K(\Theta)$ is the unsaturated hydraulic conductivity, K_s is the saturated hydraulic conductivity and l and m are curve fitting parameters. The Θ, effective saturation, is defined by

$$\Theta = \frac{\theta - \theta_r}{\theta_s - \theta_r} \qquad \text{Eq. [12]}$$

The aforementioned models have been used to determine the behaviour of hydraulic conductivity in the presence of an entrapped gaseous phase. Experimental data measured as part of this thesis research were used to assess the ability of the van Genuchten (1980) and Faybishenko (1995) numerical models in predicting the effects of dynamic entrapped air content on quasi-saturated hydraulic conductivity. The incorporation of water table dynamics and the chosen fitting conditions do not represent rigorous sensitivity analyses but are intended to provide illustrations of the behaviour of quasi-saturated flow to changes in entrapped air content as a function of water table fluctuations.

Table 3.1: Types of sand used within each core

Core designation	Porous material	Supplier
2010	Quartz sand	Unimin Canada Ltd- 2010
Ottawa	Quartz sand	Unimin Corporation-Ottawa, IL. 61350
Opta 56-A	Silica sand	Opta Minerals- 56/3/10
Opta 56-B	Silica sand	(Opta Minerals- 56/3/10)
Mix1	Quartz and silica sands	Unimin Canada Ltd- 2010, Opta Minerals- 71/11/8 and Opta Minerals- 56/3/10
Mix2	Quartz sands	Unimin Corporation-Ottawa, IL. 61350 and Unimin Corporation- Le Sueur, MN. 56058

Table 3.2: Summary of sand core characteristics

	Core designation					
Parameter	***2010***	***Ottawa***	***Opta 56-A***	***Opta 56-B***	***Mix1***	***Mix2***
Length (cm)	38.1	38.1	38.1	38.3	38.1	38.1
Volume (cm^3)	2932.8	2932.8	2932.8	2948.2	2932.8	2932.8
Bulk density ($g\ cm^{-3}$)	1.81	1.84	1.81	1.81	1.83	1.84
Porosity	0.38	0.30	0.32	0.32	0.31	0.31

Table 3.3: Summary of instruments used within experimental set-up

Instrument	Model	Manufacturer
Time domain reflectometry (TDR) system	-	DYNAMAX VADOSE
TDR software	-	TACQ
Cable tester	1502C	Tektronix
Multiplexer	-	Dynamax Inc. Vadose™
Differential pressure transducer	DP 15-30	Validyne Engineering Corporation
Tubing	-	Nalgene®
Peristaltic pump	MINIPULS 3	GILSON®

Table 3.4: Summary of the number of times each air emplacement method was performed on sand cores

	Air emplacement method	
Core designation	***Upward water flow***	***Ponded infiltration***
2010	2	2
Ottawa	2	0
Opta 56-A	2	0
Opta 56-B	1	2
Mix1	1	2
Mix2	2	2

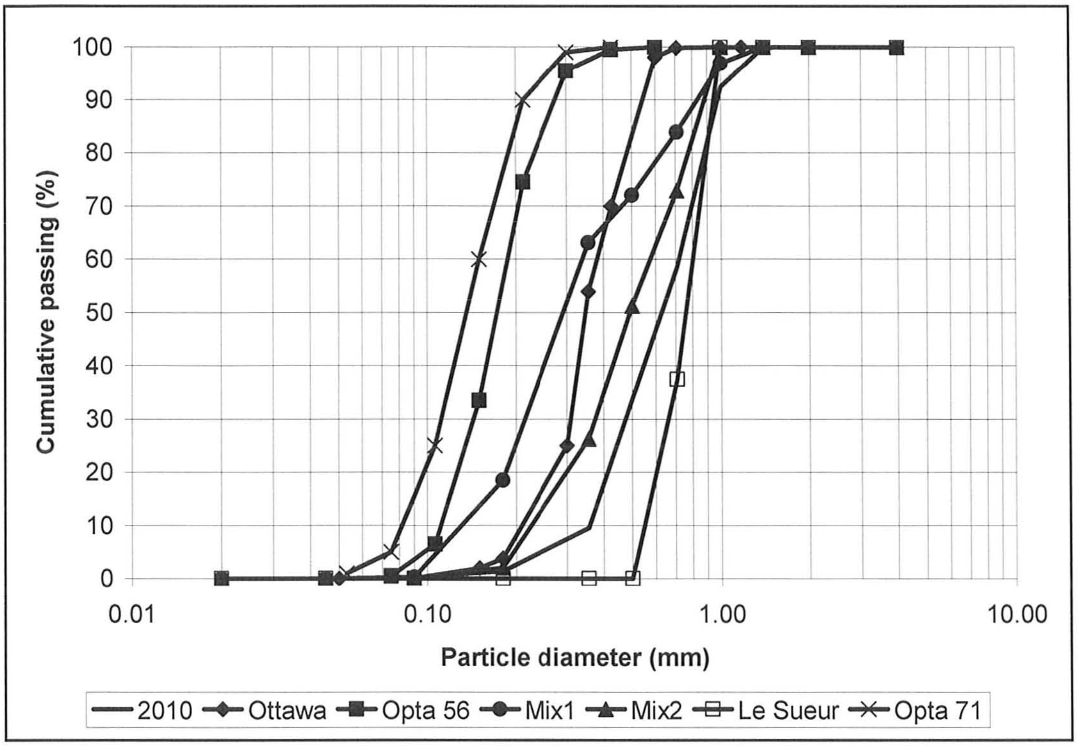

Figure 3.1: Grain size distribution for all sands used

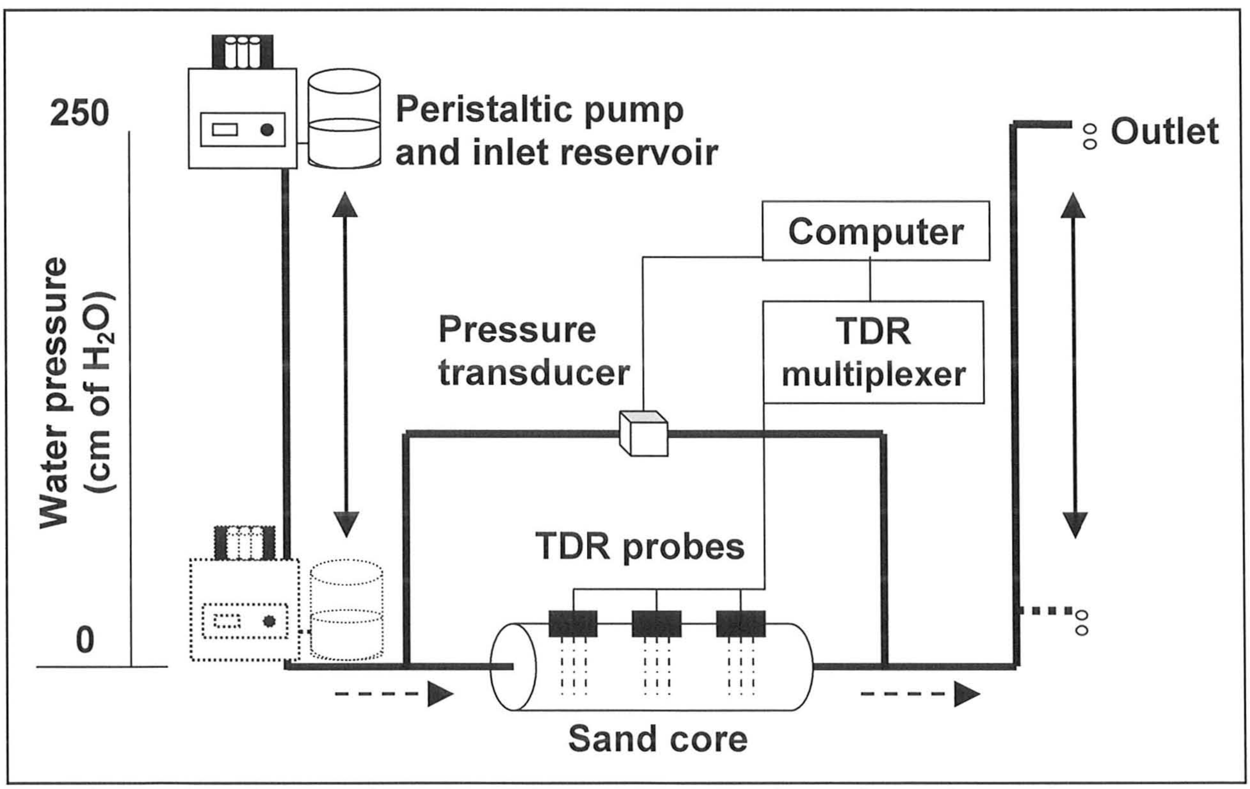

Figure 3.2: Schematic diagram of laboratory set-up and experimental over-view

4.0 EXPERIMENTAL RESULTS AND DISCUSSION

4.1 Pressures Affecting Entrapped Air

The air entrapped in these quasi-saturated systems is affected by water pressures (as a result of changing water table position) in addition to atmospheric and capillary pressures. This relationship can be expressed as

$$P_{ea} = P_{atm} + P_c + P_{wt} \qquad \text{Eq. [13]}$$

where, P_{ea} is the entrapped air pressure, P_{atm} is atmospheric pressure, P_c is capillary pressure , and P_{wt} is the pressure due to water table position.

As atmospheric pressure remains constant through the duration of these short experiments, changes caused by fluctuating water table pressures will affect both capillary and entrapped air phase pressure as both are dependant on the size of the entrapped air structure. As previously discussed, entrapped air is often described as "bubbles" due to the simple empirical relationships that define the structure of a sphere. As a result, the equation of the volume of a sphere can be applied to represent the volume of entrapped air and is defined as

$$V = \frac{4}{3}\pi r^3 \qquad \text{Eq. [14]}$$

where, V is the volume of a sphere and r is the radius of the sphere. The LaPlace equation describes the capillary pressure for a curved interface (Eq. [4]).

Assessing the change in air phase and capillary pressure (assumed using the air entry pressure for each specific sand) as a result of water pressure fluctuations requires analysis of the radius parameter within both equations. For example, for standard atmospheric pressure (1034 cm) and a capillary pressure of an entrapped air bubble of approximately 20 cm (1054 cm total pressure), the spherical bubble would have a radius of 7.34 $\times 10^{-3}$ cm and volume of 1.66 $\times 10^{-3}$ cm^3. An increase of 250 cm of pressure (1304 cm total pressure), decreases the volume to 1.34 $\times 10^{-6}$ cm^3 and the radius of the entrapped air bubble to 6.84 $\times 10^{-3}$ cm. An air bubble of that radius will have a capillary pressure of approximately 21.5 cm. This additional 1.5 cm of capillary pressure represents less than 1% of the 250 cm increase in pressure thus demonstrating that changes in capillary pressure has a quite small relative effect on the entrapped air pressure.

To further illustrate the small role played by capillary pressure changes, analysis of the change in an initial capillary pressure of 150 cm, as would be expected in silt, induced by the presence of an additional 250 cm is considered. At atmospheric pressure, an entrapped air bubble present within silt could possess a capillary pressure of 150 cm (1184 cm total pressure) which corresponds to the spherical entrapped air bubble having a radius of 9.79×10^{-4}cm and a volume of 3.93×10^{-9} cm^3. The application of an additional 250 cm of pressure (1434 cm total pressure) causes a decrease in volume to 3.24×10^{-9} cm^3 with a radius of 9.18×10^{-4} cm. The capillary pressure of the entrapped air bubble thus would increase from 150 cm to 159.9 cm following the addition of 250 cm of pressure. The additional 9.9 cm of pressure is approximately 4% of the 250 cm increase in pressure.

The analysis of the effects of capillary pressure of entrapped gas bubbles within sands and silt demonstrates the minimal changes in pressure as a result of change in capillarity relative to changes in water table elevation. Unlike entrapped spherical air bubbles, empirically quantifying capillarity within entrapped air ganglia is not directly possible due to the complex geometry of the ganglia themselves. However, it is assumed that the effects of changes in capillary pressure as a function of water table position would remain minor in comparison to the changes in air phase pressure.

The fundamental mechanism of focus within these experimental investigations is the compression of entrapped air and its effects on hydraulic conductivity as a result of water table fluctuations. Although changes in water pressure also influence capillary pressure, analysis of the change in capillary pressure induced by the addition of 250 cm of pressure confirms that compression is the primary effect changing the volume of entrapped air within quasi-saturated systems.

4.2 Calibration of TDR System using the Ideal Gas Law

In situ calibration of the TDR system was performed within saturated sand cores using TACQ software, in which match points were set to attain TDR moisture content equal to the calculated porosity of each specific sand core. However, this procedure failed to produce accurate water contents due to the limitations of the software in selecting waveform match points. Thus the difference between measured saturated moisture content and calculated porosity was taken into account by post processing the data utilizing the measure air contents under different water pressures. The ideal gas law was used to calibrate TDR measurements made within quasi-saturated systems. According to the ideal gas law (Eq. [2]), volume is inversely proportional to pressure consequently a plot of pressure versus 1/ air volume yields a straight line with a positive slope equal to $\frac{1}{nRT}$- an assumed constant over the duration of these experiments. Therefore,

$$\frac{1}{V} = \frac{1}{nRT}P + \frac{1}{V_0} \qquad \text{Eq. [15]}$$

where, P is gauge pressure and V_0 is the air volume at barometric pressure, i.e. $P = 0$.

Upon entrapment, the pressure of the gas phase is a combination of barometric and water entry pressure due to capillarity. The water entry pressure value is the pressure at which the porous medium reaches effective saturation upon wetting (Figure 4.1). For 2010 and Ottawa sands, the water entry pressure value was measured to be 2 cm and 11 cm, respectively which is considerably lower than the air entry pressure of the drainage curves of these sands (7cm and 20 cm, respectively) (Smith, 1995; McLeod, personal communication). The water entry pressure of 2010 sand is only approximately 0.2% of barometric pressure (on average 1010 cm in this study) with Ottawa sands being only 1.09% of barometric pressure. That is, the effect of water entry pressure on the entrapped air phase is very small in comparison to barometric pressure. Thus water entry pressure and capillary pressure were excluded when considering the pressure of the entrapped air for the purpose of this air content calibration method.

The accuracy of TDR measurements are increased through the application of an offset to the measured volume of air to attain the air volume determined by the ideal gas law calibration method. This calibration technique was applied to all TDR measurements for each sand core with the calculated corrections listed within Table 4.1. All correction additions of entrapped air content were in the range of 0.2 to 1.9%, averaging 1.32%.

The initial volume of air affects the n parameter and therefore the slope of the ideal gas law line within a pressure versus 1/ air volume plot. Figure 4.2 displays a range of ideal gas law type curves for various air contents within a 3000-cm^3 sand core for pressures ranging from 0 to 250 cm. These type curves demonstrate how an increase in air volume changes (decreases) the steepness of the slope and the intercept.

For example, in Figure 4.3(a) two sets of data and two lines are shown for the 2010 (I-1) experimental investigation. The upper data (triangular data points) are the TDR measured air volumes. Note how this data is not aligned with the calculated ideal gas law calibration line which was calculated using the number of moles (n parameter) in the measured volume of air at barometric pressure. To calibrate the correct air volumes, an offset for air volume was determined using trial and error. Applying an offset to the initial air volume changes the slope of the ideal gas law calibration line. An offset and slope that fit the data points in accordance with the ideal gas law calibration line (linear regression of data points possessed the same slope as the ideal gas law calibration line- circular data points) was deemed correct. This calibrated air content was then applied to all TDR air volumes measured during that specific experimental investigation. The first equation within Figure 4.3(a) identifies the slope of the newly calibrated data points using a linear least squares regression and is promptly followed by the equation for the ideal gas law calibration which possesses a similar slope.

Each 2010 quasi-saturated sand core experiment possessed different initial air volumes and therefore different slopes for each ideal gas law calibration line (Figures 4.3(a-d)). Core 2010 (I-1) and 2010 (II-1) experiments possessed similar initial air contents of approximately 7.9% (236.0 cm^3) and 7.9% (236.8 cm^3), respectively. As a result, the calibrated data linear least squares regression line for both 2010 (I-1) and 2010 (II-1), as identified by the circular and cross data points, possess comparable slopes of 4.17×10^{-6} and 4.13×10^{-6}, respectively with each calibrated slope equating to that of the ideal gas law calibration line (Figures 4.3(a) and (c)). With a higher initial air content of 9.1% (272.4 cm^3), the 2010 (I-2) experiment possessed a relatively lower slope (3.49×10^{-6}) for the calibrated data points and the ideal gas law calibration line as compared to the aforementioned trials (Figure 4.3(b)). However, experiment 2010 (II-2) possessed the highest initial entrapped air content (9.5%, 285.7 cm^3) relative to all other experiments performed on the 2010 sand core thus resulting in a slope of 3.49×10^{-6} (Figure 4.3(d)).

The ideal gas law calibration method was applied to all TDR measured moisture contents to more accurately determine the amount of entrapped air present within each quasi-saturated sand core (Figures 4.3(e) to (r)). All experimental plots yielded linearity within an acceptable range.

4.3 Air Emplacement Methods and Soil Types

The effect of the direction of wetting the sand cores (i.e. upward and downward displacement of air by water) on the volume of entrapped air was determined for the 2010, Opta 56-B, Mix1, and Mix2 sand cores with results presented in Table 4.1. The average entrapped air content for upward water flow and ponded infiltration within the 2010 sand core was 8.5% and 8.7%, respectively, indicating an average 0.2% entrapped air difference between the two air emplacement methods within this sand. The average entrapped air difference between the upward water flow and ponded infiltration ranges between 1.1% and 1.7% for the medium to fine grade uniform and mixed sands. In general, higher entrapped air contents were emplaced via ponded infiltration within the uniform and mixed composition sand cores tested in comparison to the upward water flow method. The effect of the direction of displacement of air by water was observed on loam sands reported by Faybishenko (1995). In this study, upward water flow resulted in less than 5% air entrapment whereas ponded infiltration yielded higher entrapped air contents ranging from 5 to 10%.

The uniform sand cores possessed lower air contents than the mixed sand cores for both air emplacement methods likely due to the variations in pore size and distribution within poorly sorted mixed sands (Fetter, 1999). These poorly sorted sands possess a wider pore size range enabling a higher volume of air to be emplaced in comparison to the uniform well sorted sands. The high entrapped air contents within the Mix1 sand core are possibly present as a continuous air phase i.e. maybe connected from one end of the core to the other, however, air was not observed to exit the core during the experiment.

4.4 Water Table Elevation versus Air Content

Figure 4.4 possesses plots of water table elevation versus entrapped air content which shows water table elevations of up to 250 cm and the induced changes to entrapped air content. Figure 3.4(a) shows the amount of air emplaced within each experimental investigation performed on the 2010 sand core. More specifically, the data for the 2010 (I-1) experimental investigation (circular data points) indicates the quasi-saturated system possessed an initial entrapped air content of 7.9%. The application of

250 cm of additional height to the water table decreased the air content to approximately 6.3% resulting in a 20% decrease from the initial air content. A decrease in water table elevation from a 250 cm height increases the air content by 20% in which the 6.3% entrapped air is no longer compressed thereby returning to the initial air content of 7.9%. The initial air content was reproduced during the 2010 (II-1) experimental investigation which also produced the same response upon the addition then subtraction of 250 cm of water table height.

Analysis of the 2010 (I-2) experimental data within Figure 4.4(a) (square data points) reveals that the initial air content was decreased from 9.1% to 7.2% (20% decrease initial entrapped air content) upon increasing the water table elevation by 250 cm. Following a decrease in water table height by that same interval, the air content returned to its initial volume at which it was entrapped. Comparison of the slopes of the least squares regression line for each experimental data set as identified within Table 4.2 indicate that entrapped air content within the majority of the experimental investigations experienced the same change in air content induced by a 250 cm increase and then return to the initial water table elevation thereby indicating no hysteresis effect.

The relationship between entrapped air content and water table position is a linear function and can be expressed as

$$\theta_a(wt) = m \bullet wt + \theta_{a0} \qquad \text{Eq. [16]}$$

where, wt is water table elevation, $\theta_a(wt)$ is the air content dependent on water table elevation, θ_{a0} is the initial air content, and m is

$$m = \frac{\theta_a - \theta_{a0}}{wt - wt_0} \qquad \text{Eq. [17]}$$

where θ_a is air content, wt_0 is initial water table elevation. The difference in air content as a function of water table elevation ($\Delta\theta_a(wt)$) can be expressed as

$$\Delta\theta(wt) = \theta_a - \theta_{a0}(wt) \qquad \text{Eq. [18]}$$

Defining entrapped air content as a function of water table elevation can be related to volumetric water content which can also be expressed as a function of water table position ($\theta(wt)$),

$$\theta(wt) = \theta_0 + \Delta\theta_a(wt) \qquad \text{Eq. [19]}$$

where, θ is the volumetric water content, θ_0 is the initial volumetric water content which is at a water table elevation of zero.

Within the quasi-saturated systems investigated, increases in water table elevation induced decreases in the volume of entrapped air. Regression output for each sand core demonstrates the highly significant linear relationship (possessing a 95% confidence interval) between water table position and entrapped air content (Table 4.3).

4.5 Water Table Elevation, Air Content, and Quasi-Saturated Hydraulic Conductivity Relationship

The effect of water table elevation and air content on quasi-saturated hydraulic conductivity was quantified through these experimental investigations and can be analyzed through the experimental results plotted within Figure 4.5 (water table elevation versus quasi-saturated hydraulic conductivity) and Figure 4.6 (air content versus quasi-saturated hydraulic conductivity). Figure 3.5(a) displays the measured quasi-saturated hydraulic conductivity data at increasing water table elevations of up to 250 cm for the 2010 (I-1) and 2010 (I-2) experimental investigations. The 2010 (I-1) (circular data points) show that at actual atmospheric pressure (water table possesses no additional height) the satiated system possesses a quasi-saturated hydraulic conductivity of 0.0671 cm s^{-1}. As water table elevation is increased up to 250 cm, the quasi-saturated hydraulic conductivity increased to 0.0890 cm s^{-1} indicating that hydraulic conductivity was 133% larger than at its initial state. Analysis of the 2010 (I-2) (square data points) indicate that the sand core possessed an initial hydraulic conductivity 0.0693 cm s^{-1} at the initial water table elevation; however, as the water table position was increased up to 250 cm hydraulic conductivity increased to approximately 0.0882 cm s^{-1} which is 126% larger than 0.0693 cm s^{-1}. This percentage increase in quasi-saturated hydraulic conductivity with an increase in water table elevation of 250 cm is 127% (0.0698 cm s^{-1} increased to 0.0889 cm s^{-1}) and 131% (0.0640 cm s^{-1} increased to 0.0837 cm s^{-1}) within the 2010 (II-1) and (II-2) experimental trials, respectively (Figure 3.5(b)). The experimental results observed for the 2010 sand core were highly reproducible over four trials was with an average increase in quasi-saturated hydraulic conductivity of 129%.

The quasi-saturated hydraulic conductivity can also be analyzed as a function of entrapped air content. Figure 4.6(a) depicts the behaviour of quasi-saturated hydraulic conductivity in the presence of entrapped air for all experimental trials conducted on the 2010 sand core. Each experimental trial undergoes the same percentage increase in quasi-saturated hydraulic conductivity caused by an increase in water table elevation; however, is expressed as a function of entrapped air content. For example, the increase in water table height of 250 cm decreased the initial entrapped air content from 7.9% to 6.3% (20% decrease in initial air content) resulting in the increase in quasi-saturated hydraulic conductivity of 133%. The same change in water table elevation resulted in a 20% decrease in initial air content for 2010 (I-2) (9.1% to 7.2%), 2010 (II-1) (7.9% to 6.3%), and 2010 (II-2) (9.5% to 7.6%), respectively.

Figure 4.5(c) displays the experimental data measured for the two trials conducted on the Ottawa sand core. The increase in water table elevation of up to 250 cm, causing a decrease in initial air content of 21%, increased the initial quasi-saturated hydraulic conductivity from 0.0205 cm s^{-1} to 0.0261 cm s^{-1} which is a 127% percentage increase in conductivity. A 129% increase in initial quasi-saturated hydraulic conductivity (0.0202 cm s^{-1} to 0.0261 cm s^{-1}) was produced during the Ottawa (I-2) experimental investigation in which the 250 cm increase in water table height decreased the entrapped air content by 21%. The experimental results observed for the two trials conducted using the Ottawa sand core possessed an average increase in initial quasi-saturated hydraulic conductivity of 128%.

Experimental data measured using the Opta 56-A sand core are depicted within Figure 4.5(d). Opta 56-A (I-1) possessed an initial quasi-saturated hydraulic conductivity of 0.0120 cm s^{-1} and upon the application of 250 cm of additional water table height and induced 20% decrease in initial air content conductivity increased to approximately 0.0149 cm s^{-1} (124% increase in initial quasi-saturated conductivity). Opta 56-B (I-2) experienced a 123% increase in initial conductivity (0.0114 cm s^{-1} to 0.0140 cm s^{-1}) as a result of the same change in water table elevation (250 cm) which induced a 21%

decrease in initial air content. The two trials conducted using the Opta 56-A sand core possessed an average increase in initial quasi-saturated hydraulic conductivity of 124%.

The analysis of experimental investigations performed on the duplicate Opta 56 sand core indicates that the results between the same sand types are reproducible. Figure 4.5(e) show that an increase in 250 cm of water table height inducing a 21% decrease in initial air content increased the quasi-saturated hydraulic conductivity from 0.127 cm s^{-1} to 0.0156 cm s^{-1}, a 123% increase in hydraulic conductivity for Opta 56-B (I-1). The Opta 56-B (II-1) experimental investigation experienced percentage increase of 120% in quasi-saturated hydraulic conductivity (0.0130 cm s^{-1} to 0.0156 cm s^{-1}) as a result of the 250 cm change in water table elevation which induced a 20% decrease in initial air content. The Opta 56-B (II-2) experiment possessed an initial quasi-saturated hydraulic conductivity measuring 0.0102 cm s^{-1} that increased to 0.0125 cm s^{-1} (123% increase in conductivity) upon a 21% decrease in air content induced by a change in water table elevation of 250 cm. The experimental results observed for the three trials conducted using the Opta 56-B sand core indicate an average increase in initial quasi-saturated conductivity of 122%.

Experimental trials conducted on the Mix1 sand core produced higher percentage changes in quasi-saturated hydraulic conductivity in comparison to the changes measured on uniform sand cores. Figure 4.5(f) shows that for the Mix1 (I-1) experiment an increase in water table elevation of 250 cm induced a 19% change in initial air content that increased the quasi-saturated hydraulic conductivity from 4.30×10^{-3} cm s^{-1} to 6.20×10^{-3} cm s^{-1} resulting in an increase in initial conductivity of 144%. For Mix1 (II-1) this addition in water table height resulted in a 19% change in initial air content which increased the initial quasi-saturated hydraulic conductivity by 162% ($3.12x10^{-3}$ cm s^{-1} to $5.06x10^{-3}$ cm s^{-1}). Mix 1 (II-2) experienced an increase in initial quasi-saturated hydraulic conductivity of 164% ($2.84x10^{-3}$ cm s^{-1} to $4.67x10^{-3}$ cm s^{-1}) as a result of a 20% decrease in air content. The three trials conducted on the Mix1 sand core possessed an average initial increase in quasi-saturated hydraulic conductivity of 157%.

Figure 4.5(g) displays the experimental investigations conducted on the Mix2 sand core. For the Mix2 (I-2) experiment a 250 cm increase in water table elevation induced a decrease in initial air content of 22% thereby decreasing the initial quasi-saturated hydraulic conductivity by 123% (0.0248 cm s^{-1} to 0.0305 cm s^{-1}). A 128% increase in initial quasi-saturated hydraulic conductivity (0.0225 cm s^{-1} to 0.0286 cm s^{-1}) as the result of a 21% decrease in initial air content. For the Mix2 (II-1) experimental investigation the initial quasi-saturated hydraulic conductivity of 0.0248 cm s^{-1} increased by 126% (0.0313 cm s^{-1}) as a result of a 21% decrease in air content induced by an increase in water table elevation of 250 cm. For the Mix2 (II-2) experiment a 127% increase in quasi-saturated hydraulic conductivity (0.0201 cm s^{-1} to 0.0255 cm s^{-1}) was observed for a 20% decrease in air content due to 250 cm addition in water table height. An average increase in quasi-saturated conductivity of 126% was measured for all four experimental trials conducted using the Mix2 sand core.

The experimental results for all sand cores indicate that the quasi-saturated hydraulic conductivity decreases with increases in water table elevation (Figure 4.5) or decreases in entrapped air content (Figure 4.6). The greater percentage increase in quasi-saturated hydraulic conductivity within the Mix1 sand core can be attributed to the pore size variation within the mixed composition sand core.

The changes in quasi-saturated hydraulic conductivity observed within the experimental results are caused by the compression mechanism of the entrapped air due to fluctuations in water table position. As water table elevation was increased, inducing a decrease in the volume of entrapped air, the quasi-saturated hydraulic conductivity increased. Entrapped air occupies the larger pore spaces within the medium due to weaker capillary forces. The large pores dominate as water transport pathways thus obstruction of these pore bodies and throats by the gaseous phase significantly reduces the quasi-saturated hydraulic conductivity of the system. Increased water table height caused the compression of the entrapped air structures. The resulting decrease in volume of entrapped air increased the flow of water through the previously obstructed conductivity conduits as seen within the experimental data (Table 4.4).

Strong linearity was observed between water table elevation and quasi-saturated K through regression analyzes at a 95% confidence level (Table 4.3). Low F-test and t-test probabilities indicate that there is a statistically significant association between water table elevation and quasi-saturated K. This correlation is reinforced through the fact that error in quasi-saturated K was low as high precision balances were used to measure discharge and error in pressure measurements are less than 0.25% of full scale and less than half of a centimeter. In addition, 1% error in TDR measurements suggests these changes are not a result of systematic error but are statistically significant.

4.6 Saturated Hydraulic Conductivity versus Quasi-Saturated Hydraulic Conductivity

A comparison of the saturated hydraulic conductivity and the quasi-saturated conductivity identifies the change in conductivity as a result of the static presence of air within the system. Figure 4.6(a) displays all of the experimental investigations performed on the 2010 sand core. Under saturated conditions, the 2010 sand core possessed a saturated hydraulic conductivity of 0.116 cm s^{-1}. A comparison of the saturated conductivity and initial quasi-saturated conductivity of 0.061 cm s^{-1} as measured during the 2010 (I-1) experimental investigation indicates a change in conductivity by a factor of 1.73 due to the presence of 7.9% entrapped air. The initial quasi-saturated hydraulic conductivities attained for the 2010 (I-2), 2010 (II-1), and 2010 (II-2) were measured at 0.0693 cm s^{-1}, 0.00698 cm s^{-1}, and 0.0640 cm s^{-1}, respectively for air contents ranging from 7.9 to 9.5%. The average change in conductivity for all four trials within the 2010 sand core equated to a factor of 1.72.

For the Ottawa sand core, a saturated conductivity of a 0.0351 cm s^{-1} was measured and compared to the quasi-saturated conductivities of 0.205 cm s^{-1} and 0.202 cm s^{-1} for Ottawa (I-1) and Ottawa (I-2), respectively. With the presence of approximately 7.4 to 8.9% entrapped air within the Ottawa sand core the hydraulic conductivity was decreased by an average factor of 1.76.

At saturated conditions the Opta 56-A sand core possessed a saturated hydraulic conductivity of 0.0227 cm s^{-1} which decreased by a factor of 1.89 (0.0120 cm s^{-1}) with the presence of 7.9% entrapped air during the Opta 56-A (I-1) experiment. With a higher initial entrapped air content of 8.7%, the Opta 56-A (I-2) satiated system possessed a quasi-saturated hydraulic conductivity of 0.0114 cm s^{-1}, decreased the conductivity by approximately 2.0 times. Thus an average decrease in saturated hydraulic conductivity was 1.94 times for the two trials conducted on the Opta 56-A sand core.

For the Opta 56-B sand core, a saturated conductivity of 0.0252 cm s^{-1} was measured. The initial air emplacement of 8.0% resulted in a change in conductivity by a factor of 1.98 resulting in a quasi-saturated conductivity of 0.0127 cm s^{-1}. Air contents of 8.0% and 10.3% within the experimental investigations of Opta 56-B (II-1) and Opta 56-B (II-2), respectively, decreased the hydraulic conductivity by a factor of 1.94 and 2.10, respectively.

Greater air contents of 8.4 to 11.2% were emplaced within the Mix2 sand as compared to all uniform sand cores. Regardless, the saturated hydraulic conductivity of 0.0527 cm s^{-1} was reduced by an averaged factor of 2.31, consistent with the cores possessing uniform sand composition. Generally, the presence of entrapped air within uniform and mixed sand reduces the quasi-saturated hydraulic conductivity by a factor of 2.0 (Table 4.5).

As previously discussed, air entrapped within the Mix1 sand core was present in the form of continuous connected trapped gas. Possessing a saturated hydraulic conductivity of 0.0211 cm s^{-1}, the presence of air occupying 14.7 to 16.7% of pore space, reduces the saturated hydraulic conductivity by a factor of 6.37. This was the largest change in quasi-saturated hydraulic conductivity and can be attributed to the presence of continuous entrapped air resulting in a larger reduction than that caused by the entrapment of discontinuous air. Faybishenko (1995) observed a reduced quasi-saturated hydraulic conductivity by as much as 5 to 8 times when air was entrapped within the largest pores of a hydraulic system. Fry et al. (1997) observed a decrease in hydraulic conductivity by 5 to 6 times in the presence of a wide entrapped air content range of 14 to 55%. In addition, Sakaguchi et al. (2005) determined that entrapped air contents ranging from 9.0 to 10.5% reduced the quasi-saturated hydraulic conductivity by 6 to 7 times.

Analysis of the saturated hydraulic conductivity and the quasi-saturated hydraulic conductivity as a function of entrapped air demonstrates the influence of pore size distribution and the nature of entrapped air. In Figure 4.6(a) extrapolating the linear trend from the air content quasi-saturated hydraulic conductivity measurements, has an intercept at 0% entrapped air (100% water saturation) which is greater than the measured saturated hydraulic conductivity, i.e., it predicts a saturated hydraulic conductivity greater than that measured. This overshooting in the prediction of the saturated hydraulic conductivity based on the measured hydraulic conductivity as a result of a variable air contents is also demonstrated by the data for the Ottawa sand core. Analysis of both Opta 56-A and Opta 56-B indicate that if linearly extrapolated, the measured quasi-saturated hydraulic conductivities would predict the measured saturated conductivity accurately. Both Mix1 and Mix2 sand cores exhibit data indicating that linear extrapolation of the measured data would predict a saturated hydraulic conductivity less than that of the measured saturated hydraulic conductivity. These differences in behaviour are a function of the pore size distribution and the nature of entrapped air. They are further discussed within section 5.0.

Table 4.1: Summary of saturation, TDR measured initial air contents, calculated ideal gas law offsets, and ideal gas law calibrated air contents for each sand core

Experiment designation	**Saturation rate (cm^3min^{-1})**	**TDR measured air content (%)**	**Air content offset (%)**	**IGL calibrated air content (%)**
2010				
(I-1)	20	6.6	1.3	7.9
(I-2)	20	7.6	1.5	9.1
(II-1)	10	6.5	1.4	7.9
(II-2)	20	8.1	1.4	9.5
Ottawa				
(I-1)	20	7.1	1.8	8.9
(I-2)	20	7.0	1.9	8.9
Opta 56-A				
(I-1)	20	6.4	1.5	7.9
(I-2)	20	7.7	1.0	8.7
Opta 56-B				
(I-1)	20	6.4	1.6	8.0
(II-1)	20	6.3	1.7	8.0
(II-2)	20	9.0	1.3	10.3
Mix1				
(I-1)	20	13.4	1.3	14.7
(II-1)	10	15.2	0.8	16.0
(II-2)	10	16.5	0.2	16.7
Mix2				
(I-1)	20	7.1	1.5	8.6
(I-2)	20	7.7	1.0	8.7
(II-1)	10	7.4	1.0	8.4
(II-2)	10	9.7	1.5	11.2

Table 4.2: Linear least squares regression slope for increase water table elevations up to 250 cm

Experiment designation	Air Emplacement Method	Initial air content (%)	Air content at 250 cm water table elevation (%)	Slope of linear regression of water table elevation versus air content
2010				
(I-1)	Upward water flow	7.9	6.3	-6.16×10^{-3}
(1-2)	Upward water flow	9.1	7.2	-7.35×10^{-3}
(II-1)	Ponded infiltration	7.9	6.3	-6.16×10^{-3}
(II-2)	Ponded infiltration	9.5	7.6	-7.64×10^{-3}
Ottawa				
(I-1)	Upward water flow	8.9	7.0	-4.95×10^{-3}
(I-2)	Upward water flow	8.9	6.1	-5.39×10^{-3}
Opta 56-A				
(I-1)	Upward water flow	7.9	6.3	-5.98×10^{-3}
(I-2)	Upward water flow	8.7	6.9	-6.82×10^{-3}
Opta 56-B				
(I-1)	Upward water flow	8.0	6.3	-6.30×10^{-3}
(II-1)	Ponded infiltration	8.0	6.4	-6.43×10^{-3}
(II-2)	Ponded infiltration	10.3	8.9	-8.35×10^{-3}
Mix1				
(I-1)	Upward water flow	14.7	11.9	-1.19×10^{-2}
(II-1)	Ponded infiltration	16.0	13.0	-1.32×10^{-2}
(II-2)	Ponded infiltration	16.7	13.4	-1.37×10^{-2}
Mix2				
(I-1)	Upward water flow	8.6	6.7	-6.57×10^{-3}
(I-2)	Upward water flow	8.7	6.9	-6.95×10^{-3}
(II-1)	Ponded infiltration	8.4	6.6	-6.57×10^{-3}
(II-2)	Ponded infiltration	11.2	9.0	-9.09×10^{-3}

Table 4.3: Regression output for sand cores

Experiment designation	Regression component	Water table elevation vs air content	Water table elevation vs $K_{quasi\text{-}sat}$	Air content vs $K_{quasi\text{-}sat}$
2010				
(I-1)	Correlation (r^2)	0.989	0.971	0.959
	F-test critical value		3.98	
	F-test value and F-test and T-test Probabilities	3394 5.30×10^{-38}	1222 6.10×10^{-30}	873 2.47×10^{-27}
(1-2)	Correlation (r^2)	0.991	0.969	0.940
	F-test critical value		3.98	
	F-test value and F-test and T-test Probabilities	3647 3.54×10^{-36}	1051 3.71×10^{-27}	530 2.58×10^{-22}
(II-1)	Correlation (r^2)	0.996	0.916	0.923
	F-test critical value		3.97	
	F-test value and F-test and T-test Probabilities	3948 1.25×10^{-42}	198 6.78×10^{-20}	313 1.82×10^{-20}
(II-2)	Correlation (r^2)	0.993	0.969	0.947
	F-test critical value		3.97	
	F-test value and F-test and T-test Probabilities	2432 1.84×10^{-38}	1301 3.21×10^{-27}	907 2.99×10^{-23}
Ottawa				
(I-1)	Correlation (r^2)	0.981	0.995	0.968
	F-test critical value		3.92	
	F-test value and F-test and T-test Probabilities	175 2.42×10^{-19}	265 1.79×10^{-23}	1782 8.75×10^{-46}
(I-2)	Correlation (r^2)	0.945	0.974	0.934
	F-test critical value		3.96	
	F-test value and F-test and T-test Probabilities	305 9.45×10^{-20}	1425 2.23×10^{-31}	540 4.66×10^{-24}
Opta 56-A				
(I-1)	Correlation (r^2)	0.989	0.970	0.990
	F-test critical value		3.98	
	F-test value and F-test and T-test Probabilities	3191 3.36×10^{-35}	1091 2.01×10^{-27}	3210 3.03×10^{-35}
(I-2)	Correlation (r^2)	0.997	0.973	0.966

	F-test critical value	3.98		
	F-test value and F-test and T-test Probabilities	13017 1.60 x10^{-45}	1233 2.67 x10^{-28}	966 1.50 x10^{-26}
Opta 56-B				
(I-1)	Correlation (r^2)	0.990	0.921	0.950
	F-test critical value	3.97		
	F-test value and F-test and T-test Probabilities	3844 5.41 x10^{-39}	429 5.90 x10^{-22}	699 1.27 x10^{-25}
(II-1)	Correlation (r^2)	0.993	0.967	0.954
	F-test critical value	3.97		
	F-test value and F-test and T-test Probabilities	5600.12 5.41 x10^{-42}	1073 6.27 x10^{-29}	765 2.58 x10^{-26}
(II-2)	Correlation (r^2)	0.994	0.969	0.955
	F-test critical value	3.97		
	F-test value and T-test slope (P)	5936 1.85 x10^{-42}	1163 1.47 x10^{-29}	792 1.39 x10^{-26}
Mix1				
(I-1)	Correlation (r^2)	0.996	0.994	0.992
	F-test critical value	3.97		
	F-test value and F-test and T-test Probabilities	8948 9.72 x10^{-46}	6614 2.54 x10^{-43}	4627 1.80 x10^{-40}
(II-1)	Correlation (r^2)	0.992	0.979	0.956
	F-test critical value	3.97		
	F-test value and F-test and T-test Probabilities	4401 4.51 x10^{-40}	1726 1.19 x10^{-32}	799 1.19 x10^{-26}
(II-2)	Correlation (r^2)	0.994	0.996	0.986
	F-test critical value	3.97		
	F-test value and F-test and T-test Probabilities	6103 1.11 x10^{-42}	8477 2.63 x10^{-45}	2653 4.76 x10^{-36}
Mix2				
(I-1)	Correlation (r^2)	0.878	0.848	0.972
	F-test critical value	3.97		
	F-test value and F-test and T-test Probabilities	266 1.75 x10^{-18}	207 1.00 x10^{-16}	1295 2.14 x10^{-30}
(I-2)	Correlation (r^2)	0.991	0.965	0.957
	F-test critical value	3.97		

	F-test value and F-test and T-test Probabilities	3948 3.32×10^{-39}	1015 1.68×10^{-28}	825 6.72×10^{-27}
(II-1)	Correlation (r^2)	0.977	0.842	0.894
	F-test critical value		3.97	
	F-test value and F-test and T-test Probabilities	3948 5.67×10^{-32}	198 2.03×10^{-16}	313 1.21×10^{-19}
(II-2)	Correlation (r^2)	0.985	0.972	0.961
	F-test critical value		3.97	
	F-test value and F-test and T-test Probabilities	2432 2.33×10^{-35}	1301 7.96×10^{-30}	907 1.26×10^{-17}

Table 4.4: Comparison of the effect of entrapped air on quasi-saturated hydraulic conductivity with a 250- cm water pressure above atmospheric

Experiment designation	**$K_{quasi-sat}$ at 0cm (cms^{-1})**	**$K_{quasi-sat}$ at 250cm (cms^{-1})**	**$K_{quasi-sat(250\ cm)}/K_{quasi-sat(0\ cm)}$**	**Average $K_{quasi-sat(250\ cm)}/K_{quasi-sat(0\ cm)}$**
2010				
(I-1)	0.0671	0.0890	1.33	1.29
(I-2)	0.0693	0.0882	1.26	
(II-1)	0.0698	0.0889	1.27	
(II-2)	0.0640	0.0837	1.31	
Ottawa				
(I-1)	0.0205	0.0261	1.27	1.28
(I-2)	0.0202	0.0261	1.29	
Opta 56-A				
(I-1)	0.0120	0.0149	1.24	1.24
(I-2)	0.0114	0.0140	1.23	
Opta 56-B				
(I-1)	0.0127	0.0156	1.23	1.22
(II-1)	0.0130	0.0156	1.20	
(II-2)	0.0120	0.0125	1.23	
Mix1				
(I-1)	0.0043	0.0062	1.44	1.57
(II-1)	0.0031	0.0051	1.62	
(II-2)	0.0028	0.0047	1.64	
Mix2				
(I-1)	0.0248	0.0305	1.23	1.26
(I-2)	0.0225	0.0286	1.27	
(II-1)	0.0248	0.0313	1.26	
(II-2)	0.0201	0.0255	1.27	

Table 4.5: Comparison of quasi-saturated hydraulic conductivity relative to saturated hydraulic conductivity

Experiment designation	K_{sat} (cms^{-1})	$K_{quasi\text{-}sat}$ at 0cm (cms^{-1})	$K_{sat}/K_{quasi\text{-}sat}$	Average $K_{sat}/K_{quasi\text{-}sat}$
2010				
(I-1)	0.116	0.0671	1.73	1.72
(I-2)		0.0693	1.67	
(II-1)		0.0698	1.66	
(II-2)		0.0640	1.81	
Ottawa				
(I-1)	0.0357	0.0205	1.74	1.76
(I-2)		0.0202	1.77	
Opta 56-A				
(I-1)	0.0227	0.0120	1.89	1.94
(I-2)		0.0114	2.00	
Opta 56-B				
(I-1)	0.0252	0.0127	1.98	2.01
(II-1)		0.0130	1.94	
(II-2)		0.0120	2.10	
Mix1				
(I-1)	0.0211	0.0043	4.91	6.37
(II-1)		0.0031	6.76	
(II-2)		0.0028	7.43	
Mix2				
(I-1)	0.0527	0.0248	2.13	2.31
(I-2)		0.0225	2.34	
(II-1)		0.0248	2.13	
(II-2)		0.0201	2.62	

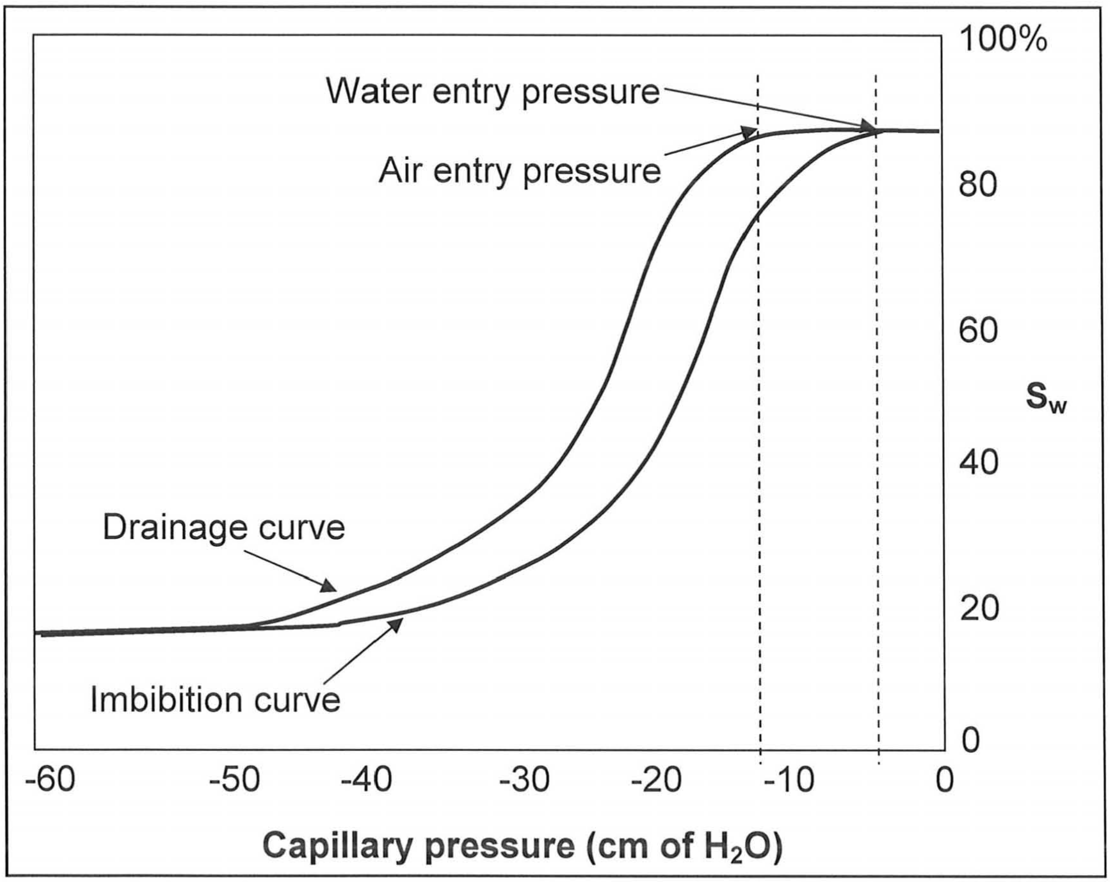

Figure 4.1: Schematic water retention curve for a sand showing the air entry pressure of a drainage curve and the water entry pressure of an imbibition curve

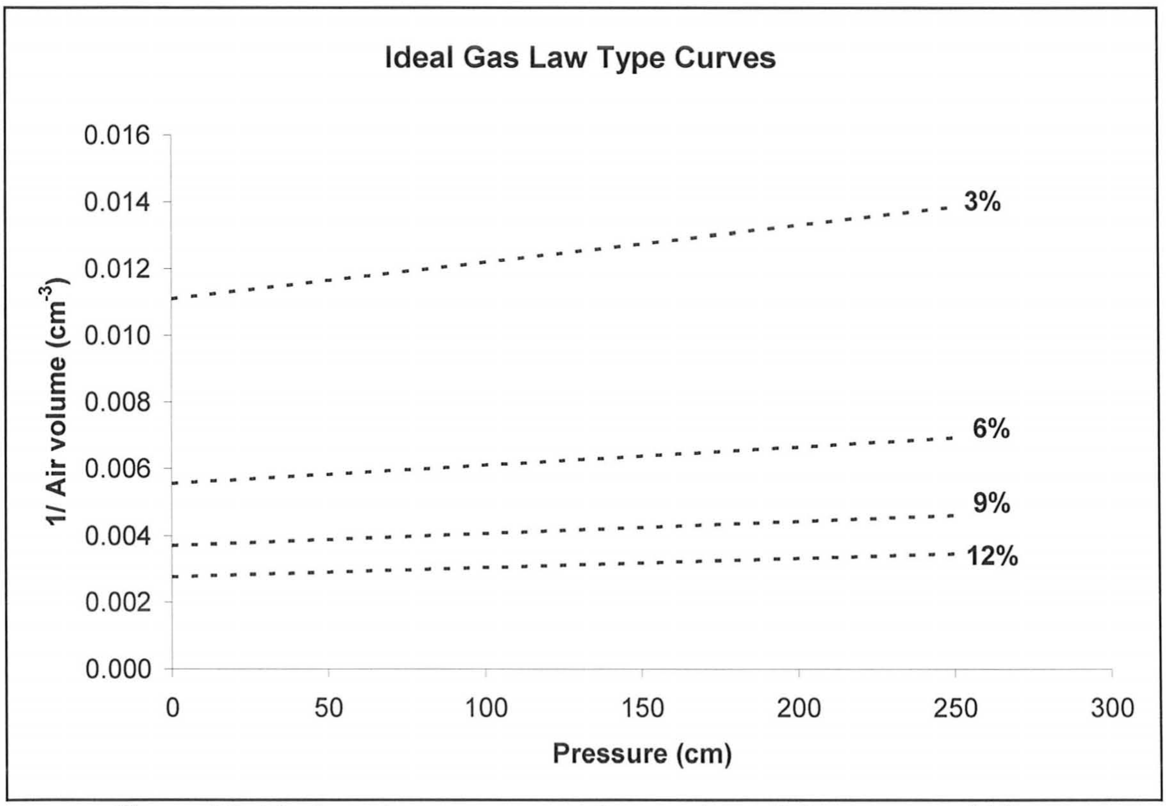

Figure 4.2: Ideal gas law type curves for a variety of air contents within a sand core with a volume of 3000 cm^3

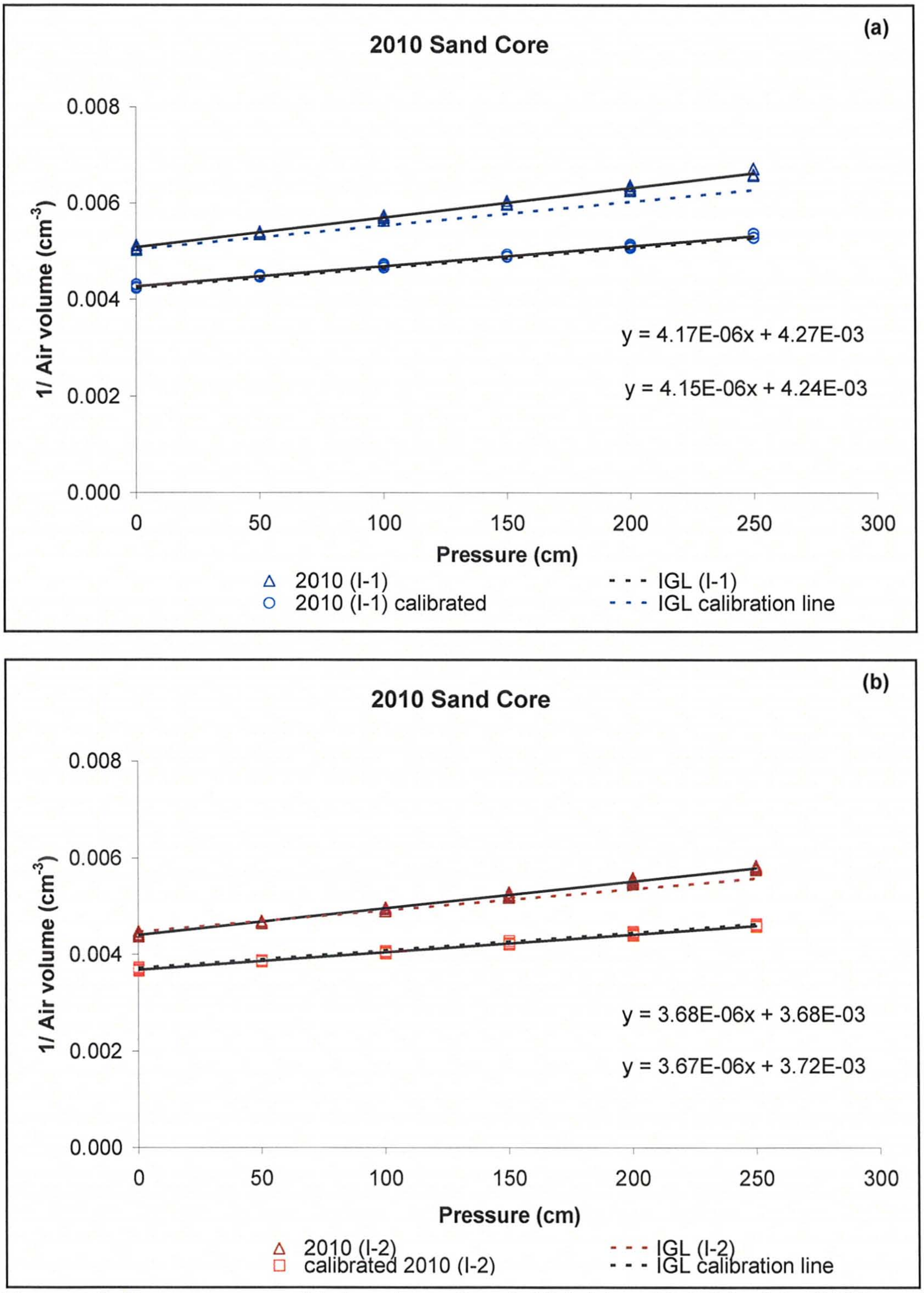

Figure 4.3: Pressure versus 1/ air volume for trial I-1 (a) and I-2 (b) of the 2010 sand core; first equation is the linear least squares regression for the calibrated air contents and the second equation is the corresponding ideal gas law calibration line

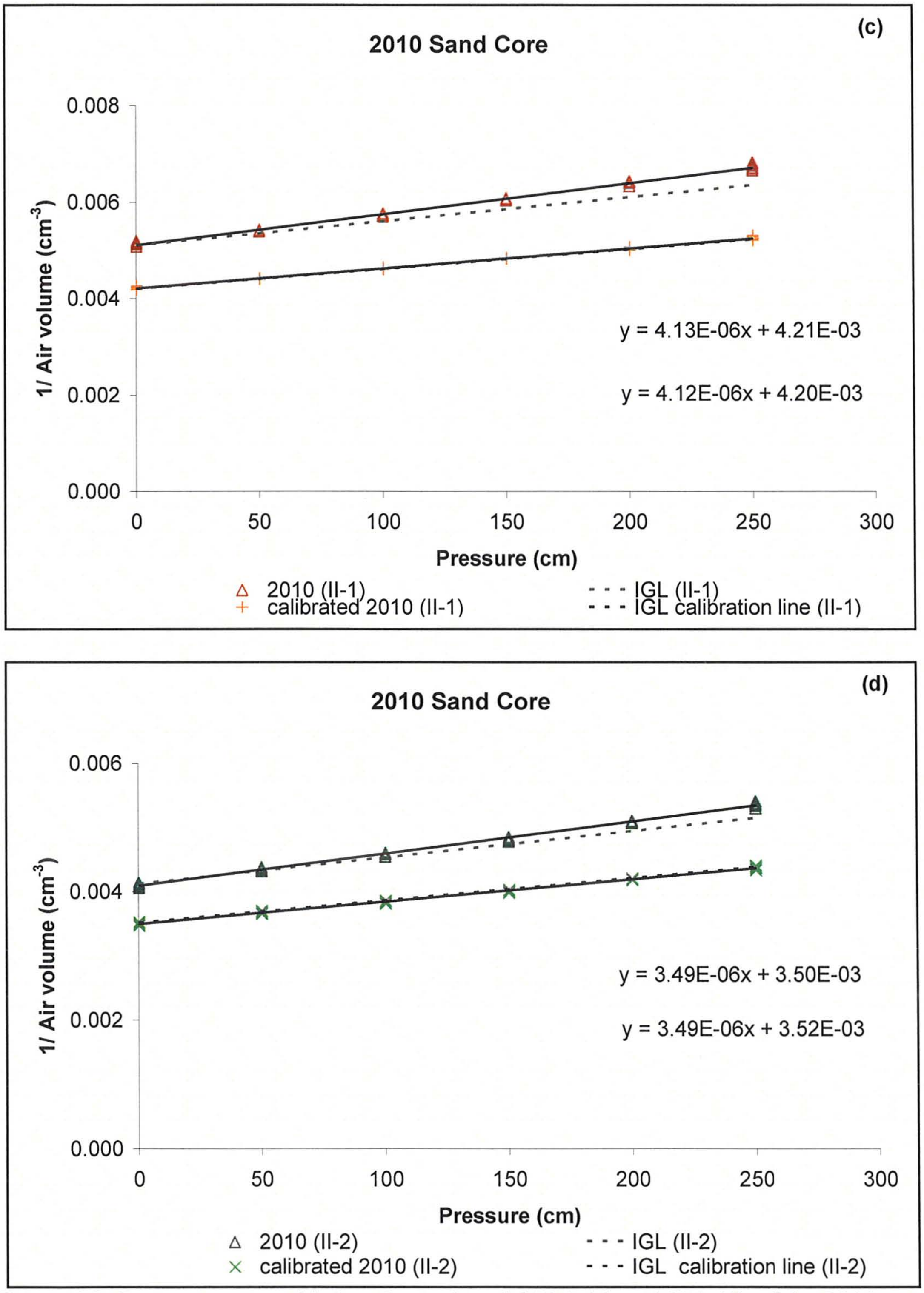

Figure 4.3: Pressure versus 1/ air volume for trial II-1 (c) and II-2 (d) of the 2010 sand core; first equation is the linear least squares regression for the calibrated air contents and the second equation is the corresponding ideal gas law calibration line

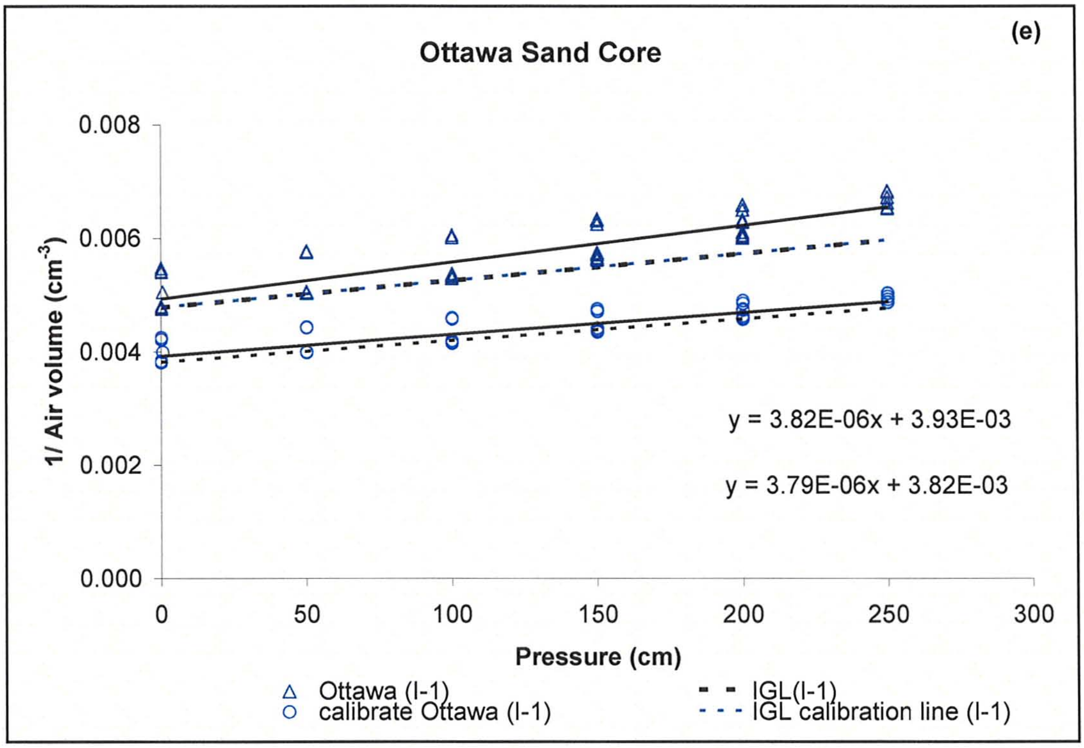

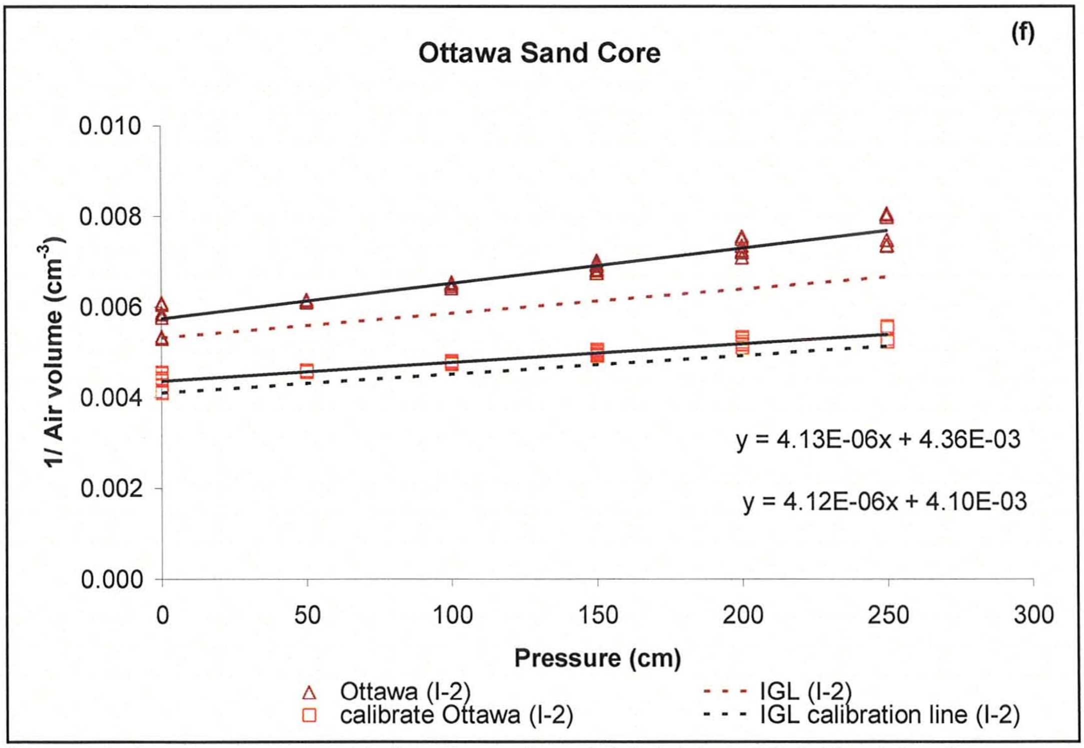

Figure 4.3: Pressure versus 1/ air volume for trial I-1 (e) and I-2 (f) of the Ottawa sand core; first equation is the linear least squares regression for the calibrated air contents and the second equation is the corresponding ideal gas law calibration line

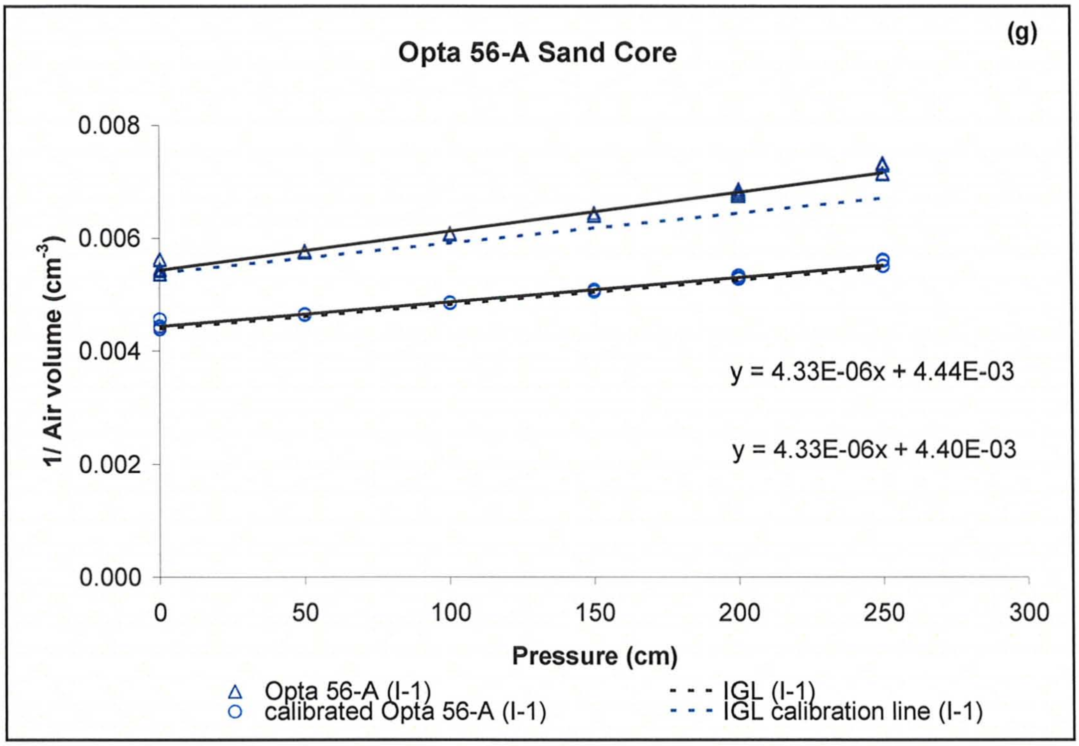

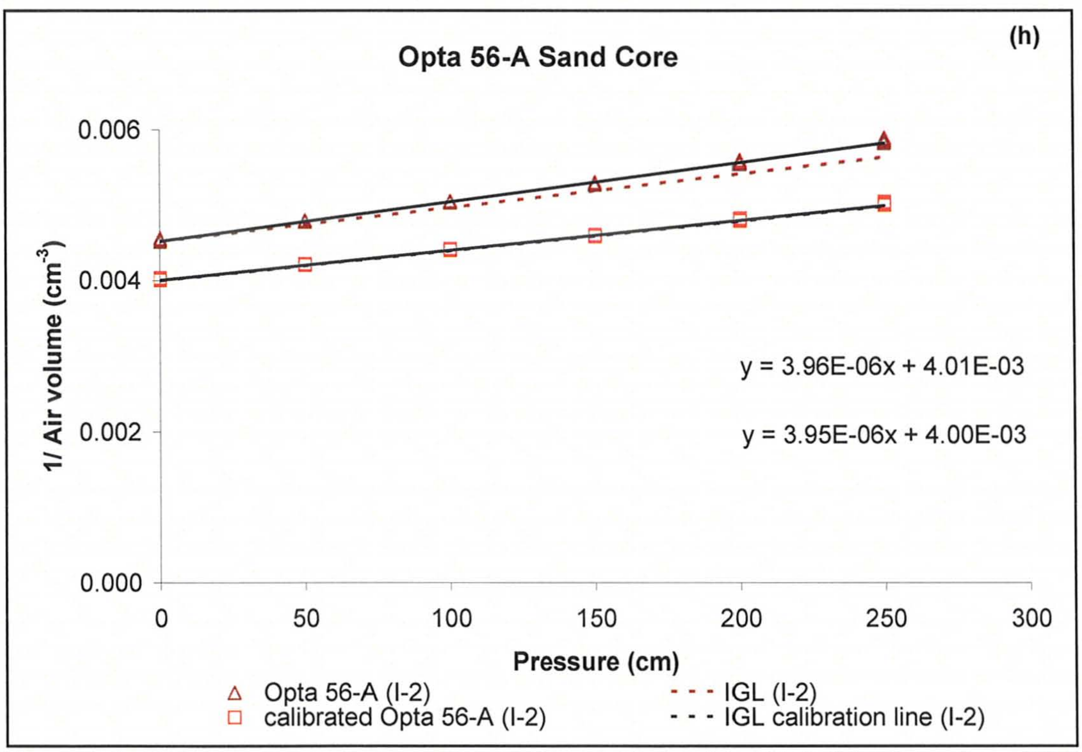

Figure 4.3: Pressure versus 1/ air volume for trial I-1 (g) and I-2 (h) of the Opta 56-A sand core; first equation is the linear least squares regression for the calibrated air contents and the second equation is the corresponding ideal gas law calibration line

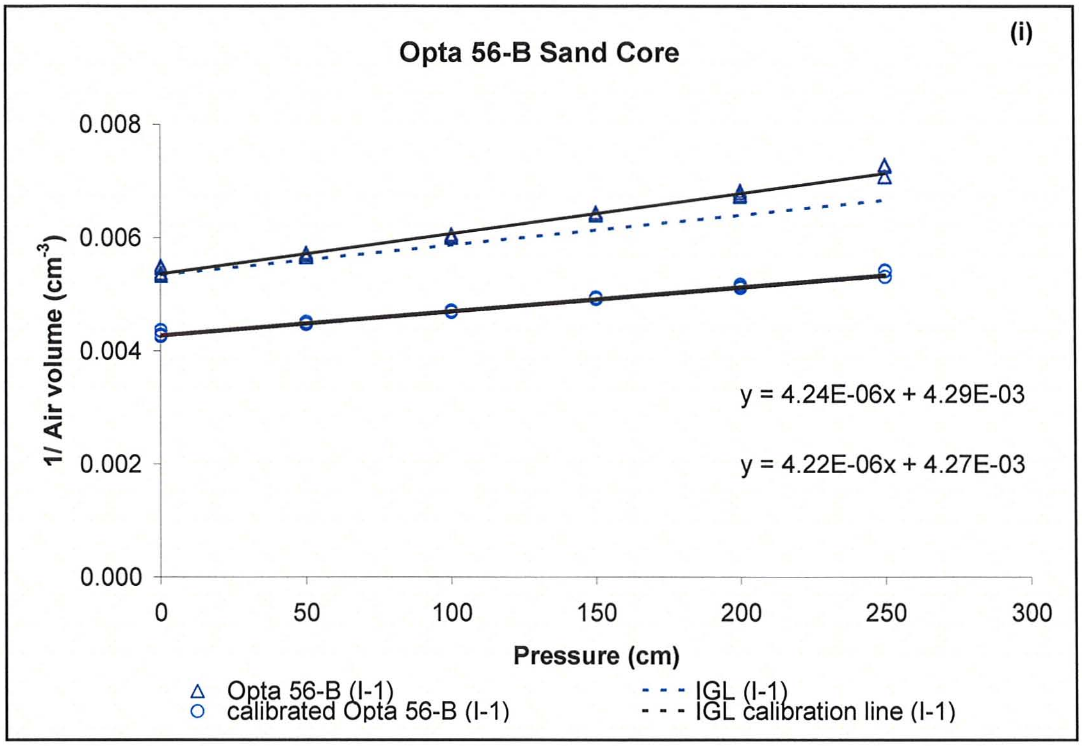

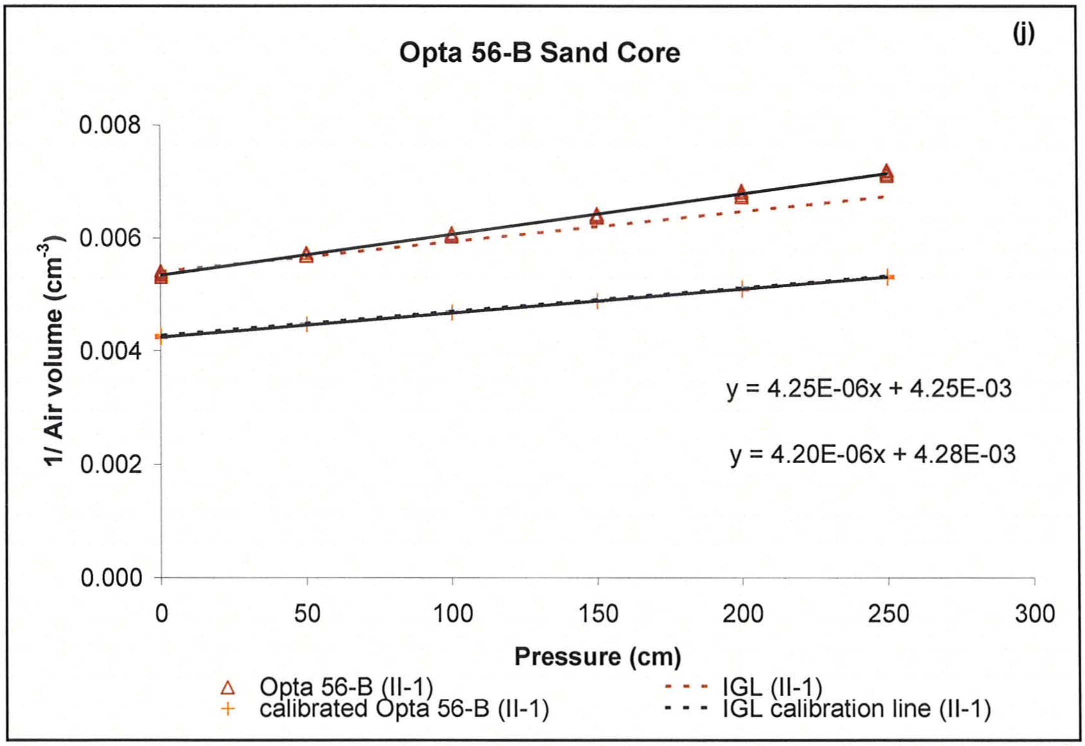

Figure 4.3: Pressure versus 1/ air volume for trial I-1 (i) and II-1 (j) of the Opta 56-B sand core; first equation is the linear least squares regression for the calibrated air contents and the second equation is the corresponding ideal gas law calibration line

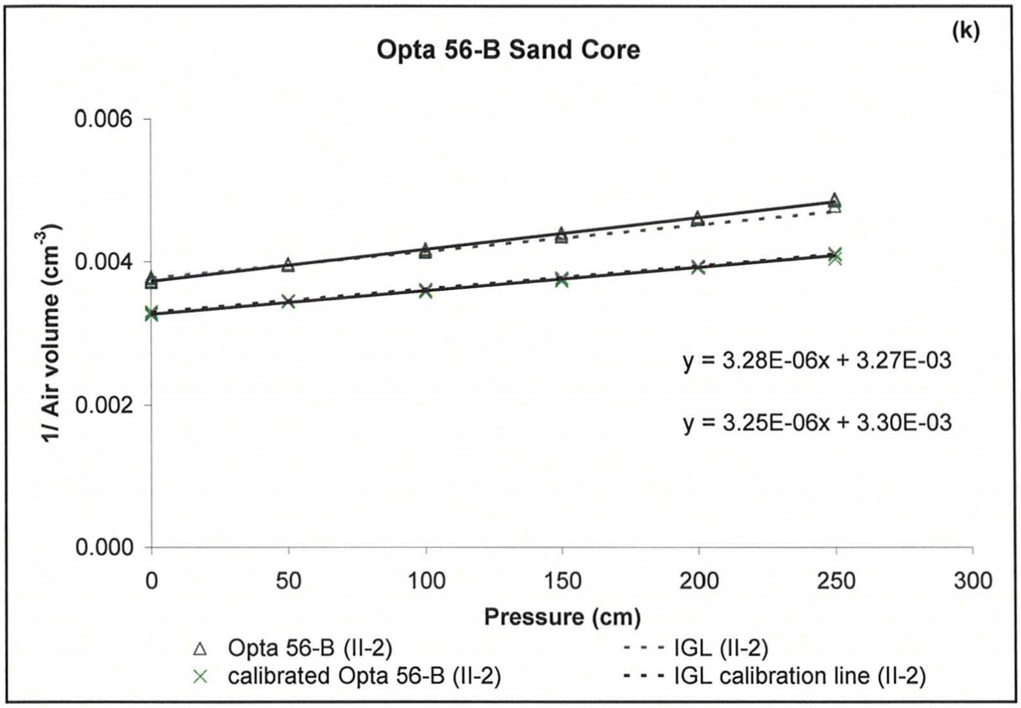

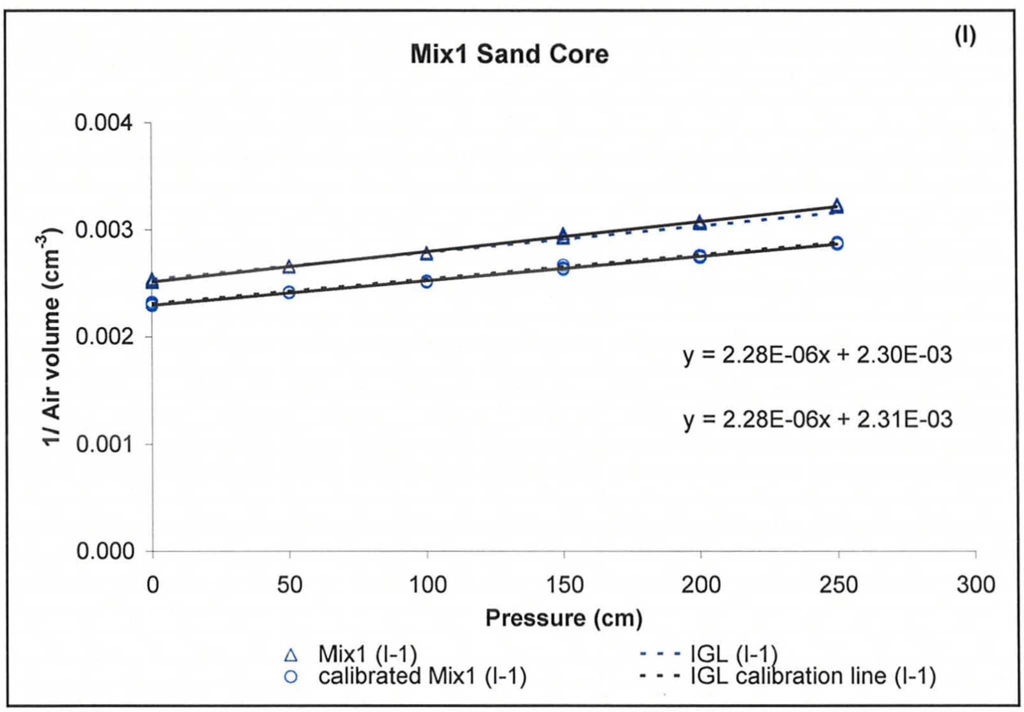

Figure 4.3: Pressure versus 1/ air volume for trial II-2 (k) and trial I-1 (l) of the Opta 56-B and Mix1 sand cores, respectively; first equation is the linear least squares regression for the calibrated air contents and the second equation is the corresponding ideal gas law calibration line

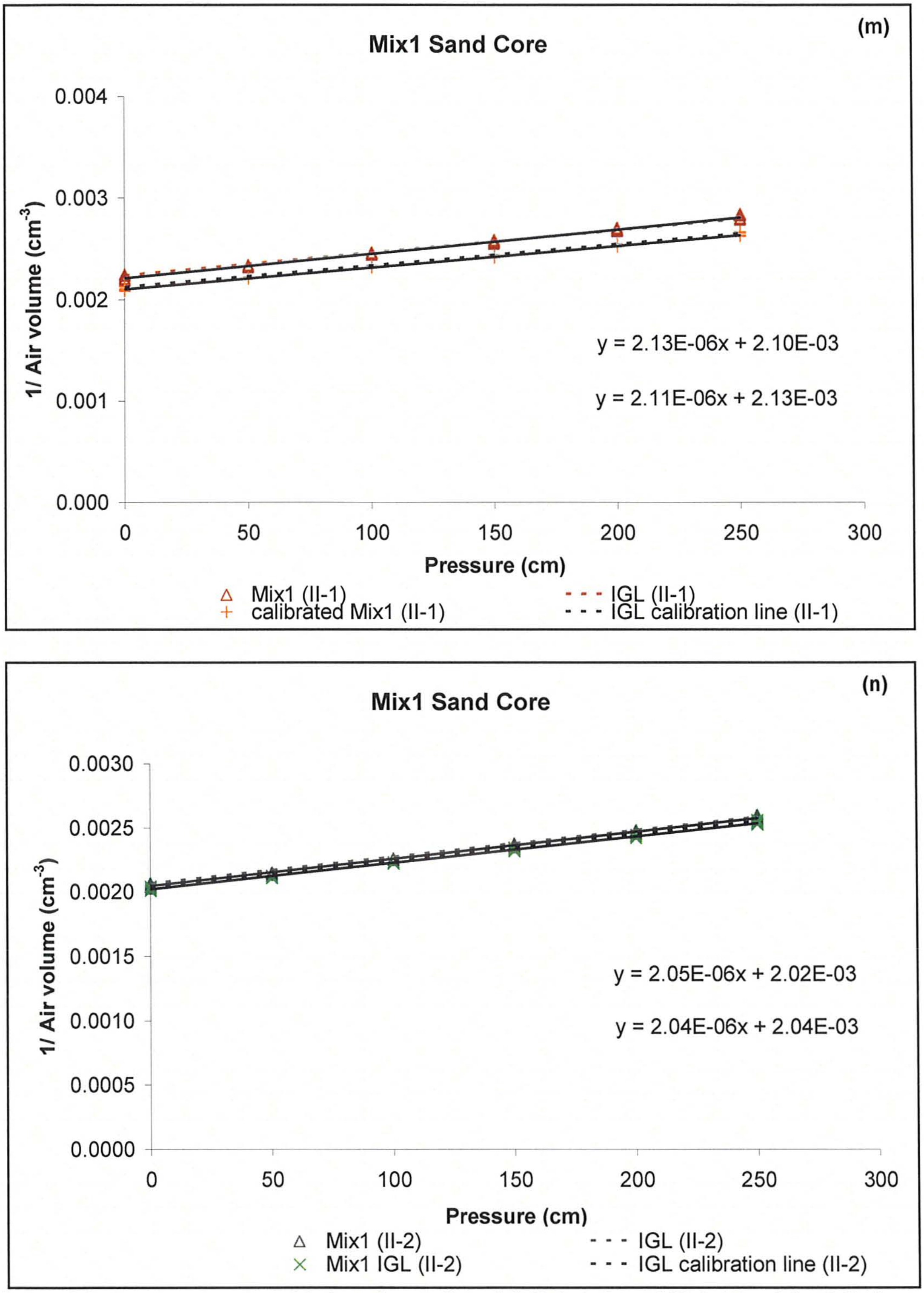

Figure 4.3: Pressure versus 1/ air volume for trial II-1 (m) and II-2 (n) of the Mix1 sand core; first equation is the linear least squares regression for the calibrated air contents and the second is that of the corresponding ideal gas law calibration line

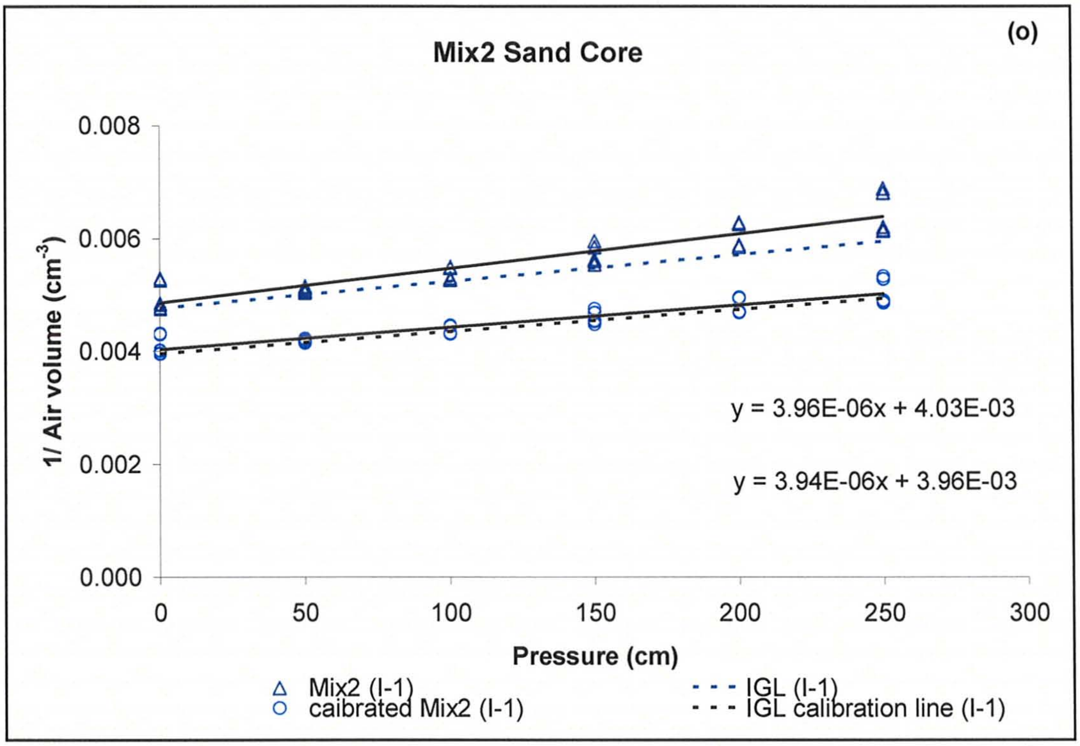

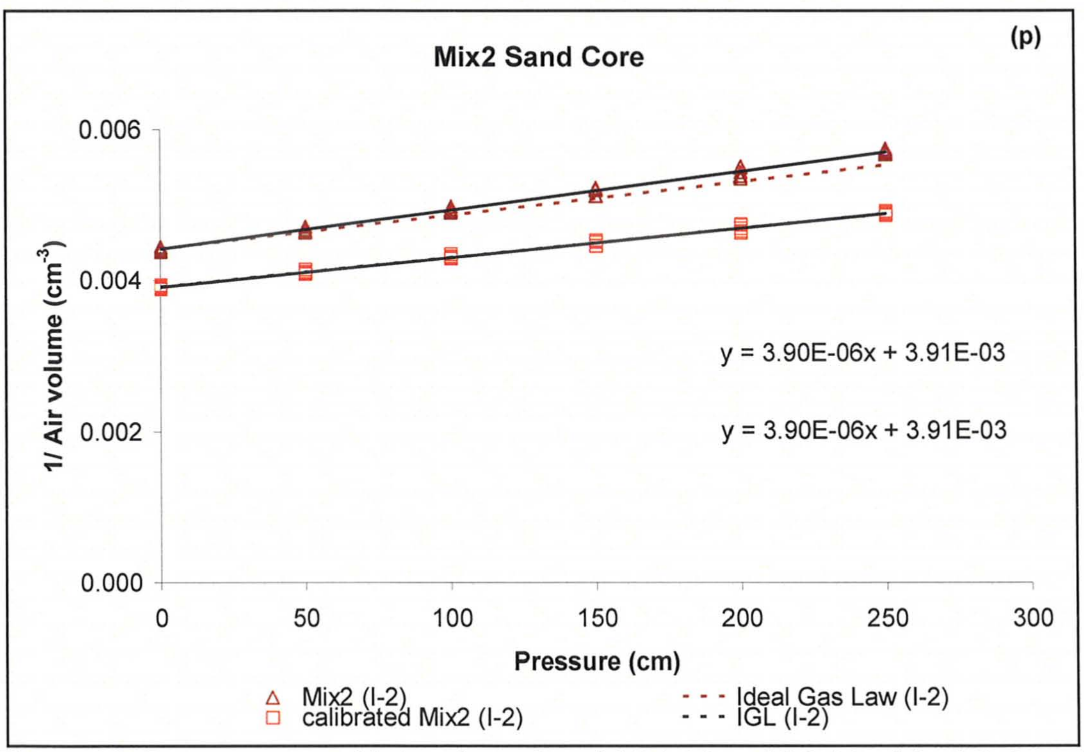

Figure 4.3: Pressure versus 1/ air volume for trial I-1 (o) and I-2 (p) of the Mix2 sand core; first equation is the linear least squares regression for the calibrated air contents and the second equation is the corresponding ideal gas law calibration line

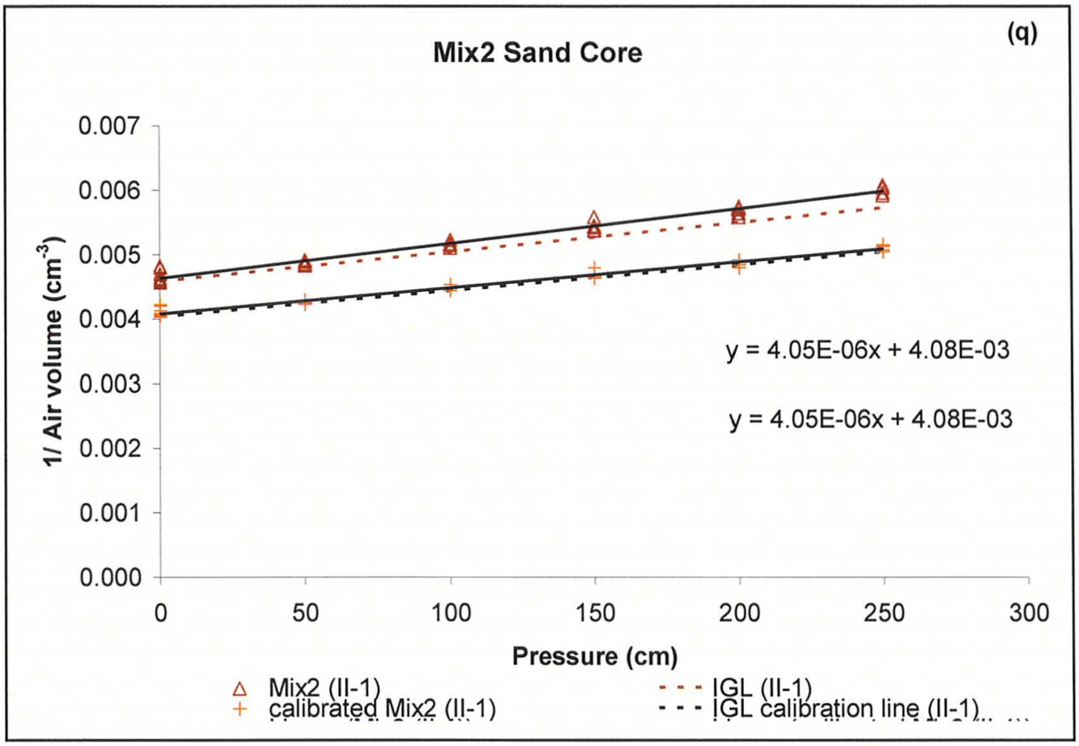

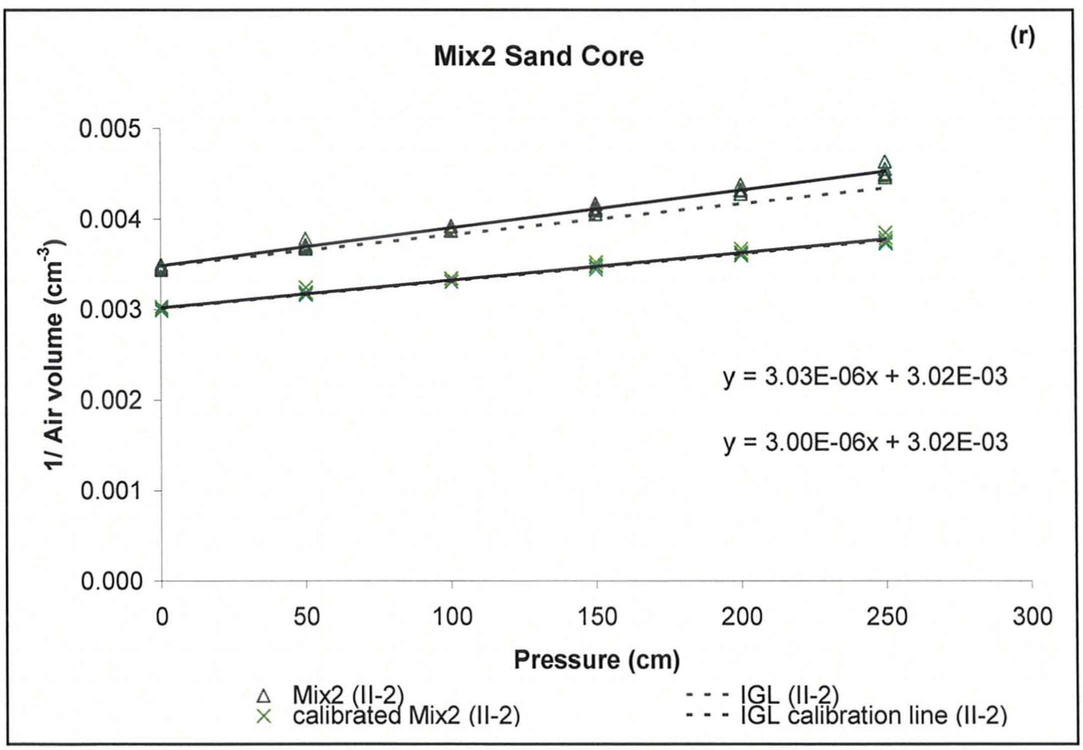

Figure 4.3: Pressure versus 1/ air volume for trial II-1 (q) and II-2 (r) of the Mix2 sand core; first equation is the linear least squares regression for the calibrated air contents and the second equation is the corresponding ideal gas law calibration line

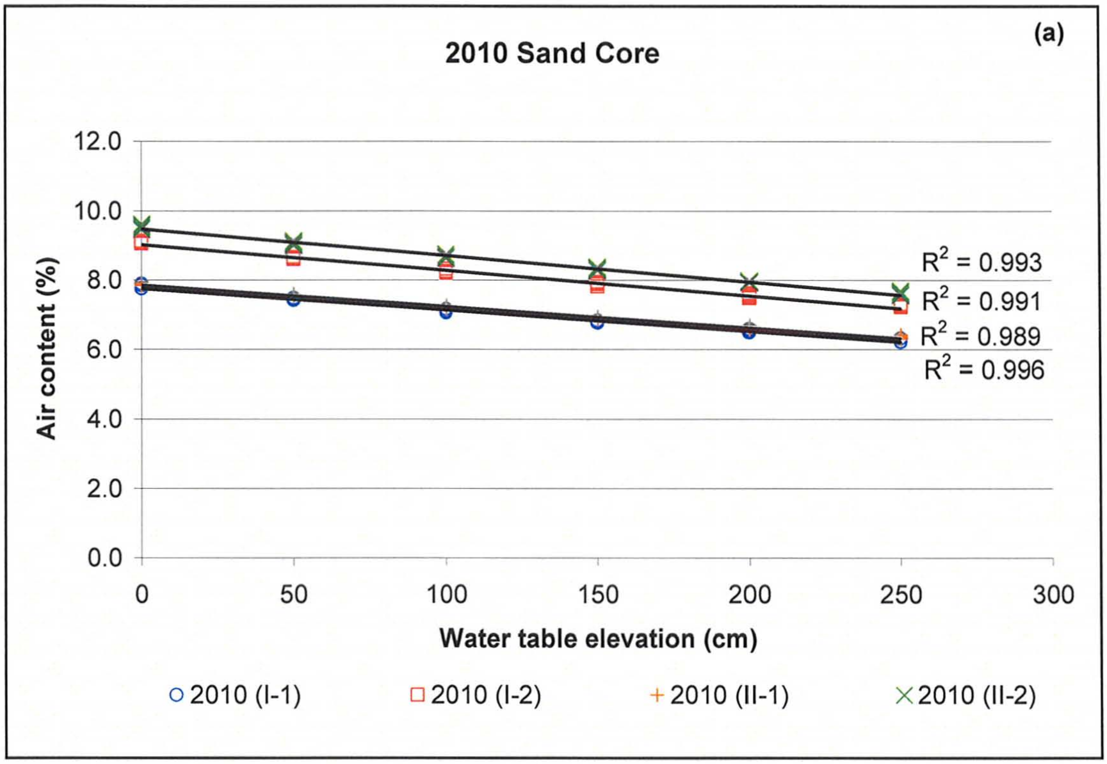

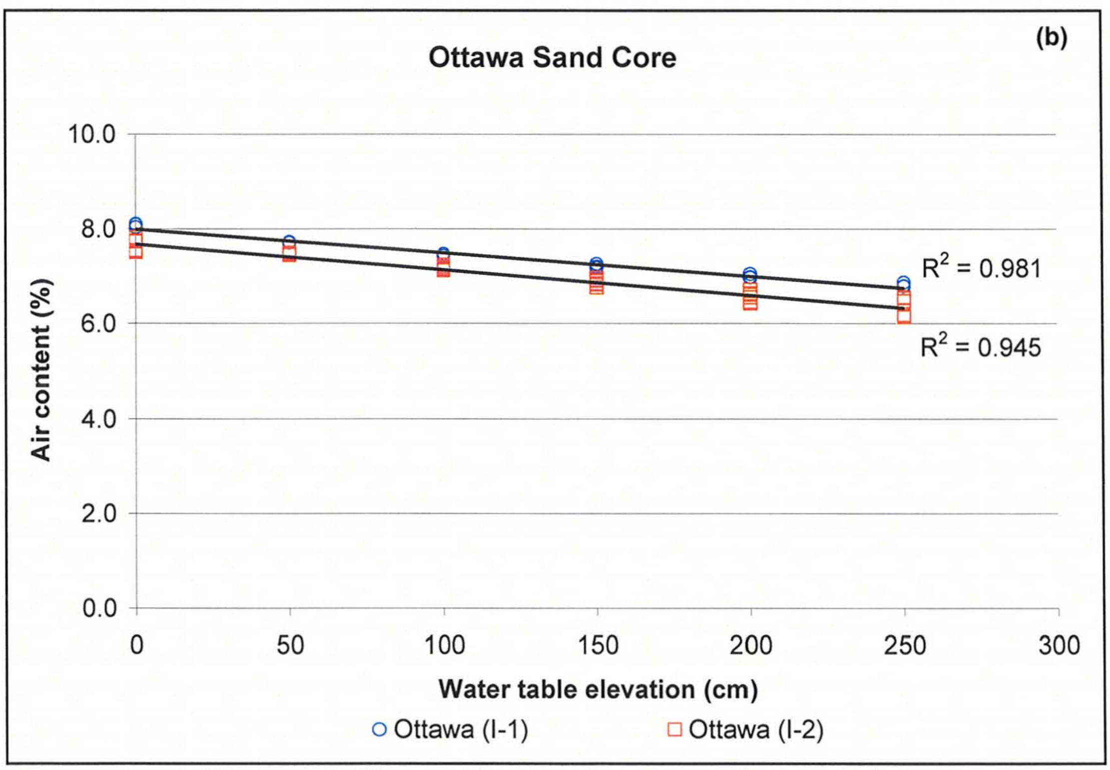

Figure 4.4: Water table elevation versus air content for 2010 (a) and Ottawa (b) sand cores

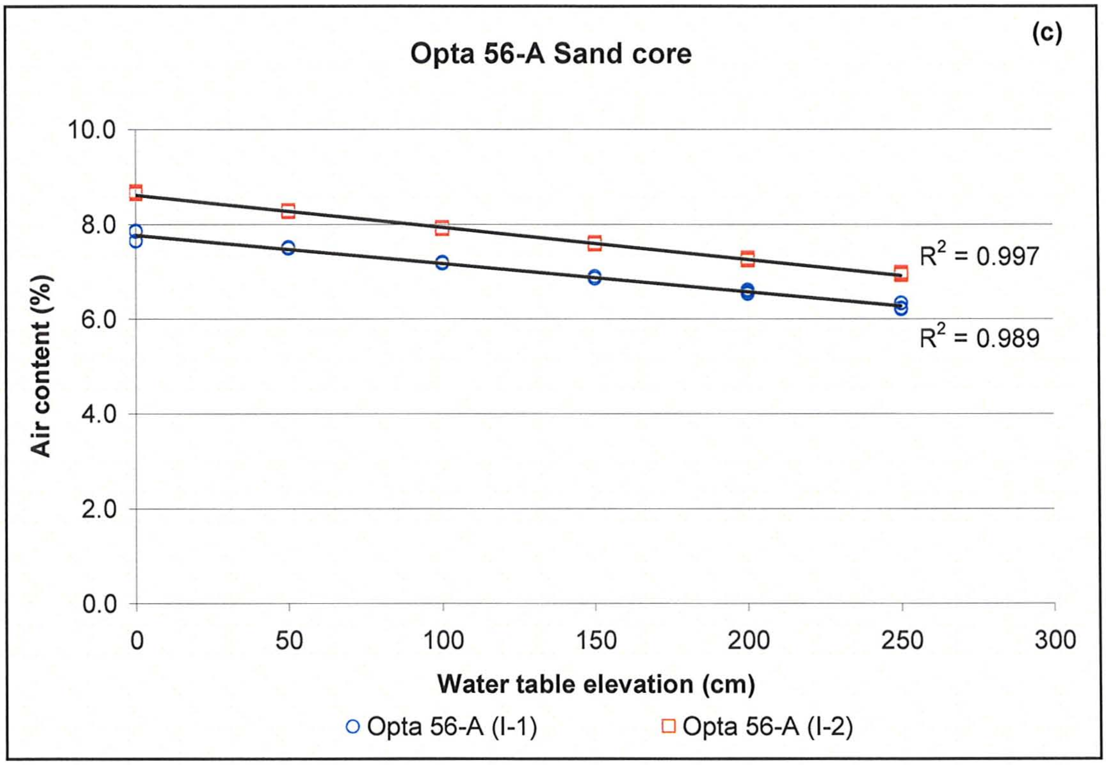

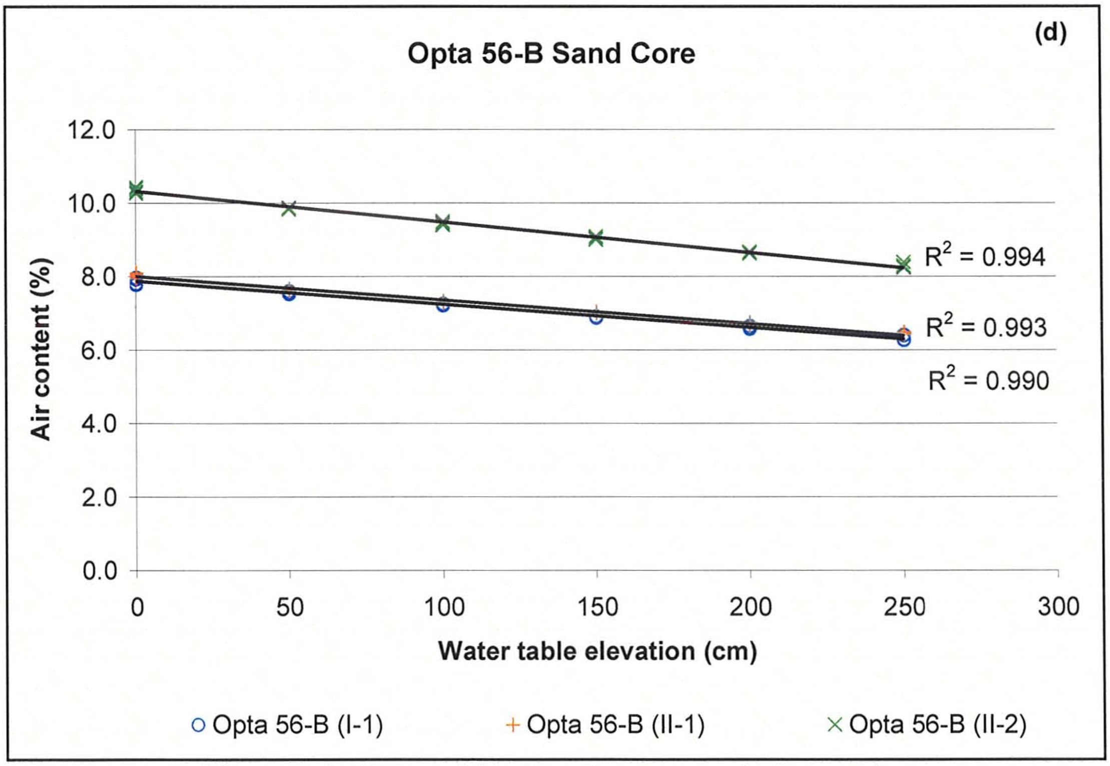

Figure 4.4: Water table elevation versus air content for Opta 56-A (c) and Opta 56-B (d) sand cores

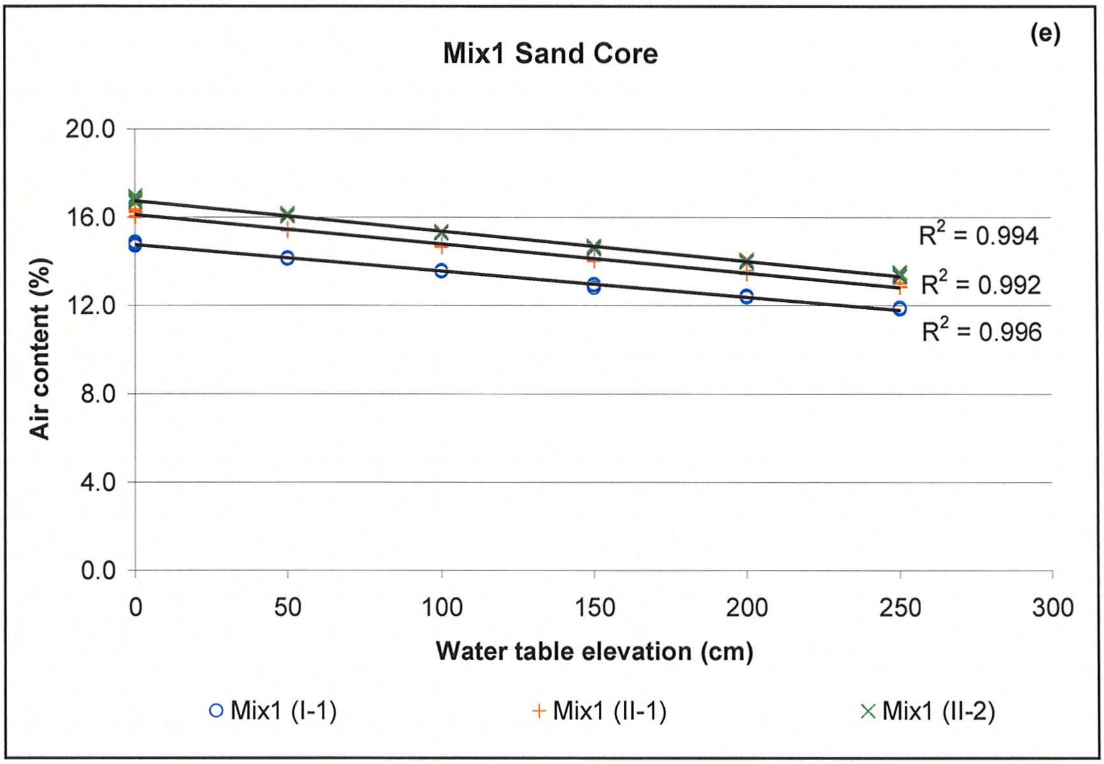

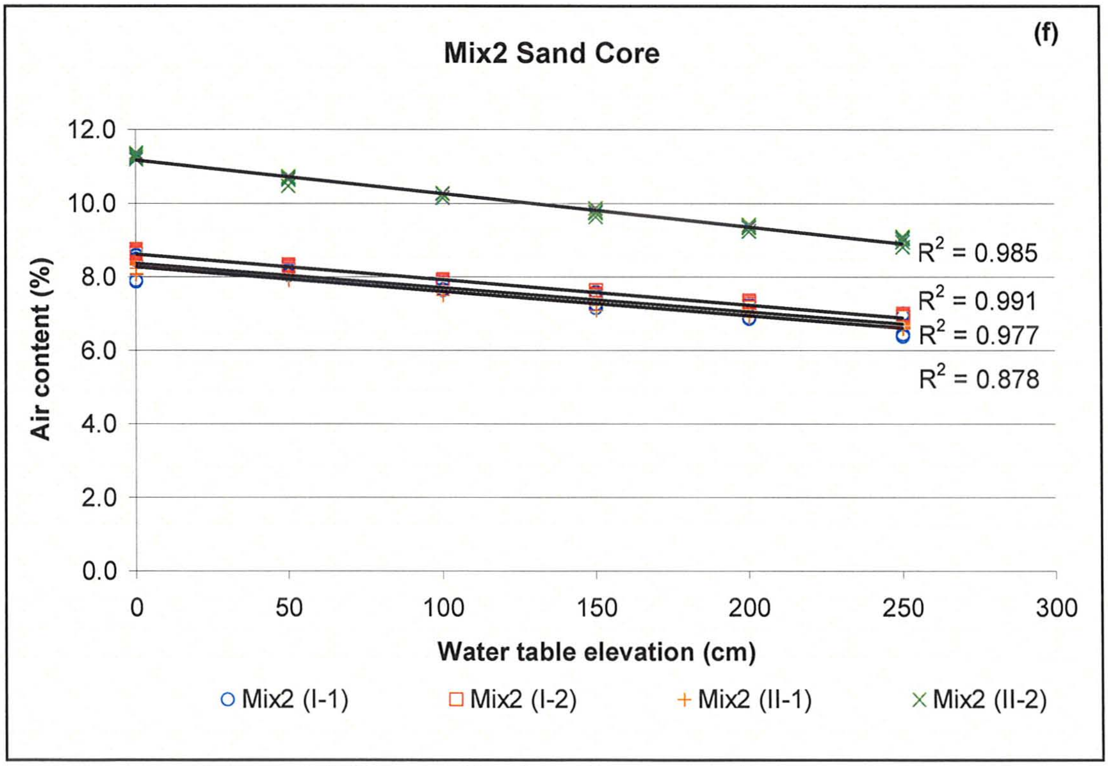

Figure 4.4: Water table elevation versus air content for Mix1 (e) and Mix2 (f) sand cores

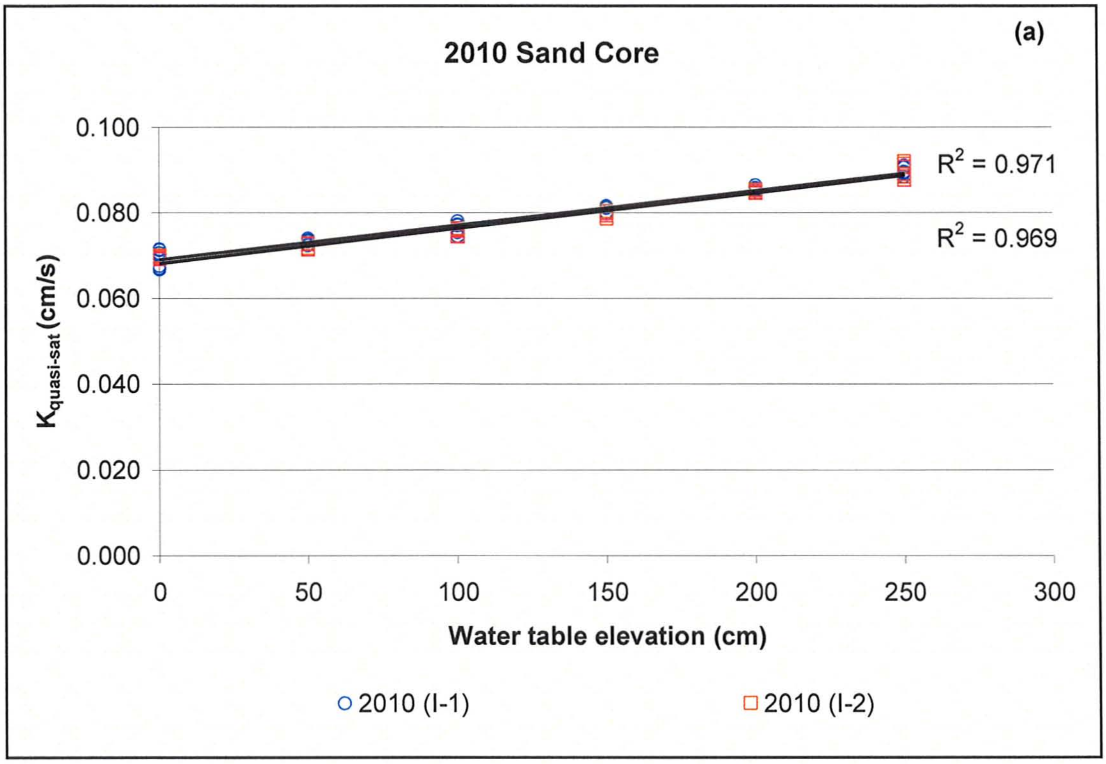

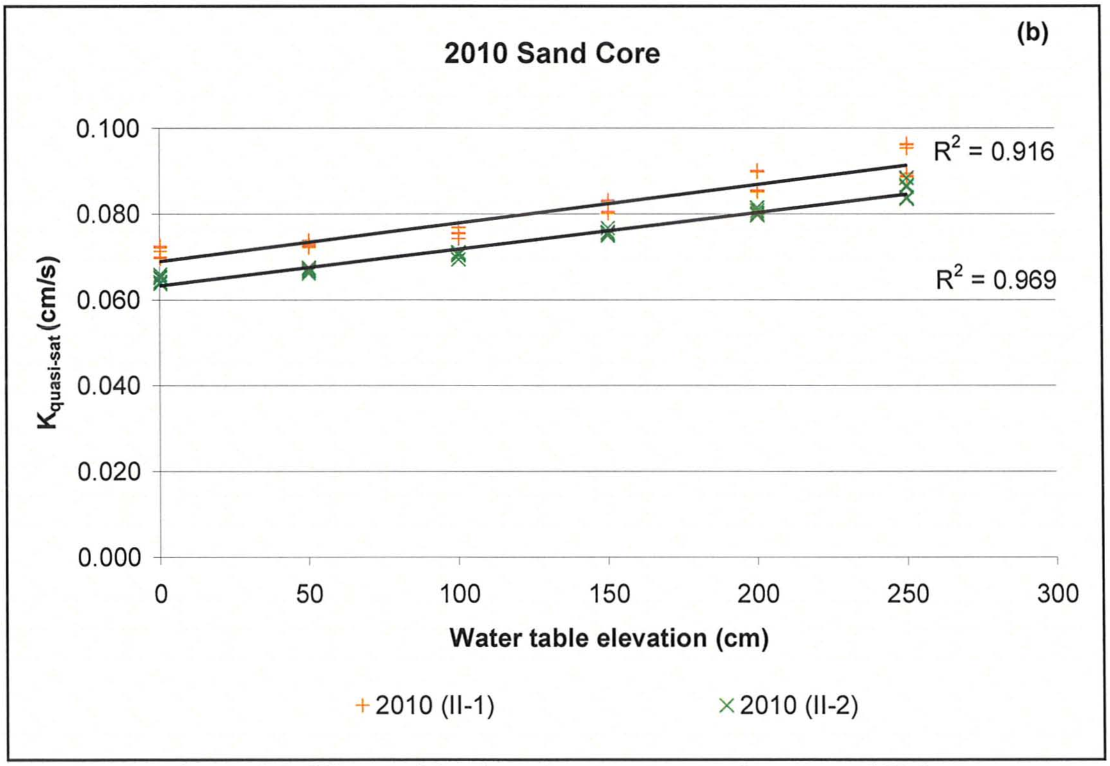

Figure 4.5: Water table elevation versus quasi-saturated K for trial (I-1) (a) and trial (1-2) (b) for the 2010 sand core

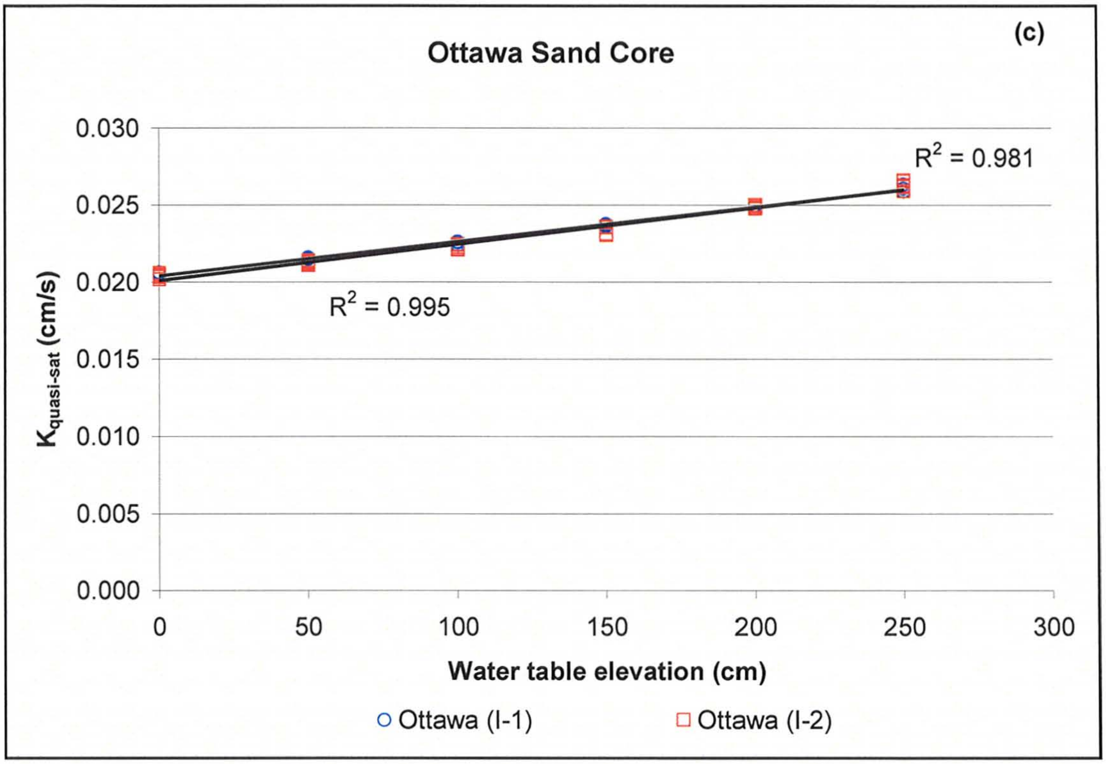

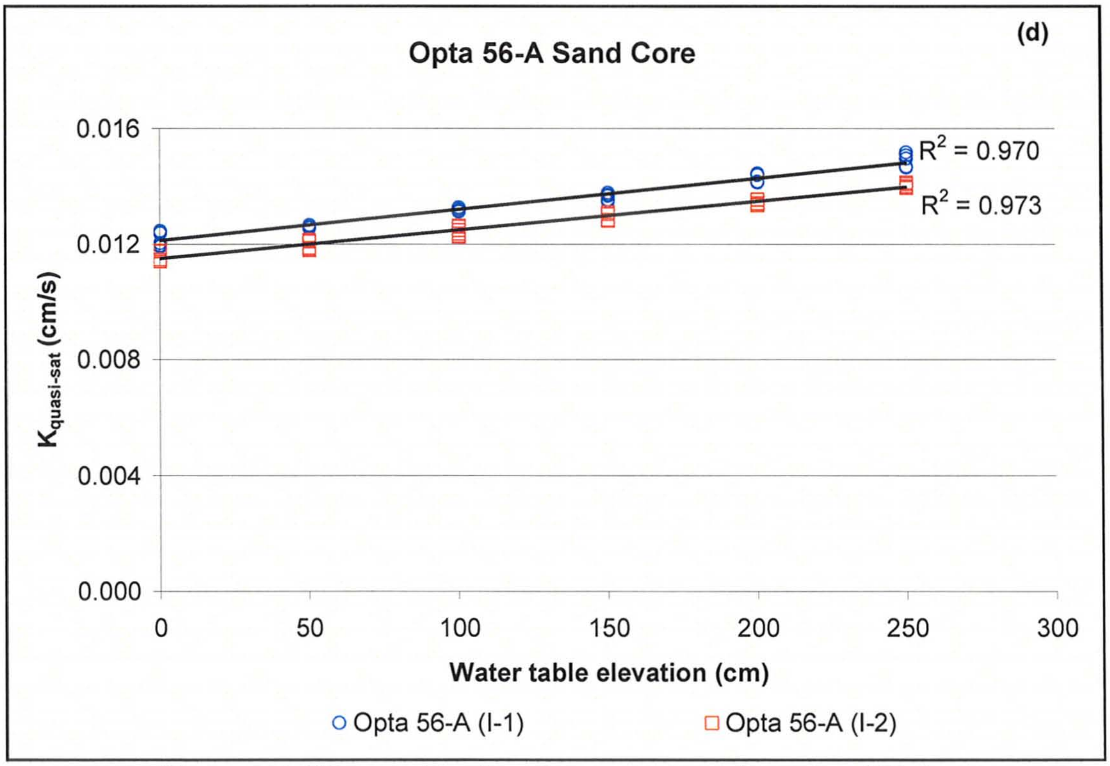

Figure 4.5: Water table elevation versus quasi-saturated K for the Ottawa (c) and Opta 56-A (d) sand cores

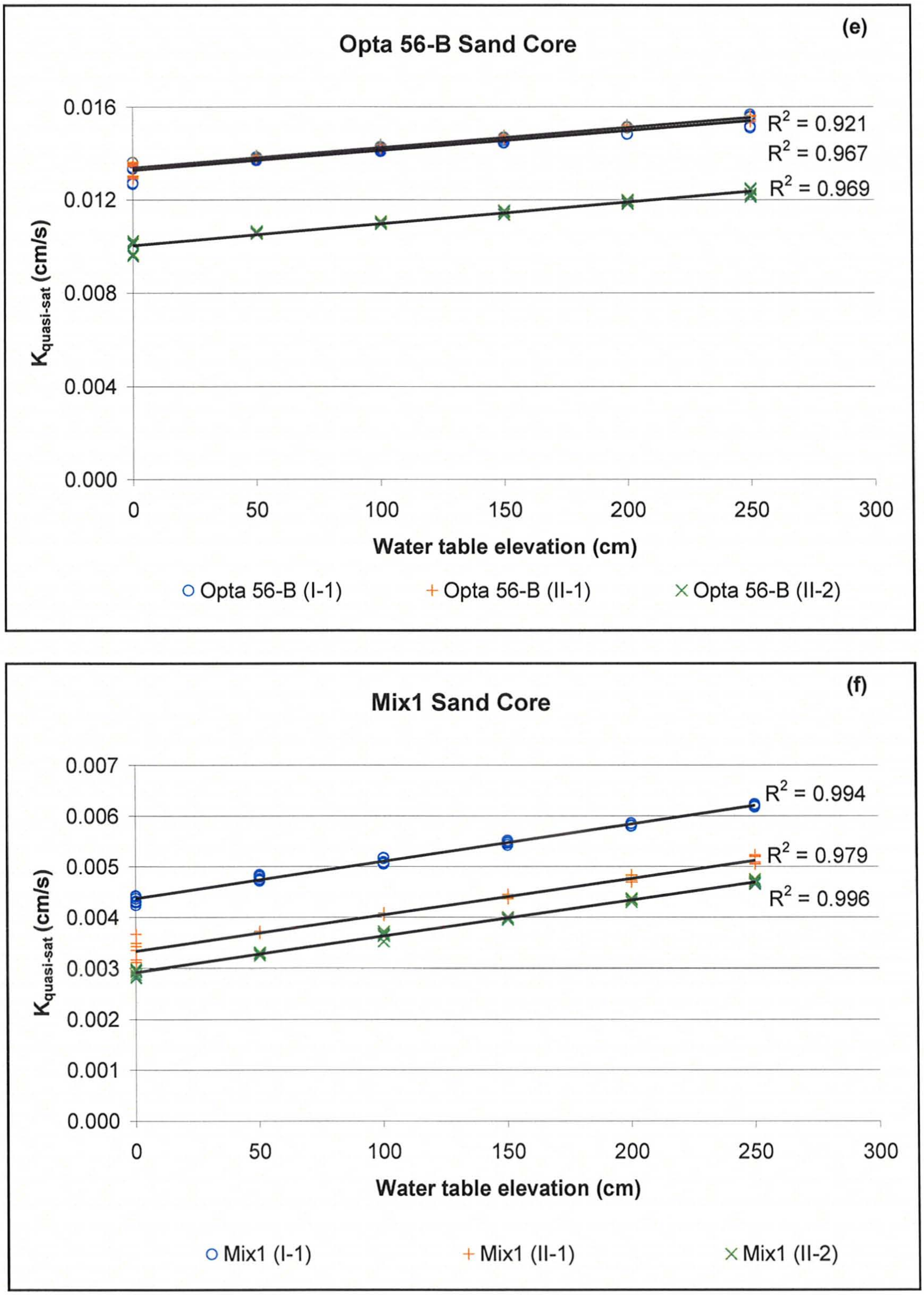

Figure 4.5: Water table elevation versus quasi-saturated K for the Opta 56-B (e) and Mix1 (f) for the 2010 sand cores

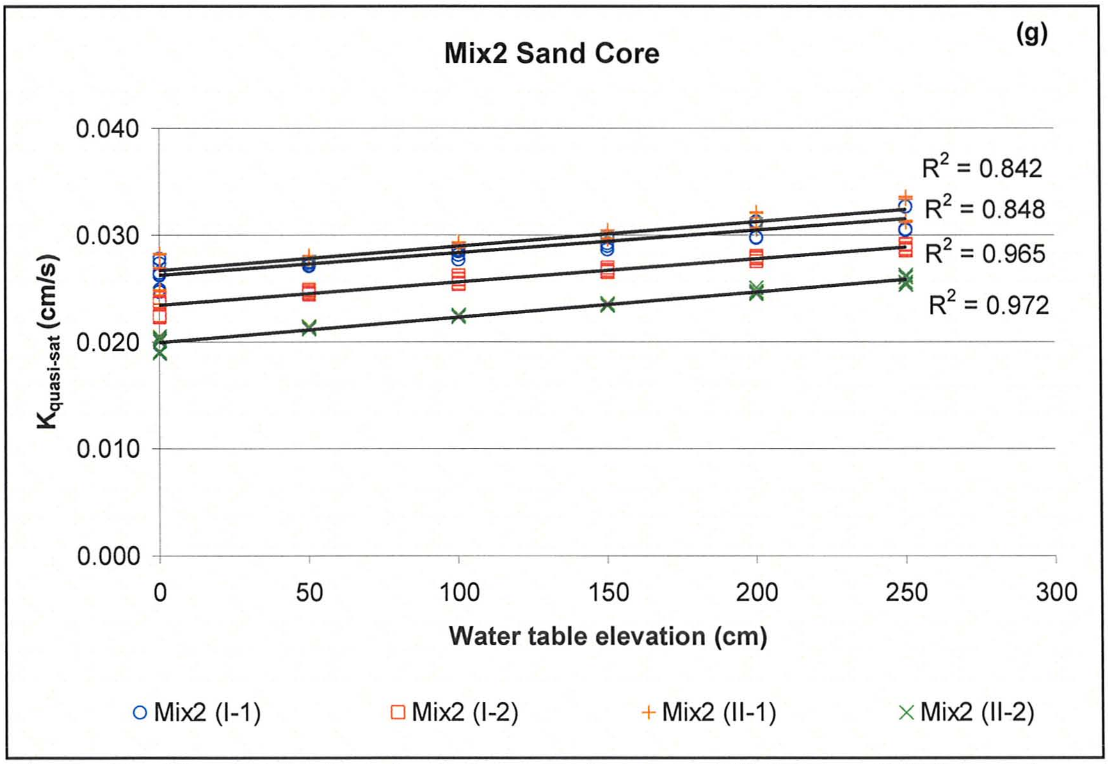

Figure 4.5: Water table elevation versus quasi-saturated K for the Mix2 (g) sand core

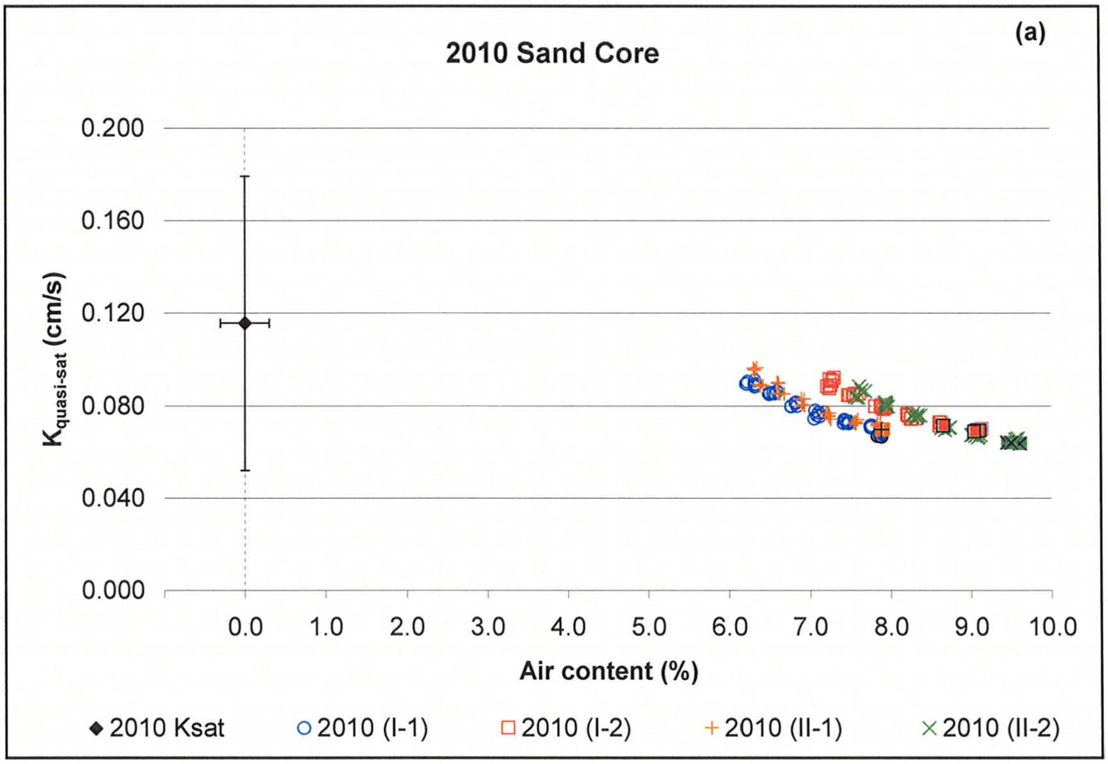

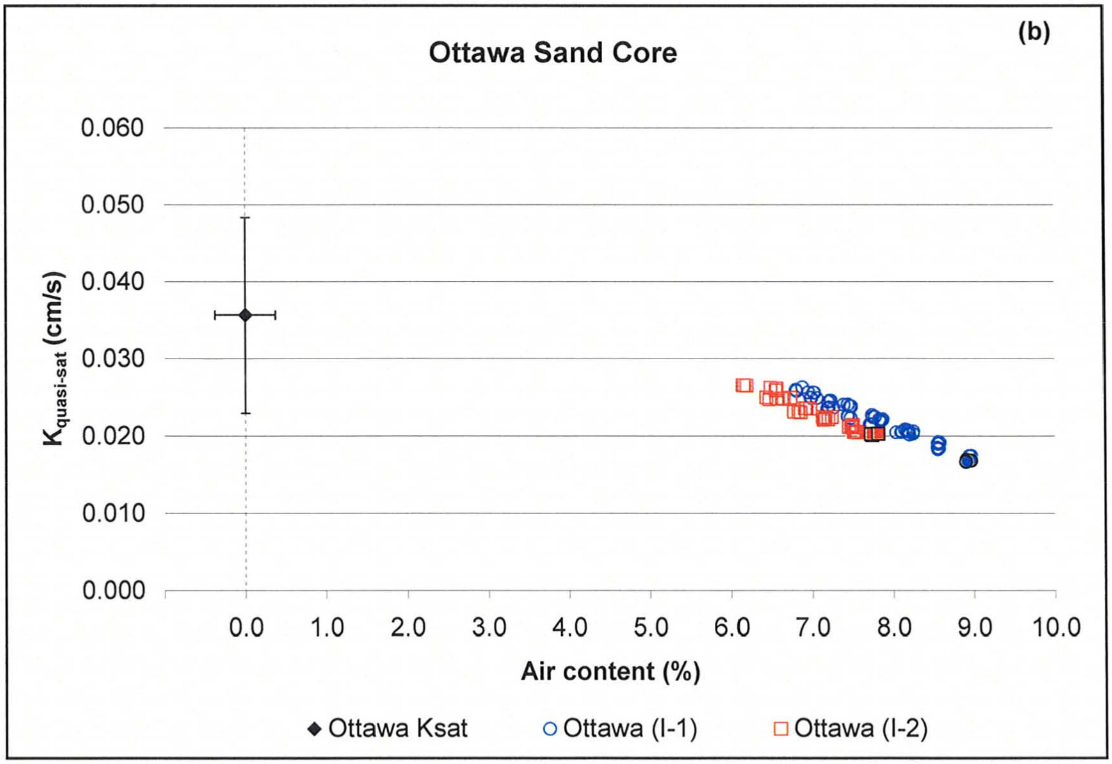

Figure 4.6: Air content versus quasi-saturated hydraulic conductivity for 2010 (a) and Ottawa (b) sand cores

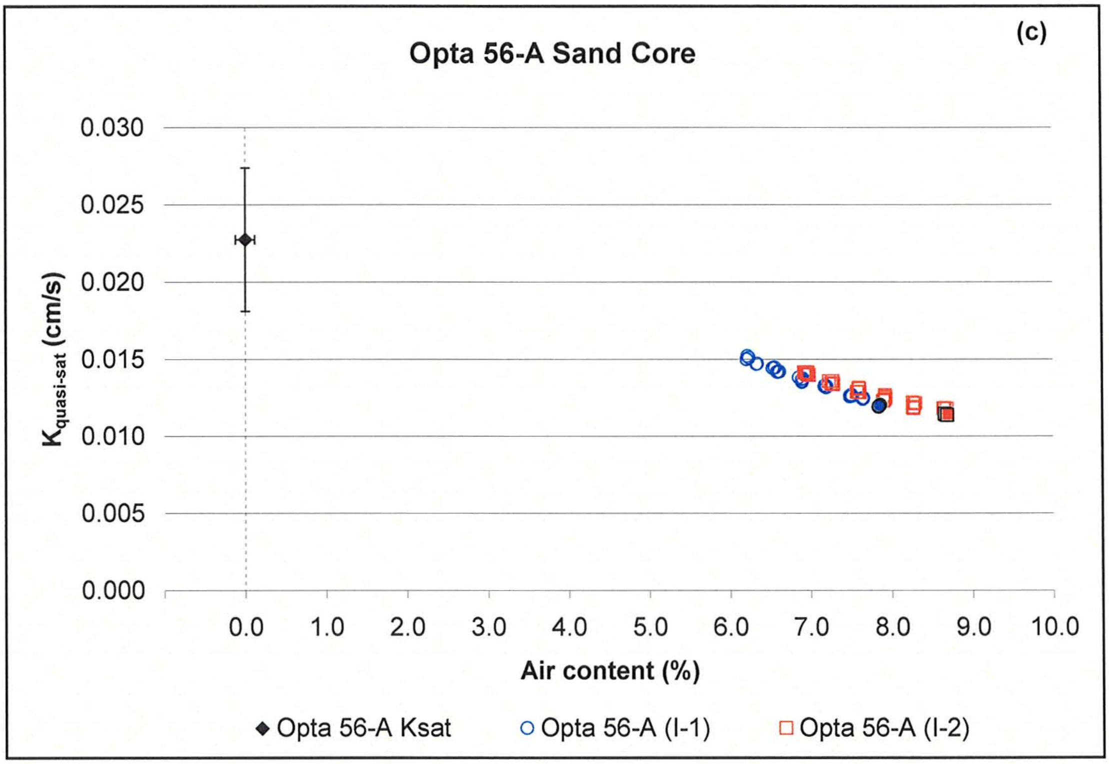

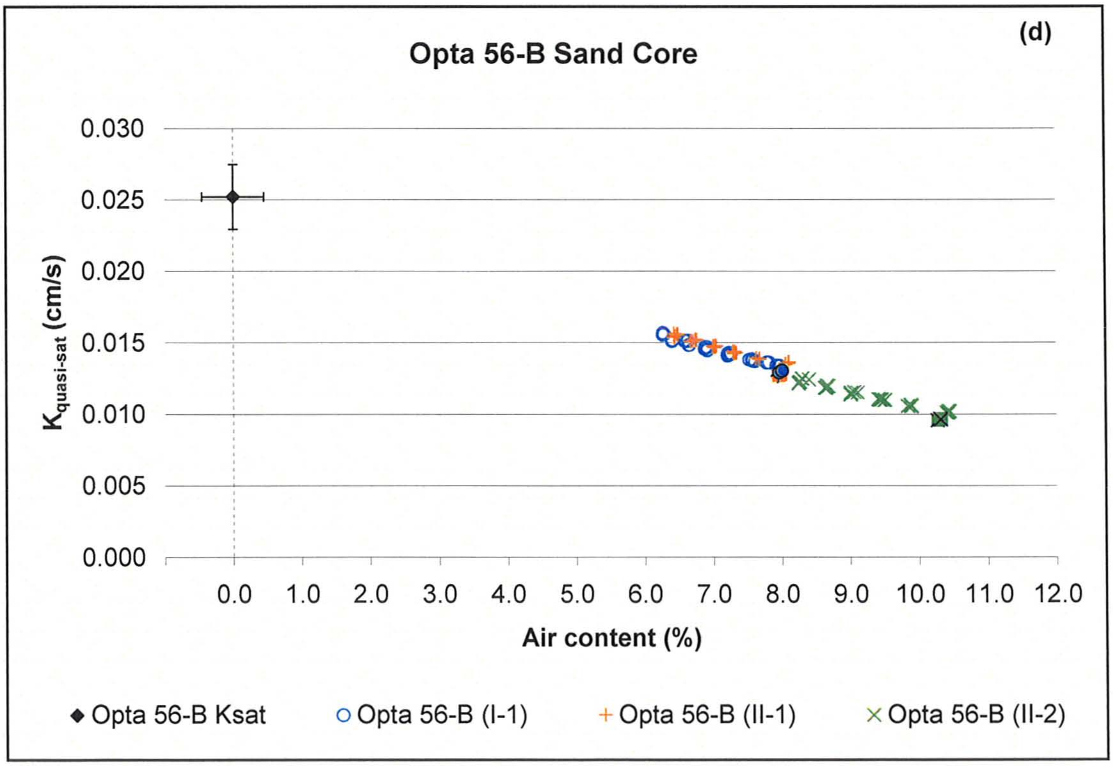

Figure 4.6: Air content versus quasi-saturated hydraulic conductivity for Opta 56-A (c) and Opta 56-B (d) sand cores

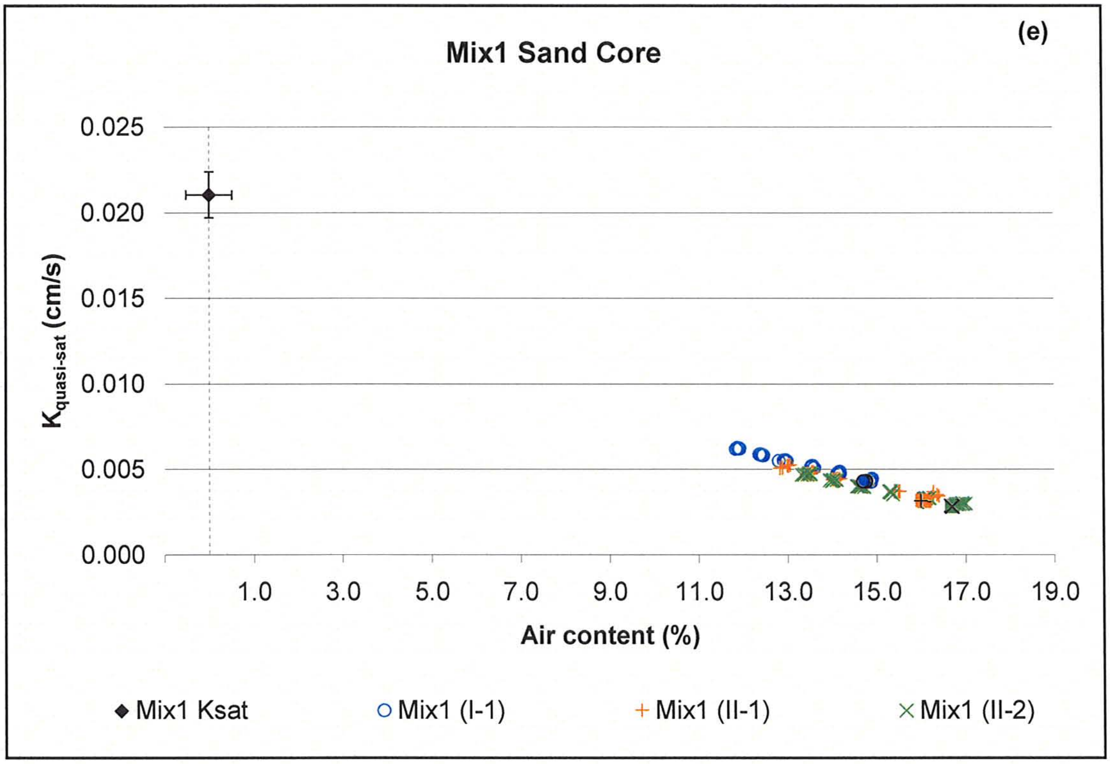

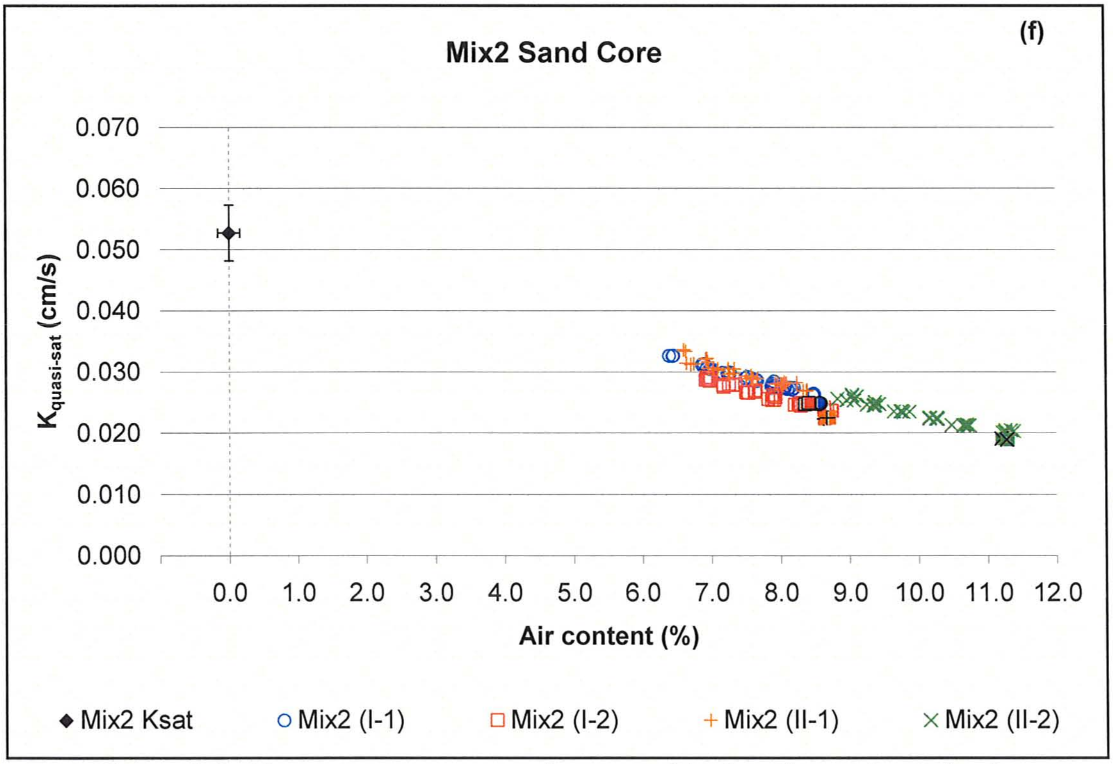

Figure 4.6: Air content versus quasi-saturated hydraulic conductivity for Mix1 (e) and Mix2 (f) sand cores

5.0 MODEL RESULTS AND DISCUSSION

5.1 Quasi-Saturated Hydraulic Conductivity and Entrapped Air: Faybishenko (1995) Function

Figure 5.1 displays the fitting of the modified Aver'yanov (1950) formula derived by Faybishenko (1995) quasi-saturated hydraulic conductivity equation to the measured data. The empirical formula derived by Faybishenko (1995) (Eq. [9]) correctly reflects the decrease quasi-saturated hydraulic conductivity due to increases in entrapped air as a result of increasing water table elevation. The fit of the data is quantified through the analysis of the generated regression coefficients specified within Table 5.1. All experimental data measured for each sand core were utilized to determine the behaviour of quasi-saturated hydraulic conductivity as predicted by the Faybishenko (1995) empirical equation.

Figures 5.1(a) and (b) depict the fit of the Faybishenko (1995) equation and the measured experimental data for the 2010 and Ottawa sand cores which exhibit that a minor increase in entrapped air results in an almost linear response by the quasi-saturated hydraulic conductivity. The measured data for both the 2010 and Ottawa sand core possess a steep slope in comparison to the function predicted by the Faybishenko (1995) equation. For these sand cores, the Faybishenko (1995) function trends across the data. The fitting of measured data for sand cores Opta 56-A and Opta 56-B using the Faybishenko (1995) function shows that the quasi-saturated hydraulic conductivity will decrease linearly with increases in air content (Figure 5.1(c) and (d)). Figure 5.1(e) and (f) for Mix1, and Mix2, respectively each show substantial decreases in hydraulic conductivity occurred at low air contents with little increase in air volume and at higher air contents hydraulic conductivity decreases less. The data generated on the Opta 56 and Mix sand cores trend well along the Faybishenko (1995) function. The pore size distribution effects the air entrapment influence on the quasi-saturated hydraulic conductivity as a function of entrapped air are similar to that reported by Sakaguchi et al. (2005) in that larger changes are seen at lower air contents which would be occupying larger pores.

The results generated through the fitting of measured data and the Faybishenko (1995) equation of quasi-saturated hydraulic conductivity demonstrates the ability of this function in predicting the nature of conductivity in the presence of dynamic entrapped air. Following from Faybishenko (1995) Eq. [8] can be adapted such that quasi-saturated hydraulic conductivity is expressed as a function of volumetric water content as a result of water table position (wt) is expressed as

$$K(\omega) = K_0 + (K_s - K_0)\left(\frac{\theta(wt) - \theta_{qs}}{\theta_s - \theta_{qs}}\right)^n \qquad \text{Eq. [20]}$$

$\theta(wt)$ is the volumetric water content dependant on the water table position and is expressed as Eq. [19]. This modified formula now acknowledges and incorporates the presence and behaviour of entrapped air variability due to water table variations thereby allowing a more accurate determination of the quasi-saturated hydraulic conductivity within a dynamic system.

5.2 Quasi-Saturated Hydraulic Conductivity and Entrapped Air: van Genuchten (1980) Function

The van Genuchten (1980) function is commonly used to simulate flow in unsaturated porous media. Simulations of each experimental investigation were performed using the unsaturated hydraulic conductivity equation developed by van Genuchten (1980). The input parameters and generated regression coefficients are outlined within Table 5.1.

Analysis of Figure 5.2(a) and (b) shows that the measurements made for all experimental trials conducted on the 2010 and Ottawa sand cores do not possess the same slope as the generated van Genuchten (1980) function. Although there is a slight difference in quasi-saturated hydraulic conductivity at equal saturations, this is a small secondary concern.

For example, Figure 5.2 identifies that for the same core a 0.83 initial saturation (7.9% entrapped air) for the 2010 (II-1) experimental investigation which is approximately equal to the saturation attained as a result of 200 cm of increased water table elevation within 2010 (II-2). The mean quasi-saturated hydraulic conductivity (average of six measurements) for equal saturations within the 2010 (II-1) and 2010 (II-2) experimental trials were calculated to be 0.071 cm s^{-1} (standard deviation= 0.001) and 0.081 cm s^{-1} (standard deviation= 0.001), respectively. However, a t-test performed at a 95% confidence level (α=0.05) indicated no significant difference between these values.

The analysis of Figure 5.2 indicates that e measured data for all experimental investigations conducted within sand cores Opta 56-A, Opta 56-B, Mix1 and Mix2 sand cores trends well along the van Genuchten (1980) function. The analysis of the van Genuchten (1980) equation and the experimental data indicates that the function sufficiently describes the effects of changing air content on hydraulic conductivity in the presence of a fluctuating water table.

The van Genuchten (1980) numerical model is a general description that relates volumetric water content and hydraulic conductivity through a function that is widely accepted. The goodness of fit of the measured experimental data indicates that not only is the van Genuchten (1980) function able to predict the changes in unsaturated hydraulic conductivity but can also sufficiently predict hydraulic behaviour within quasi-saturated systems where air contents can change with water table elevation.

Table 5.1: Summary of simulation parameters and regression coefficients for Faybishenko (1995) and van Genuchten (1980) functions

Parameters	**Core designation**					
	2010	***Ottawa***	***Opta 56-A***	***Opta 56-B***	***Mix1***	***Mix2***
K_s (cm/s)	0.116	0.0357	0.0227	0.0252	0.0211	0.0527
Faybishenko (1995)						
$\omega_{\max}$	0.0960	0.896	0.0868	0.0913	0.170	0.0987
K_0 (cm/s)	0.0630	0.0160	0.0110	0.0100	0.003	0.020
n	0.767	0.621	0.978	1.061	1.444	1.244
Correlation (r^2)	0.673	0.871	0.969	0.985	0.987	0.910
Van Genuchten (1980)						
l	0.313	1.00×10^{-8}	0.201	0.371	1.00×10^{-4}	1.00×10^{-3}
m	1.00	1.00	1.00	1.00	0.890	0.965
Correlation (r^2)	0.654	0.766	0.960	0.980	0.988	0.907

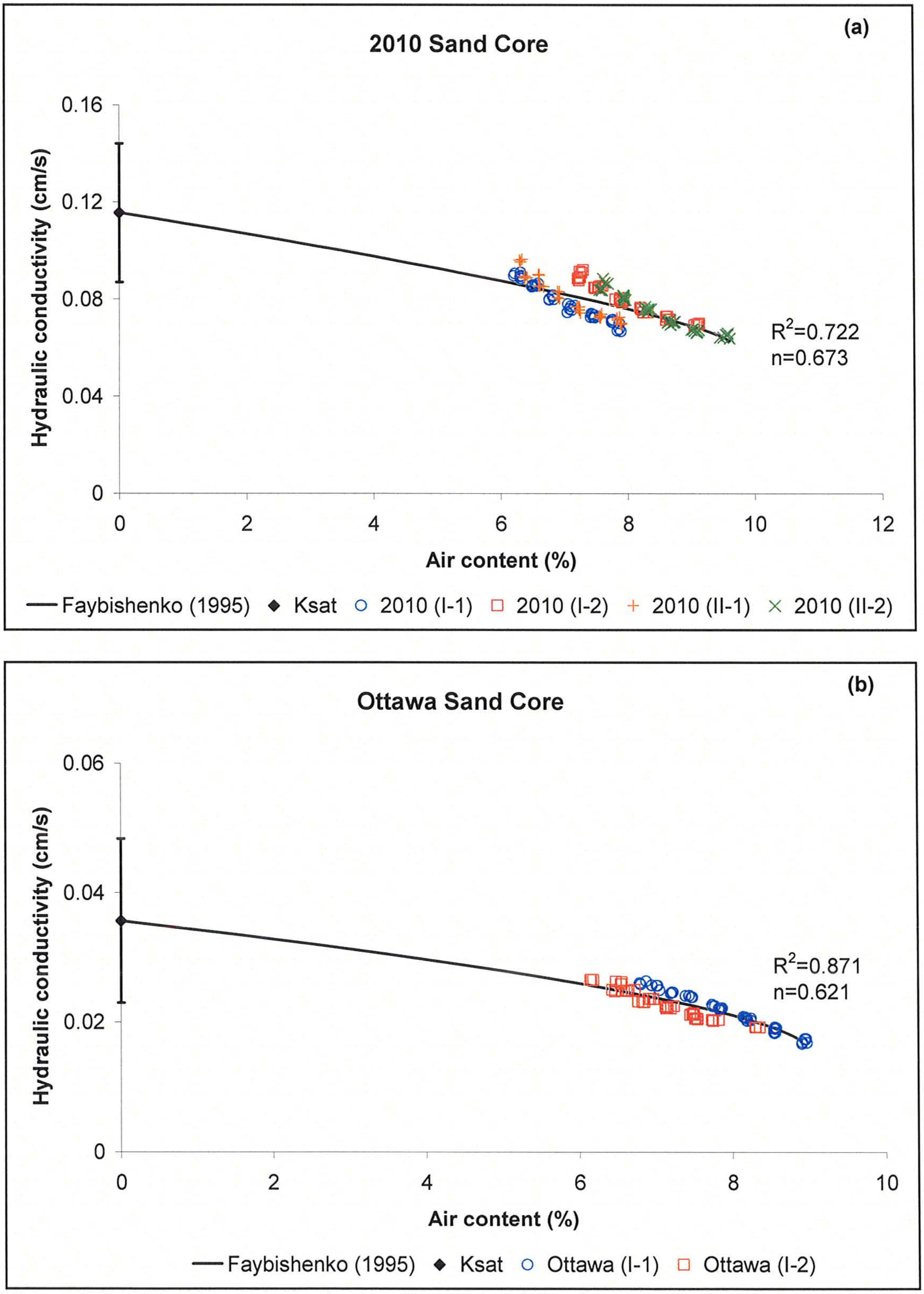

Figure 5.1: Air content versus hydraulic conductivity for 2010 (a) and Ottawa (b) sand cores as fitted by the Faybishenko (1995) function

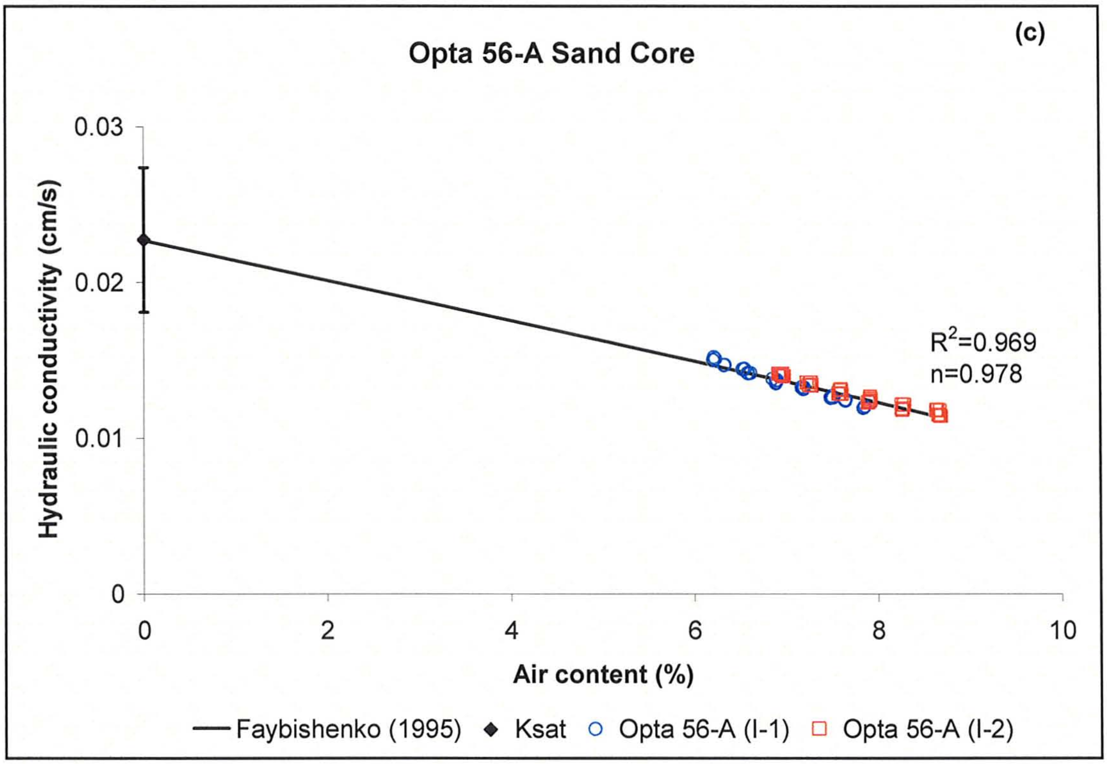

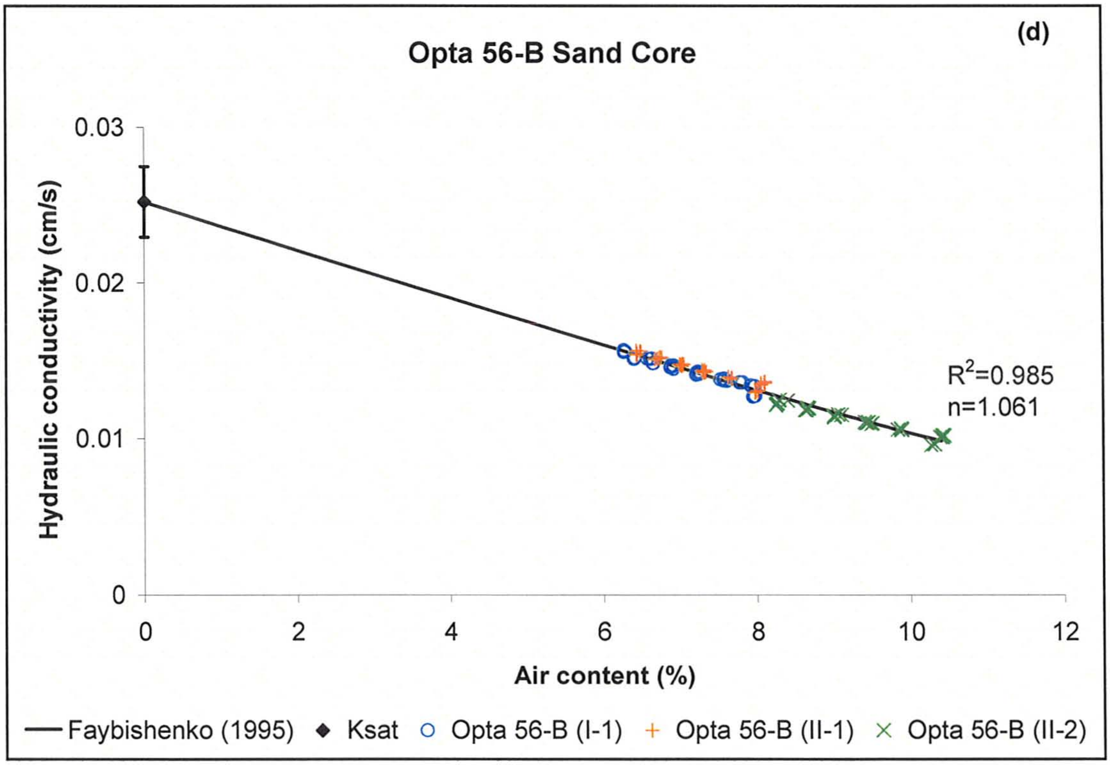

Figure 5.1: Air content versus hydraulic conductivity for Opta 56-A (c) and Opta 56-B (d) sand cores as fitted by the Faybishenko (1995) function

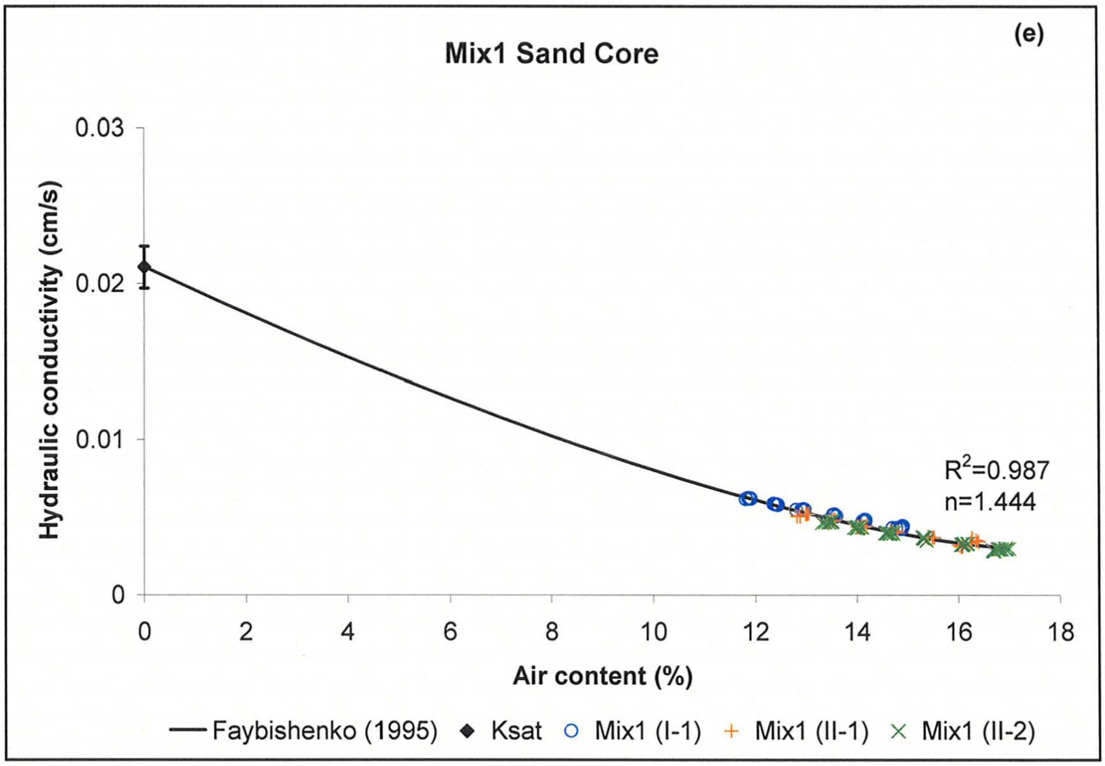

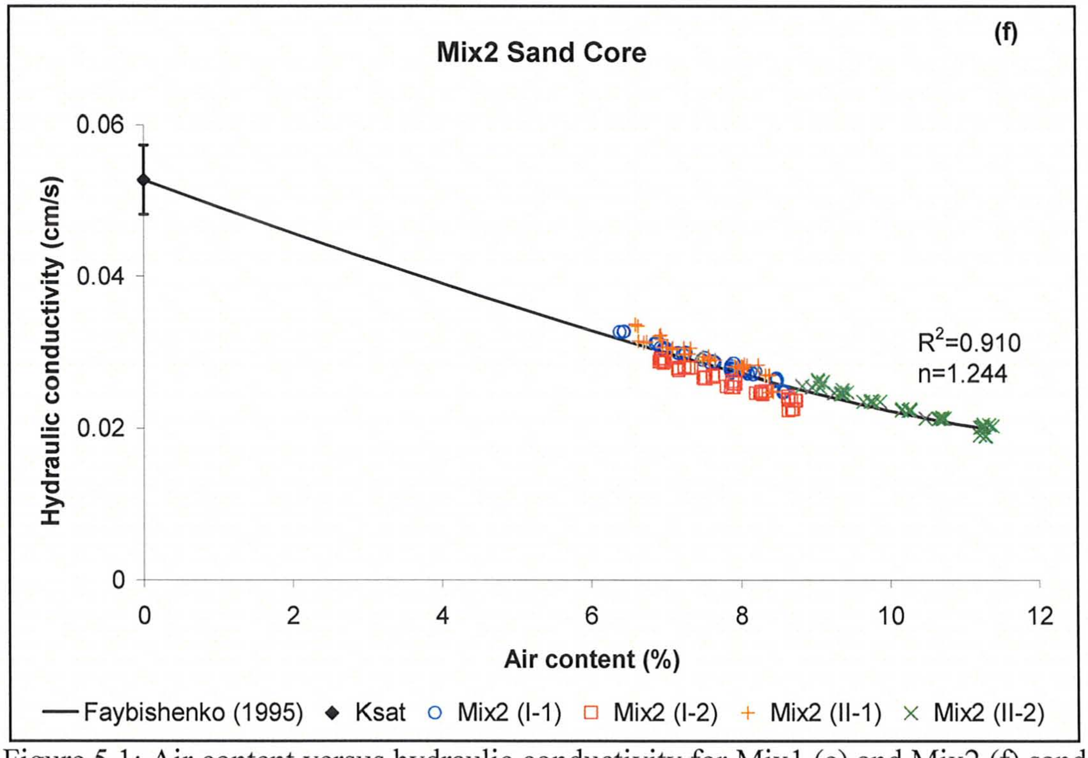

Figure 5.1: Air content versus hydraulic conductivity for Mix1 (e) and Mix2 (f) sand cores as fitted by the Faybishenko (1995) funtion

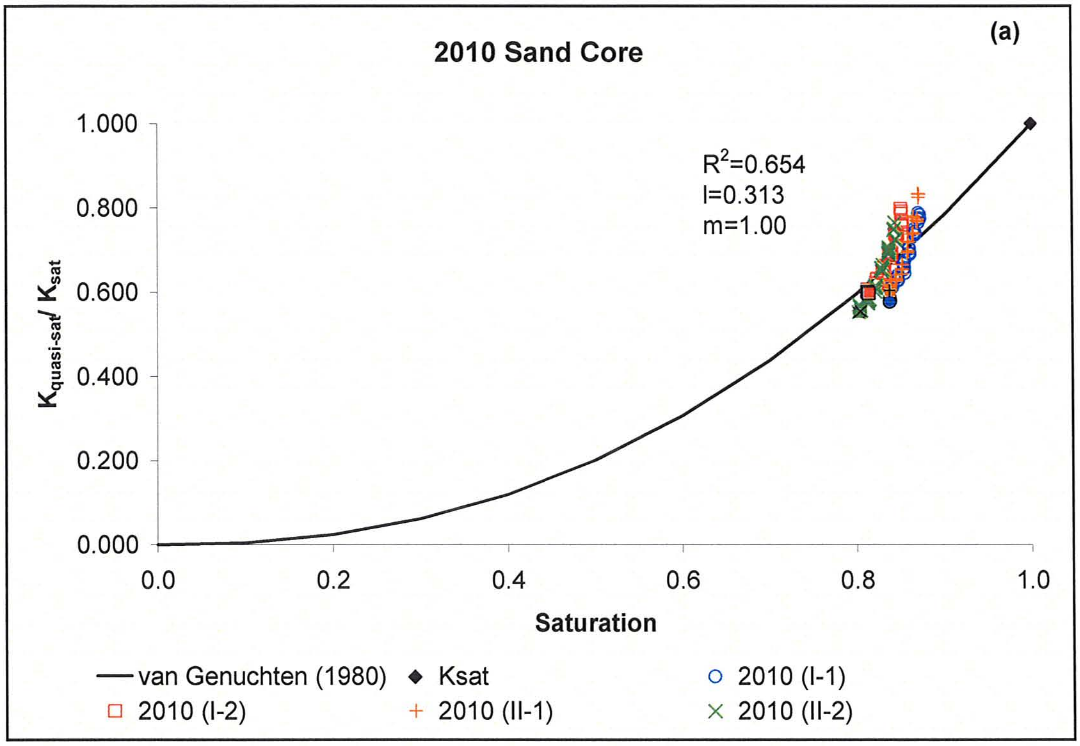

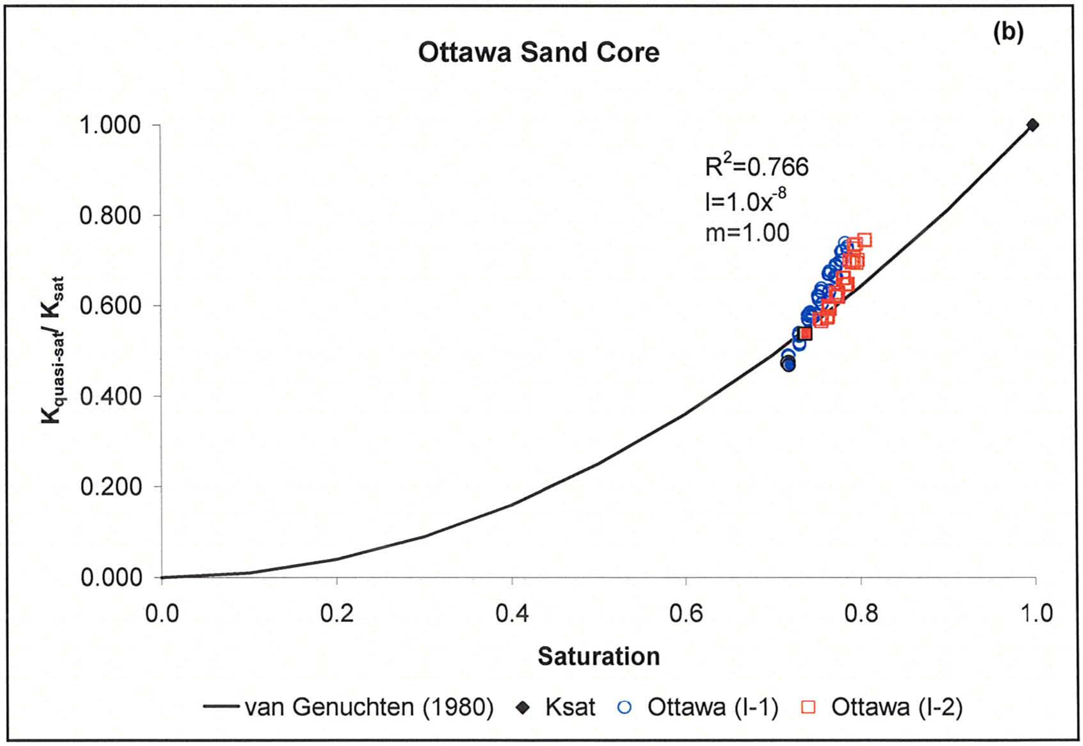

Figure 5.2: Saturation versus relative hydraulic conductivity for 2010 (a) and Ottawa (b) sand cores as fitted by the van Genuchten (1980) function; solid symbols indicate initial measured parameters

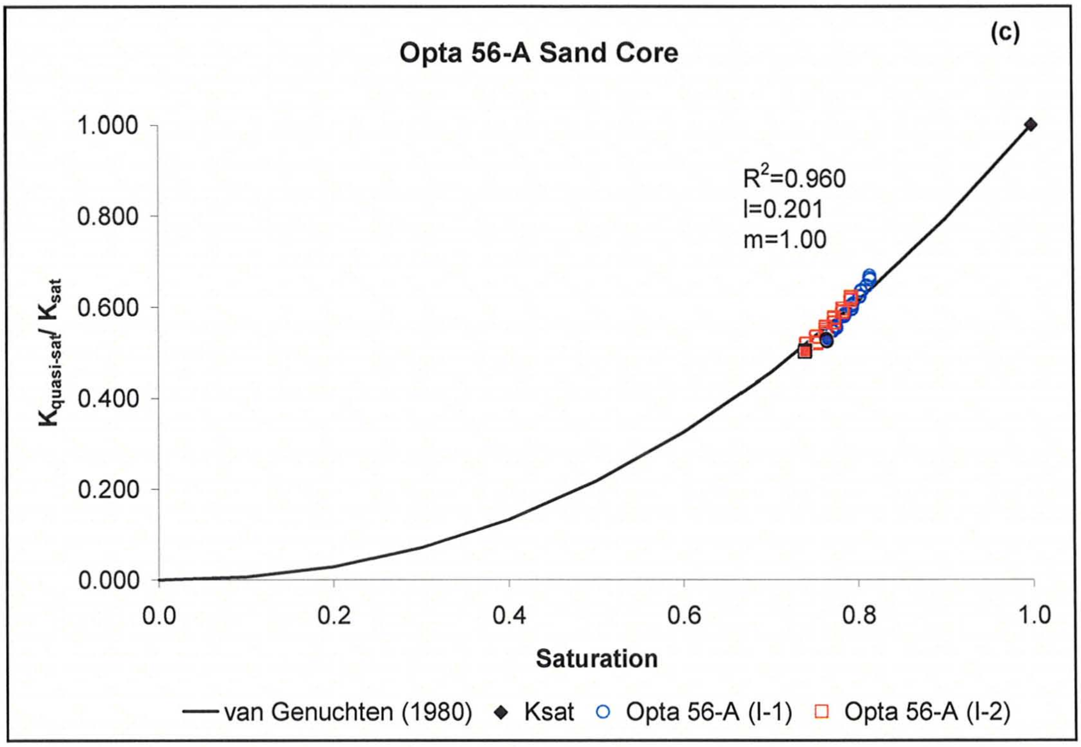

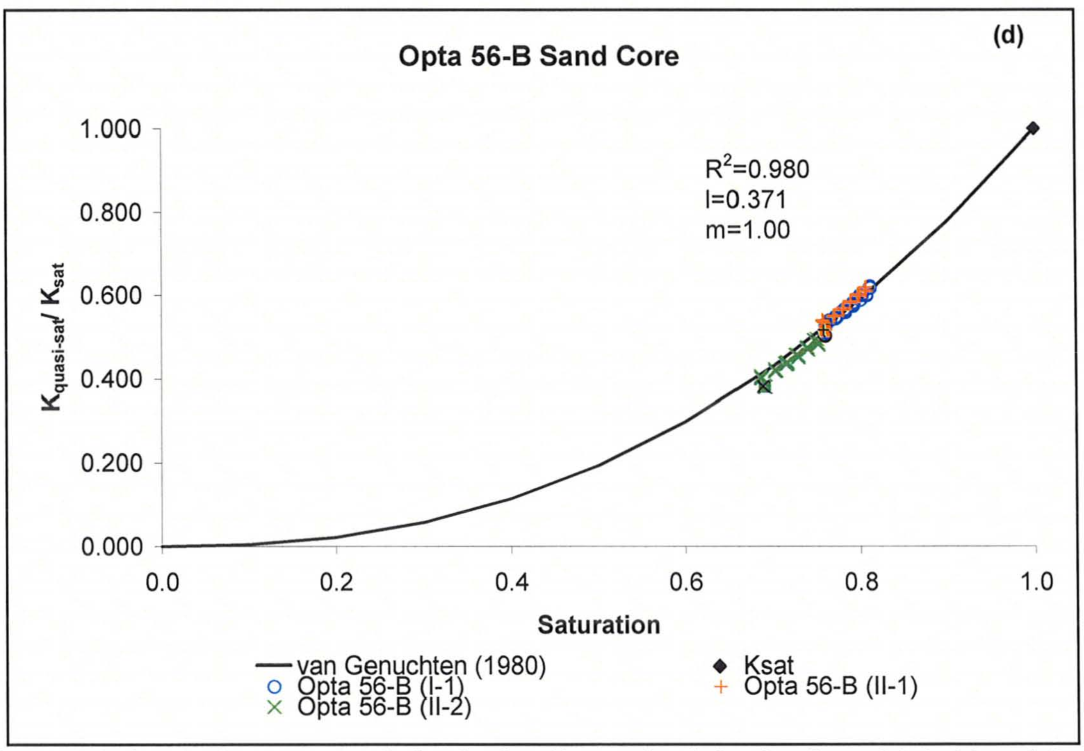

Figure 5.2: Saturation versus relative hydraulic conductivity for Opta 56-A (c) and Opta 56-B (d) sand cores as fitted by the van Genuchten (1980) function; solid symbols indicate initial measured parameters

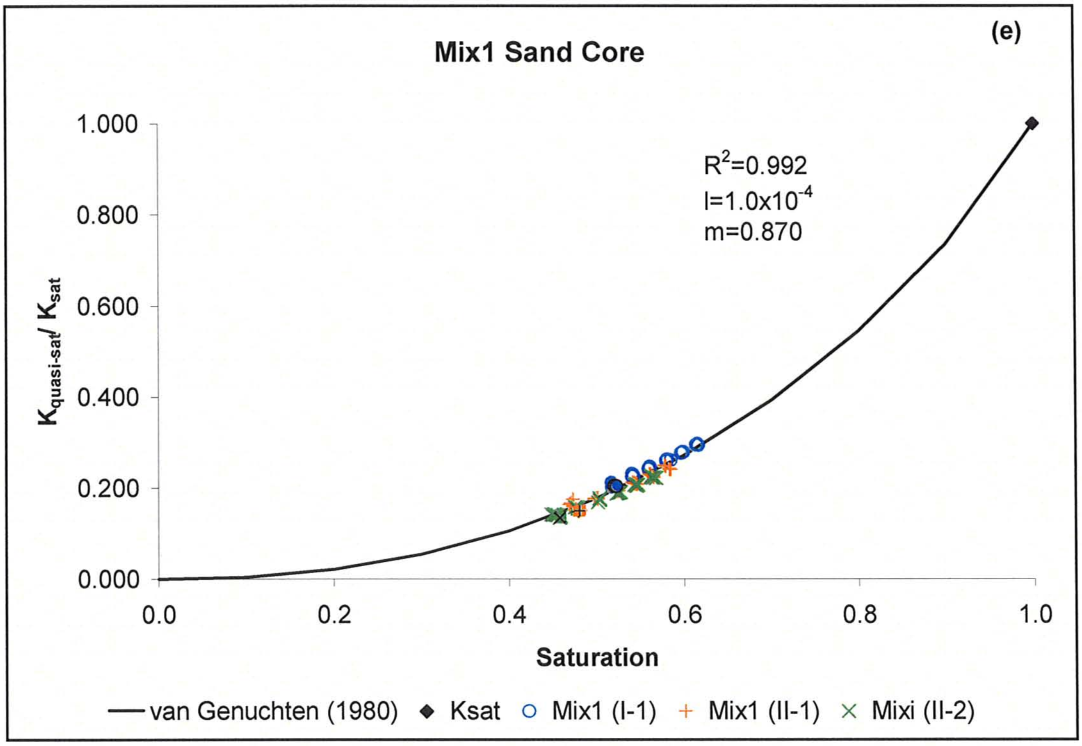

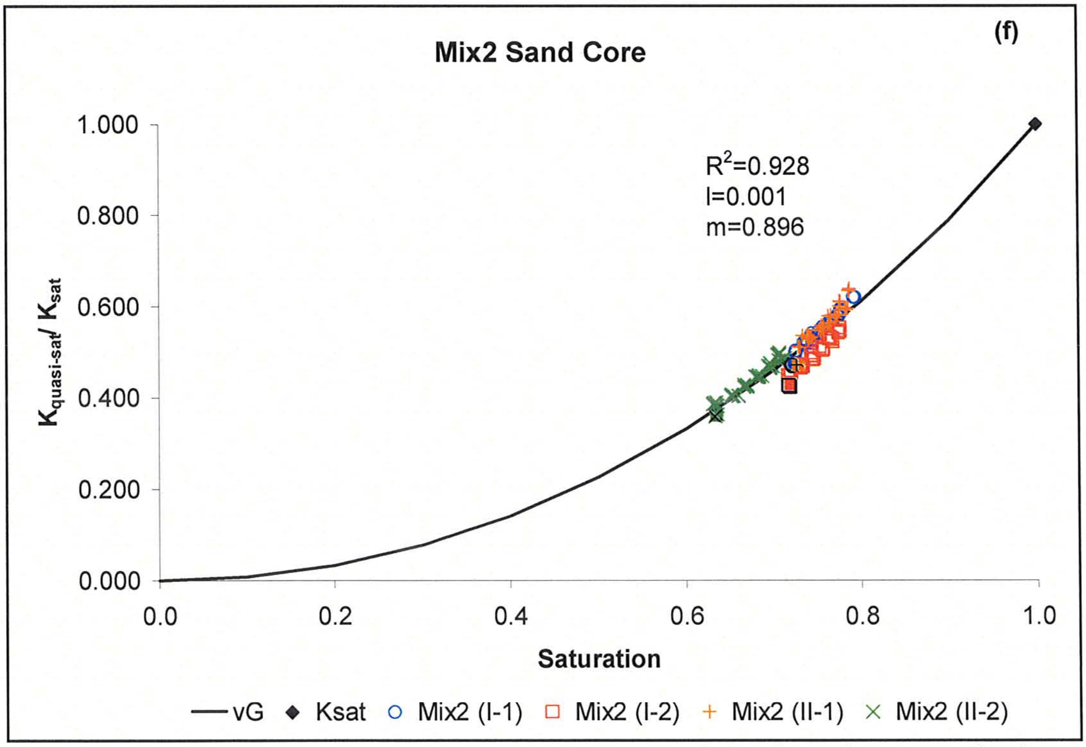

Figure 5.2: Saturation versus relative hydraulic conductivity for Mix1 (e) and Mix2 (f) sand cores as fitted by van Genuchten (1980) function; solid symbols indicate initial measured parameters

6.0 CONTRIBUTIONS

There are no papers in the peer reviewed scientific literature reporting or acknowledging this mechanism of systematic change in hydraulic conductivity associated with entrapped near the water table. The data generated within this thesis has made the following contributions to science:

1. Demonstrated systematic changes in air content induced by water table fluctuations and its effects on quasi-saturated hydraulic conductivity.
2. Developed an ideal gas law based TDR calibration for discontinuous discrete entrapped air.
3. Showed that existing hydraulic functions in numerical models can be relatively easily adapted to incorporate water table fluctuations effects on air content and quasi-saturated hydraulic conductivity (e.g. HYDRUS-1D, 2D, 3D; TOUGH2VOC; UTCHEM, etc.)

Given the ubiquitous occurrence of this fundamental compression mechanism induced by water table fluctuations understanding its effects on quasi-saturated hydraulic conductivity is relevant within all natural unconfined groundwater systems. Changes in water table position can occur naturally through extreme precipitation events/ seasonal changes and biogenic processes. In addition, anthropogenic processes can change water table position by shallow groundwater resource exploitation or through a variety of remediation techniques including pump and treat, air sparging, and the introduction of microbes, etc.

7.0 CONCLUSIONS

This research on the influence of entrapped air on hydraulic conductivity has brought forth new information on the dynamic behaviour of these systems in the presence of water table fluctuations. The quasi saturated hydraulic conductivity of the sands with initial entrapped air contents of 6.3 to 16.5% observed in this study were factors of 2 to 6 times lower than the saturated hydraulic conductivity values which are consistent with values reported in the literature.

The hypothesis that the magnitude of entrapped air would be sensitive to water table elevation due to the change in water pressure surrounding entrapped air clusters was proven to be the correct. Entrapped air contents decreased by 20% when subjected to an increase in water pressure of 250 cm which represents a 250 cm increase in elevation of a water table. This is consistent with a change in air volume caused by a change in absolute pressure as described by the ideal gas law. Predictions using a simple spherical model of entrapped air clusters generated results supporting that associated changes in capillary pressure do not play a significant role in changes in entrapped air contents. This is primarily due to fact that both the pressure of the wetting phase (water) and the entrapped non-wetting phase (air) change with water table elevation, and any changes in capillary pressure are only caused by changes in the curvature of the air water meniscus within the pore space. The fact that the changes in air content are described well by the ideal gas law proved useful in improving our experimental air content data.

A spreadsheet post-processing method was developed to calibrate commercial software generated TDR data by exploiting the observed changes in the volume of entrapped air and the known changes in water pressure relative to the measured prevailing barometric pressures. Through this ideal gas law based calibration a more accurate value of the initial air content entrapped in the sand prior to pressure changes, i.e. the air content at the prevailing gauge pressure (barometric pressure) which is by definition the pressure at the water table, was calculated.

As an extension of the hypothesis that air contents would be sensitive to water table elevation, it was also hypothesized that quasi-saturated hydraulic conductivities in the presence of entrapped air would also change due to changes in water table position. The results prove this hypothesis to be true with measured hydraulic conductivities changing significantly with water table changes, i.e., a factor of 1.20 to 1.64 increase in quasi-saturated hydraulic conductivity for a 250 cm increase in water pressure above atmospheric. This mechanism and associated hydraulic conductivity changes are expected to be ubiquitously occurring whenever water table elevations increase significantly, or decrease significantly with prevailing entrapped air contents.

The ability of two existing equations of hydraulic conductivity as a function of water content to fit the observed changes in quasi-saturated hydraulic conductivity as a function of air content changes induced by water table elevation changes were evaluated. It was found in this work that introducing water content or air content as a function of water table elevation into the unsaturated hydraulic conductivity as a function of water content presented by van Genuchten (1980) (Eq. [11]), and the quasi-saturated hydraulic conductivity as a function of entrapped air content model presented by Faybishenko (1995) (Eq. [9]) fit the data relatively well. . This means that the effect on quasi-saturated hydraulic conductivity of dynamic entrapped air contents due to changes in water table elevation can be incorporated into groundwater flow models relatively easily.

This thesis constitutes significant scientific contributions to the fundamental understanding of the nature of entrapped air and its effects on hydraulic conductivity near the water table. Given the ubiquitous occurrence of unconfined aquifers and water table fluctuations this fundamental mechanism should be added to conceptual models and when warranted to numerical models to better assess and predict the behaviours of groundwater and associated processes.

REFERENCES

Amos, R.T. and K.U. Mayer. 2006. Investigating the ebullition in a sand column using dissolved gas analysis and reactive transport modeling. Environmental Science and Technology 40: 5361-5367.

Aven'yanov, S.F. 1950. O vodopronitsaemosti gruntov pri nepolnom ikh nasyschenii (On soil permeability under unsaturated conditions). Inzh. Sb 7: 3-14.

Buckingham, E. 1907. Studies on the movement of soil moisture, U.S. Dept. Agr. Bur.Soils Bull., 38, Washington DC.

Christiansen, J.E. 1944. Effect of entrapped air upon the permeability of soils. Soil Science 58: 355-365.

Cirpka, O.A. and P.K. Kitanidis. 2001. Transport of volatile compounds in porous media in the presence of a trapped gas phase. Journal of Contaminant Hydrology 49: 263-285.

Constantz, J., Herkelrath, W.N. and F. Murphy. 1988. Air encapsulation during infiltration. Soil Science Society of America Journal 52: 10-16.

Darcy, H. 1856. Les fontaines publiques de la ville de Dijon. Victor Dalmont, Paris.

Domenico, P.A. and F.W. Schwartz. 1998. Physical and Chemical Hydrogeology. New York: John Wiley & Sons, Inc.

Dunn, A.M. and S.E. Silliman. 2003. Air and water entrapment in the vicinity of the water table. Groundwater 41(6): 729-734.

Emmerton, C.A. 2001. The effect of entrapped air on hydraulic conductivity. Honors B.Sc. Senior Thesis, School of Geography and Geology, McMaster University, Hamilton, Ontario.

Faybishenko, B.A. 1995. Hydraulic behaviour of quasi-saturated soils in the presence of entrapped air: Laboratory experiments. Water Resources Research 31 (10): 2421-2435.

Fayer, M.J. and D. Hillel. 1986. Air encapsulation: I. Measurement in a field soil. Soil Science Society of America Journal 50: 568-572.

Fetter, C.W. 1999. Contaminant Hydrogeology. New Jersey: Prentice Hall.

Fireman, M. 1944. Permeability measurements on disturbed soil samples. Soil Science 58: 337-353.

Freeze, R.A. and J.A. Cherry. 1979. Groundwater. New Jersey: Prentice Hall.

Fry, V.A., Selker, J.S. and S.M. Gorelick. 1997. Experimental investigations for trapping oxygen gas in saturated porous media for in situ bioremediation. Water Resources Research 33 (12): 2687-2696.

Geistlinger, H., G. Krauss, D. Lazik, and L. Luckner. 2006. Direct gas injection into saturated glass beads: Transition from incoherent to coherent gas fl ow pattern. Water Resources Research. 42: W07403, doi: 10.1029/2005WR004451.

Glass, R.J., S.H. Conrad, and W. Peplinski. 2000. Gravity-destabilized non-wetting phase invasion in macroheterogeneous porous media: Experimental observations of invasion dynamics and scale analysis. Water Resources Research 36: 3121–3137.

Gupta, R.P. and D. Swartzendruber. 1964. Entrapped air content and hydraulic conductivity of quartz sand during prolonged liquid flow. Soil Science Society Proceedings 28: 9-12.

Jones, S.F., Evans, G.M. and K.P. Galvin. 1999. Bubble nucleation from gas cavities- a review. Advances in Colloid and Interface Science 80: 27-50.

Mualem, Y. 1976. A new model for predicting the hydraulic conductivity of unsaturated porous media. Water Resources Research 12: 513-522.

Mumford, K.G., Smith, J.E. and S.E. Dickson. 2009. New observations of gas-phase expansion above a dense nonaqueous phase liquid pool. Vadose Zone Journal 8: 404-410.

Poulovassilis, A. 1969. The effect of entrapped air on the hysteresis curves of a porous body and on its hydraulic conductivity. Soil Science 109 (3): 154-162.

Ryan, M.C., MacQuarrie, K.T.B., Harman, J., and J. McLellan. 2000. Field and modeling evidence for a "stagnant flow" zone in the upper meter of sandy phreatic aquifers. Journal of Hydrology 233: 233-240.

Ronen, D. Berkowitz, B. and M. Magaritz. 1989. The development and influence of gas bubbles in phreatic aquifers under natural flow conditions. Transport in Porous Media 4: 295-306.

Roy, J.W. and J.E. Smith. 2007. Multiphase flow and transport caused by spontaneous gas phase growth in the presence of dense non-aqueous phase liquid. Journal of Contaminant Hydrology 89: 252-269.

Sakaguchi, A., Nishimura, T., and M. Kato. 2005. The effect of entrapped air on the quasi-saturated soil hydraulic conductivity and comparison with the Unsaturated hydraulic conductivity. Vadose Zone Journal 4: 139-144.

Silliman, S.E., Berkowitz, B., Simunek, J., and M. Th. Van Genuchten. 2002. Fluid flow and solute migration within the capillary fringe. Groundwater 40 (1): 76-84.

Smith, J.E. 1995. The effect of solute concentration dependent surface tension on vadose zone flow and transport. Ph.D Thesis in Earth Sciences, Waterloo University, Waterloo, Ontario.

Storestrom, D.A. and J. Rubin. 1989. Water content dependence of trapped air in two soils. Water Resources Research 25 (9): 1947-1958.

Topp, G.C., Davis, J.L., and A.P. Annan. 1980. Electromagnetic determination of soil water content: Measurement of coaxial lines. Water Resources Research 16: 574-582.

Van Genuchten, M.Th. 1980. A closed-form equation for predicting the hydraulic conductivity of unsaturated Soils. Soil Science Society of America Journal 44: 892-898.

Validyne Engineering, General Operating Instructions: www.validyne.com.

Wang, Z., Feyen, J., Van Genuchten, M.Th., and D.R. Nielsen. 1998. Air entrapment effects on infiltration rate and flow instability. Water Resources Research 34 (2): 213-222.

Zlotnik, V.A., Eisenhauer, D.E., Schlautman, D.J., Zurbuchen, B.R. and D. Van Peursem. 2007. Entrapped air effects on dipole flow test in sand tank experiments: Hydraulic conductivity and head distribution. Journal of Hydrology 339: 193-205.